

Effects of a Non-Condensable Gas on the Vapex Process

by

Karen Friedrich

A thesis
presented to the University of Waterloo
in fulfillment of the
thesis requirement for the degree of
Master of Applied Science
in
Chemical Engineering

Waterloo, Ontario, Canada, 2005

© Karen Friedrich 2005

Author's Declaration

I hereby declare that I am the sole author of this thesis. This is a true copy of the thesis, including any required final revisions, as accepted by my examiners.

I understand that my thesis may be made electronically available to the public.

Abstract

It is estimated that Canada has 1.7 trillion barrels of oil contained in oil sands located mainly in Alberta. However, the oil contained in the oil sands is a very viscous, tar-like substance that does not flow on its own and cannot be produced with conventional methods. Economical production of this vast resource requires new technology and research. Research in Canada has helped maintain leadership in heavy oil recovery technology.

One method of viscosity reduction is through dilution, which is controlled by two mechanisms – mass transfer and gravity drainage. In the vapour extraction (Vapex) process, vapour of a light hydrocarbon solvent is injected into the reservoir. The mass transfer of vapour into bitumen is driven by a concentration gradient; the vapour diffuses into the heavy oil, causing a reduction in viscosity. The viscosity reduced oil is referred to as “live oil” and is now able to flow by gravity to a horizontal production well. At the surface, solvent can be easily separated and recovered from the produced oil through a flash separation/distillation process.

Under reservoir conditions, extraction solvents such as butane and pentane would condense, increasing the amount of solvent required and decreasing the density difference between solvent and bitumen. The solvent can be maintained in a gaseous phase, by co-injecting a non-condensable gas (NCG), reducing the partial pressure of the solvent and thus preventing condensation. Two types of models were used to observe the VAPEX process while varying the concentration of air and pentane in the system. Experimental results will help to determine the effect of increasing NCG concentration on the rate of live oil production.

The apparatus consists of a porous media model saturated with bitumen and placed inside acrylic housing. NCG (air) exists in the housing before liquid pentane is added. Pentane vapour continuously evolves from a reservoir of liquid pentane, maintained at constant temperature. A concentration gradient was established allowing pentane to flow into the

system where the partial pressure of pentane in the bitumen phase is lower than the vapour pressure of pentane. The bitumen, diluted at the bitumen-gas interface, drains under the action of gravity. The advancement of the bitumen-gas interface was monitored to determine the live oil production rate. By varying the temperature of liquid pentane, the partial pressure of pentane in the extraction vessel was varied.

Results from five experiments in trough models and two in micromodels show that the rate of interface advancement in the presence of a NCG is proportional to the square root of time. Similarly, cumulative volume of oil produced was proportional to the square root of time. Previous works [Ramakrishnan (2003), James (2003), Oduntan, (2001)] have shown that interface advancement and production using a pure solvent was proportional to time. In the experimental range examined (24-32°C) temperature did not effect the rate of production for a given time or interface location.

The average steady state effective diffusion coefficient was calculated from production data to be 0.116 cm²/s, five times larger than estimated from the Hirschfelder Equation.

Live oil properties were found to be consistent throughout each experiment and between experiments. On average, live oil contained 46-48 wt% pentane and viscosity was reduced by four orders of magnitude from 23,000 mPa•s to 4-6 mPa•s.

Acknowledgements

I would like to thank everyone who helped produce this thesis and supported me in every way possible. I would like to directly thank the following people:

- My supervisors Dr. John Chatzis and Dr. Ali Lohi for their wealth of knowledge, support and guidance.
- Dr. Marios Ioannidis for moral support and the best transport phenomena class in existence. Dr. Xianshe Feng for his assistance in preparing this thesis.
- The Chemical Engineering staff, especially Liz Bevan, Pat Anderson, Wendy Irving, Bert Habicher, Ralph Dickhout, and Siva Ganeshlingam for help in all aspects of administrative and technical assistance.
- John Bolt for help in designing and producing my apparatus.
- Sumit Kundu and Lesley James, the best and smartest friends anyone could ask for. Thank you for the motivation, lab guidance and memories.
- My parents for letting me be a professional student for two more years. Thank you for teaching me all the right stuff in life.
- Alex Everett for always standing by me, putting up with me and being there for me. You always make me smile when I need it most.

Table of Contents

1.0	Introduction	1
1.1	General Aspects	1
1.2	Difficulties with Bitumen Production.....	4
1.3	Enhanced Oil Recovery Techniques.....	5
1.4	Motivation and Objectives of This Study	9
2.0	Literature Review.....	11
2.1	Initial Development of the Vapex Process	11
2.2	Viscosity Reduction.....	16
2.2.1	Solvent Concentration Profile.....	16
2.3	Solvent Selection.....	20
2.3.1	Maintaining the Solvent as a Gas Phase	20
2.3.2	Asphaltenes	25
2.3.3	De-Asphalting in Vapex.....	29
3.0	Solvent Diffusion	33
3.1	Diffusion Through a Stagnant Gas	33
3.2	Experimental Determination of Diffusion Coefficient.....	39
3.3	Diffusion Coefficients.....	42
3.3.1	Diffusion of Pentane into Air	42
3.3.2	Diffusion of Pentane into Liquid Bitumen	43
4.0	Materials and Methods.....	45
4.1	Interface Advancement Over a Curved Surface	45
4.2	Bitumen and Solvent Properties	46
4.2.1	Vapex Extraction Using Various Porous Media.....	47
4.2.2	Data Acquisition System.....	50
4.2.3	Vapour Extraction with 2-D Pore Network Micromodels.....	52
4.2.4	Viscosity Variation with Temperature and Pentane Content.....	54
4.3	Analysis of Experimental Data	55
4.3.1	Solution Viscosity.....	55

4.3.2	Live Oil Density	55
4.3.3	Determination of Solvent Fraction in Filtrate/Live Oil	56
4.3.4	Asphaltene Content	57
4.3.5	Residual Oil Saturation.....	57
5.0	Results and Discussion	59
5.1	Movement of an Interface over a Curved Surface.....	59
5.2	Viscosity of Heavy Oil with Temperature and Solvent Fraction.....	61
5.2.1	Effect of Asphaltenes on Stock Heavy Oil.....	61
5.2.2	Effects of Temperature and Pentane Concentration on Viscosity of Bitumen	62
5.3	Summary of Vapour Extraction Experiments.....	66
5.4	Pore Scale Phenomena.....	67
5.4.1	Movement of Live Oil in Micromodels	68
5.5	Interface Advancement.....	71
5.6	Live Oil Production.....	85
5.6.1	Live Oil Properties.....	89
5.6.2	Solvent Diffusion	90
6.0	Conclusions & Recommendations.....	98
6.1	Conclusions.....	98
6.2	Recommendations	99
7.0	References.....	100
	Appendix A.....	105
	Appendix B.....	107
	Appendix C.....	108

List of Figures

Figure 1-1 - Major Heavy Oil Resources (after Smalley, 2000).....	1
Figure 1-2 - Main Heavy Oil Deposits in Canada (after Smalley, 2000).....	3
Figure 1-3 – Recoverable Canadian Conventional and Oil Sands Resources.....	3
Figure 1-4 - Typical Crude Refining Values (after CAPP, 2004).....	4
Figure 1-5 - The Vapex Process (James, 2003).....	8
Figure 2-1 - Interfacial Contact Area in Porous Media (after Das and Butler, 1998).....	13
Figure 2-2 – Distribution of Solvent in Liquid and Gas Phases.....	17
Figure 2-3 - Magnified View of a Pore Network Including Pore Throats, Pore Bodies, Bitumen and Solvent.....	18
Figure 2-4 - Effect of Solvent Mass Fraction on Bitumen Viscosity.....	19
Figure 2-5 - Butex Experimental Apparatus Used by Das and Butler (1995).....	22
Figure 2-6 - Viscosity of Original and Produced Oil in Experiment U2 (after Das and Butler, 1995).....	23
Figure 2-7 - Yield of Asphaltene Precipitate and Solubility Parameter For Various Normal Hydrocarbon Solvents.....	27
Figure 2-8 - Asphaltene Deposition in a Hele-Shaw Cell (Das and Butler, 1994).....	30
Figure 2-9 - Effect of Asphaltene Content on the Viscosity of Bitumen (after Das, 1995)	32
Figure 3-1 - Diagram of System including Co-ordinates.....	34
Figure 4-1 - Curved Interface Model.....	46
Figure 4-2 - Experimental Apparatus and Set Up.....	48
Figure 4-3 - LabView User Interface.....	51
Figure 4-4 - LabView Logic Diagram.....	52
Figure 4-5 - Micromodel Characteristics of Model OC-4 (after James and Chatzis, 2004)	53
Figure 4-6 - Cannon-Fenske routine viscometer (Cannon Instruments, 2004).....	56
Figure 4-7 - Residual Oil Sample Locations.....	58
Figure 5-1 - Measurement of Interface Advancement Perpendicular to Fluid Flow.....	59

Figure 5-2 - Corn Syrup-Air Interface Position over Time	60
Figure 5-3 - Sample of Precipitated Asphaltenes	61
Figure 5-4 - Effect of Increasing Pentane Fraction on Bitumen Solution Viscosity	63
Figure 5-5 - Relationship Between Viscosity of De-asphalted Oil and Pentane Mass Fraction at $T = 22^{\circ}\text{C}$	64
Figure 5-6 - Effect of Solvent Mass Fraction on Bitumen Viscosity by Solvent Type	65
Figure 5-7 - Pore Scale Events.....	69
Figure 5-8 - Advancement of Interface in a Trough Model at Selected Times (Experiment #5).....	73
Figure 5-9 – Photo showing the Bitumen/Vapour Capillary Interface in Glass Micromodel (Experiment #7, $t = 1860$ min)	74
Figure 5-10 - Normalized Advancement of Interface in a Trough Model at Selected Times (Experiment #5)	75
Figure 5-11 - Normalized Advancement of Interface in a Micromodel at Selected Times (Experiment #8)	76
Figure 5-12 - Effects of Lower Porosity on Live Oil Drainage in Trough Models	78
Figure 5-13 - Vapex Interface Visible from Edge and in Model Centre (Experiment #6)	79
Figure 5-14 - Location of Interface Visible from Outside Model	80
Figure 5-15 - Interface Advancement as a Function of Square Root Time (Experiment #7).....	82
Figure 5-16 – Normalized Interface Advancement as a Function of Square Root Time (Experiment #7)	83
Figure 5-17 - Interface Advancement 20 and 40 cm from Model Top (Experiment #5)	84
Figure 5-18 - Time Adjusted Interface Advancement 20 and 40 cm from Model Top (Experiment #5)	85
Figure 5-19 - Live Oil Production History (Experiment #5).....	86
Figure 5-20 - Comparison of Cumulative Production Rates for Trough Experiments	87

List of Tables

Table 1-I - Properties of Canadian Bitumen (Speight, 1991)	2
Table 2-I - Live Oil Properties	20
Table 2-II - Experimental Condition and Results for Butex (Das and Butler, 1995).....	24
Table 2-III - Atomic Composition of Asphaltenes in Canada Precipitated with n-Pentane	26
Table 2-IV - Standard Methods for Asphaltene Precipitation (Speight, 2004).....	29
Table 4-I - Properties of Bitumen and Solvents.....	47
Table 5-I - Summary of Experimental Parameters	66
Table 5-II - Time Required for Interface to Reach the Back of the Model.....	77
Table 5-III - Production Rate at Given z or t.....	88
Table 5-IV - Average Live Oil Properties for Trough Experiments.....	89
Table 5-V - Summary of Experimental Relationships for Trough Model Experiments	Error! Bookmark not defined.
Table 5-VI - Summary of Experimental Relationships for Trough Model Experiments with Shifted Time [#]	95
Table 5-VII - Effective Diffusivity (cm ² /s) Variation Resulting from Errors in Δz and Non-Ideal Solution Behaviour.....	97

Nomenclature

Symbol	Definition	Units
A	area	cm ²
A _d	interfacial area for diffusion	cm ²
A _f	area open for fluid flow	cm ²
c	concentration	g/cm ³ , mol/cm ³
D	diffusivity	cm ² /s
D _a	apparent diffusivity	cm ² /s
D _{eff}	effective diffusivity	cm ² /s
g	acceleration due to gravity	cm/s ²
H, h	height	cm
M _j	molar flux of j with respect to molar average velocity	mol/cm ² •min
k	permeability	Darcy
L	length	cm
M _j	molecular mass of j	g/mole
m	mass	g
N _j	molar flux of j with respect to a fixed reference frame	mole/cm ² •min
n	number of moles	
P	pressure	Pa
P _j	partial pressure of component j	Pa
Q	flow rate	cm ³ /min, mol/min
R	gas constant	m ³ •Pa/mol•K
S _{oi}	initial oil saturation	%Pore Volume (PV)
S _{or}	residual oil saturation	%PV
T	temperature	°C, K
t	time	min, s
V	volume	cm ³
W	width	cm
x	liquid fraction	
y	vapour fraction	
z	interface position	

Greek

Symbol	Definition	Units
β	solubility parameter	$\text{dyne}\cdot\text{mol}^{1/3}/\text{cm}^2$
γ	activity coefficient	
ϕ	porosity	
γ	surface tension	dyne/cm
λ	power value of drainage height	
μ	dynamic viscosity	mPa · s
ν	kinematic viscosity	cSt
ρ	density	g/cm^3
ω	mass fraction	
ξ_j	associate factor for j	
Ω	cementation factor	

Subscripts

Symbol	Definition
0, 1, 2	position
a	air
ave	average
b	beads, back
d	diffusion
eff	effective
f	flow
i	interface
j	Component
M	log mean
max	maximum
min	minimum
o	oil
s	solvent

Superscripts

Symbol	Definition
V	volumetric
vap	vapour pressure
°	dilute solution

1.0 Introduction

1.1 General Aspects

As conventional crude oil production declines, bitumen and heavy oil reserves have become increasingly important to the world's oil supply. Bitumen¹ is located in several parts of the world (Figure 1-1), with Canada, Venezuela, and Russia each possessing more than one trillion barrels in place (Smalley, 2000). However, the main difficulty in producing these vast reserves is bitumen is immobile under reservoir conditions due to its high viscosity (greater than 1000 mPa•s under reservoir conditions).



Figure 1-1 - Major Heavy Oil Resources (after Smalley, 2000)

¹ The terms “heavy oil” and “bitumen” will be used interchangeable in this work.

The Alberta Energy and Utilities Board (AEUB) estimates that Alberta's oil sands contain approximately 1631 billion barrels (259.3 billion m³) of crude bitumen with 315 billion barrels (5 million m³) recoverable by current or anticipated technology and economic conditions (AEUB, 2003). The Canadian deposits are located in four main areas: Athabasca, Peace River, Cold Lake and Lloydminster (as seen in Figure 1-2). Table 1-I shows properties of bitumen from Cold Lake, Lloydminster and Athabasca regions. At reservoir temperature, the oil viscosity in these areas ranges from 10,000 mPa•s to over 1,000,000 mPa•s.

Table 1-I - Properties of Canadian Bitumen (Speight, 1991)

Location	Specific Gravity	API Gravity	Physical Composition (wt/wt%)		
			Asphaltenes	Resins	Oils
Cold Lake	0.999	10.1	15.7	28.7	55.6
Lloydminster	0.966	15.0	12.9	38.4	48.7
Athabasca	1.030	5.9	16.9	34.1	49.0

Canadian oil sands production has increased greatly, surpassing conventional oil in 2001. The Canadian Associate of Petroleum Producers (CAPP) has forecast total oil production (conventional and bitumen) to rise from 2.7 million barrels per day (430,000 m³/day) in 2003 to 3.4 million barrels per day (540,000 m³/day) by 2010; during this time period, the Canadian conventional oil production will continue to decline. The amount of oil that is recoverable in oil sands reservoirs exceeds that in conventional reservoirs by 500%, as shown in Figure 1-3.

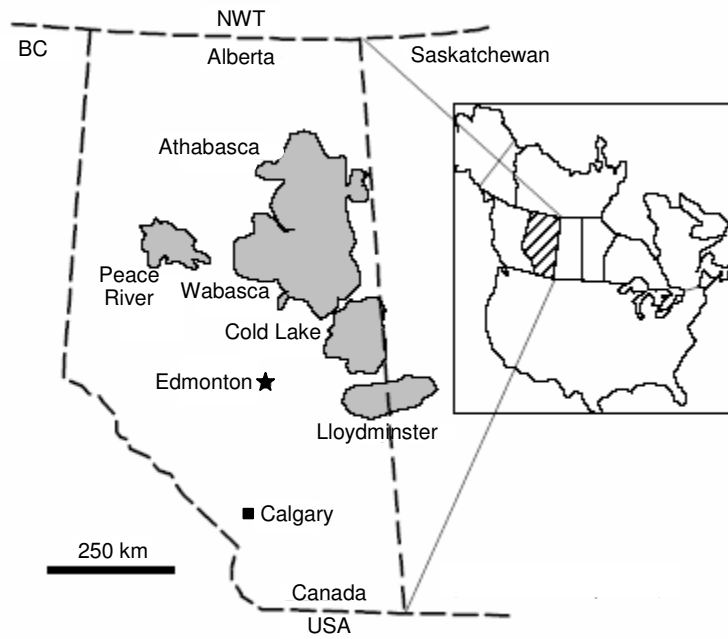


Figure 1-2 - Main Heavy Oil Deposits in Canada (after Smalley, 2000)

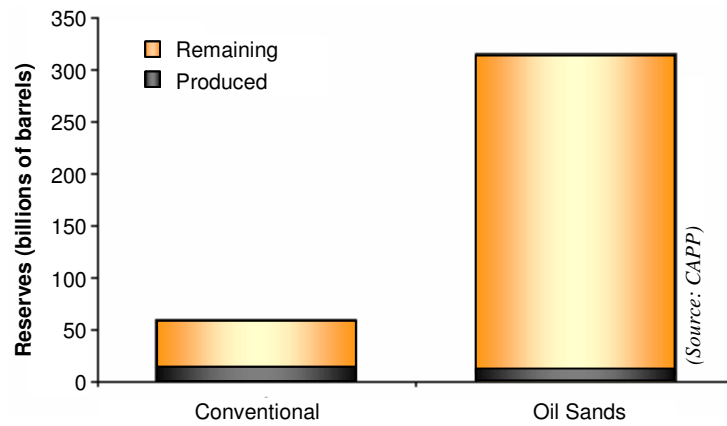


Figure 1-3 – Recoverable Canadian Conventional and Oil Sands Resources

1.2 Difficulties with Bitumen Production

The main difficulty with bitumen is that due to its high viscosity, bitumen is essentially immobile under reservoir conditions, making production by conventional means ineffective or impossible. Bitumen production requires a form of enhanced oil recovery (EOR) to be employed. In comparison to conventional crude, bitumen has high asphaltene and heavy metal (nickel, vanadium, sulphur and iron) content. Heavy metals are considered environmental contaminants and cause coking and catalyst poisoning in refineries. Bitumen also consists of generally higher molecular weight hydrocarbons than conventional crude (Figure 1-4), however it is the lighter ends, such as gasoline and diesel that generate more revenue once distilled, putting bitumen at a disadvantage. Production of bitumen often leaves large amounts of waste products to treat and dispose of. Open-pit mining and cold heavy oil production with sand (CHOPS) result in tonnes of oil-coated sand while thermal process require separation and treatment of condensed water.

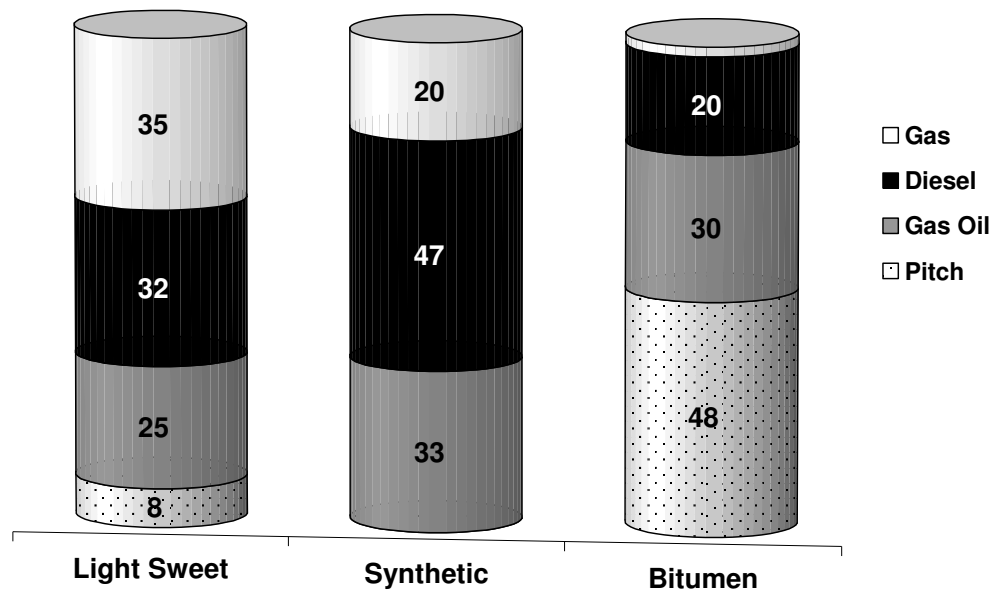


Figure 1-4 - Typical Crude Refining Values (after CAPP, 2004)

The major barrier to bitumen production is cost. Conventional crude is preferred as it is much cheaper to produce, however the yearly production from conventional reservoirs is declining while petroleum consumption is increasing. Bitumen production is the next economic alternative to meet increasing demand. The increased cost in producing bitumen comes from a variety of factors. Additional energy is required to get bitumen to the surface since artificial lift and EOR techniques are required. These methods require added capital and operating costs. Once bitumen has reached the surface, substantial refining is required to produce the more profitable lighter ends, such as gasoline and diesel. Additionally, EOR techniques often have a larger environmental impact and require the treatment and disposal of large amounts of waste products. The Canadian Association of Petroleum Producers (CAPP, 2004) lists the current cost of producing Canada's bitumen at \$8 to \$12 per barrel (bbl). The cost will continue to decrease with innovation and technology, but many EOR techniques still require world oil prices for West Texas Intermediate to remain above \$20 US/bbl to continue operating economically.

1.3 Enhanced Oil Recovery Techniques

Oil production techniques for bitumen are classified into two categories: surface mining and in-situ (in-place) production techniques. Surface mining is the oldest technique, with Suncor opening the first commercial mine in 1967. The process involves digging up the oil sand then transporting it to a treatment facility where hot water extraction is used to separate the bitumen from the sand. This technique is effective, recovering up to 75% of the oil; however it is only economical to produce oil that is less than 75 m below surface and only 5 to 10% of Canada's heavy oil is found at these depths. In addition, two tonnes of sand must be mined to produce one barrel of oil, leaving a huge volume of sand (containing the remaining 25% oil) to be disposed of. Surface mining also leaves a large footprint requiring extensive land reclamation projects. Improving the flow of oil by changing the properties of the crude oil is an in-situ enhanced oil recovery (EOR) technique. By reducing the crude oil's viscosity or changing the surface chemistry of

reservoir fluids, the oil may begin to flow, allowing for production. The use of EOR techniques can bring oil recovery to over 60% of original oil in place (RWE, 2004).

Oil viscosity is a strong function of temperature. Thermal methods increase the production flow rate of oil by increasing the reservoir temperature with the addition of heat, thereby decreasing the viscosity. Heat is added in the form of steam, hot water or in-situ combustion. Currently the most popular methods of bitumen production in Canada are steam assisted gravity drainage (SAGD) and cyclic steam stimulation (CSS). In both processes, steam is injected into the wells where it contacts cooler oil. As the steam condenses, latent heat is transferred to the reservoir, decreasing bitumen viscosity until it is able to flow to the production well. Production is maintained with continuous (SAGD) or cyclical (CSS) injection of steam.

Unfortunately, the use of steam has several disadvantages. The production of one barrel of oil requires two to four barrels of steam, a relationship known as the steam-to-oil ratio (SOR). Steam is generated by burning natural gas, thus the cost of producing steam is very sensitive to increases in the price of natural gas. Steam generation facilities account for about 30% of the capital cost in SAGD (Das, 1998). Steam production also requires a large source of water, usually a lake or aquifer. After the steam condenses in the reservoir, both oil and water will be produced, thus separators are required to remove and reclaim the injected water. A significant amount of surface equipment is required to produce steam and separate the produced oil-water mixture, including a heated de-emulsification tank, water softening system, and steam turbines. Heat loss is a major concern for thermal methods. Despite heavy insulation, steam is lost in the lines between the steam generators and the well bore, through the well casing, to the overburden and to ground water below the reservoir. Typically thermal methods can only be used economically in thick reservoirs and those without bottom water.

The use of steam also has several environmental impacts. Firstly, to produce steam, natural gas is burned, resulting in a large production of carbon dioxide (CO₂) as one of the combustion products. Secondly, since large volumes of water are required, the depletion of aquifers is a major concern. Thirdly, formation damage can also occur in

reservoirs which contain more than 10% clay. When the steam condenses into water, clay will absorb the water, resulting in clay swelling. Clay swelling phenomena lead to pore blockage, reducing permeability and halting or limiting production. The intense heat inside the reservoir, particularly for injection wells, can also lead to well shearing, a phenomenon that occurs when the reservoir expands more rapidly than the overburden. As it expands, the reservoir rock shifts under the overburden causing wells in this area to shear. Production shut-down and re-drilling costs are significant.

Vapour Extraction (Vapex) is a non-thermal alternative for bitumen production. The process uses a second method of viscosity reduction; dilution. Since the process is non-thermal, Vapex can be applied to reservoirs that are un-suitable for thermal methods such as those with low thermal conductivity, bottom water, and thin pay zones. The Vapex process starts with the injection of a highly soluble vapourized solvent² into a bitumen reservoir. Since the solvent is much less dense than bitumen, it will tend to rise in the reservoir towards the impermeable cap rock. As the solvent diffuses into the bitumen, a significant reduction in viscosity is experienced. Viscosity reduction of up to four orders of magnitude was observed by Oduntan (2001), Ramakrishnan (2003) and James (2003). When a critical concentration of the solvent has diluted the oil, the oil will begin to flow, and it is now referred to as live oil. Live oil drains along the solvent vapour-oil interface under the force of gravity to the production well. The evacuated pores are filled with solvent vapour resulting in the formation and growth of a solvent chamber. Figure 1-5 illustrates the Vapex process and the growth of the solvent chamber once the cap rock has been reached.

The production rate of Vapex is governed by two processes: mass transfer of solvent vapour into bitumen and gravity drainage. Experiments by Das and Butler (1998) have shown that the rate of mass transfer is up to ten times higher than expected by simple diffusion, partially due to constant interface renewal. When live oil drains from the bitumen-solvent interface, undiluted bitumen is exposed, maintaining a high

² Contrary to convention, in Vapex bitumen is referred to as the solute and the light hydrocarbon as the solvent.

concentration gradient and thus a high driving force for mass transfer. Production rates in porous media have also been shown to be higher than those from Hele-Shaw cells.

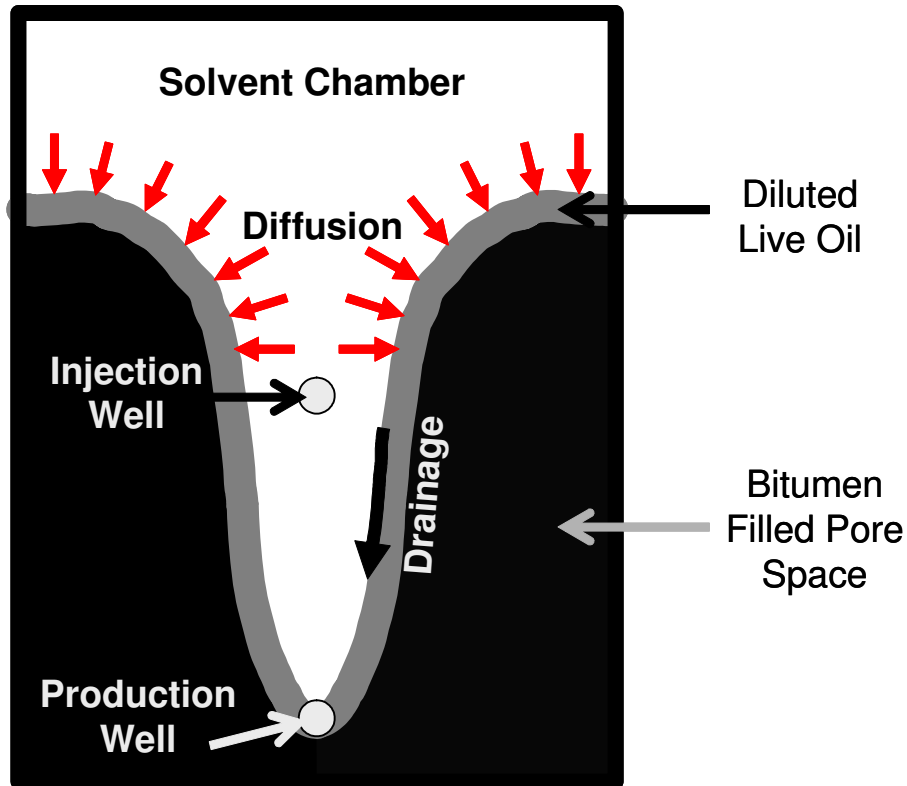


Figure 1-5 - The Vapex Process (James, 2003)

Compared to thermal oil recovery techniques Vapex has a lower capital cost, requires less energy, produces less pollution and may lead to in-situ upgrading (Karmaker & Maini, 2003). In thermal techniques significant amounts of energy are consumed for heating up reservoir rock and lost to the overburden, underburden, piping and wellbore. The solvents used in Vapex cannot escape through the cap rock, and they are insoluble in water, hence there is no loss of solvent through water zones that can exist both above and below. After oil production has ceased, the majority of the solvent held in the reservoir can be recovered through a “blowdown” procedure.

The energy requirement for Vapex is also significantly lower compared to SAGD. Since water has a larger latent heat of vapourization compared to propane or butane, the Vapex process uses only 3% of the energy required by steam processes (Das, 1998). Without the need for steam production, Das (2002) estimated that the Vapex process produces 80% less green house gas emissions than SAGD. In addition, carbon dioxide sequestration is possible with Vapex, thus reducing the volume of CO₂ released to the atmosphere.

1.4 Motivation and Objectives of This Study

Solvent selection is an important economic and process decision in Vapex. The ideal solvent depends on reservoir characteristics such as temperature, pressure and bitumen properties. It is important that the solvent remain in the gas phase to minimize the amount of solvent required to fill evacuated pore spaces. The lower density of the solvent gas (compared to liquid solvent) also aids in live oil drainage and expansion of the solvent chamber. However, a heavy oil reservoir located 100 m below surface would typically be 10°C and 1 MPa, which would cause pure solvents such as propane, butane or pentane to condense. Condensation can be prevented through the addition of a non-condensable gas (NCG), such as air or nitrogen.

If the partial pressure of the solvent remains lower than the vapour pressure at reservoir temperature, the solvent will not condense. The addition of a non-condensable gas will however reduce the rate of mass transfer as the solvent will also have to diffuse through a stagnant layer of the non-condensable gas.

The effect of NCG on production characteristics and evolution of the Vapex interface has not been addressed in past studies. The main objective of this work is to examine the effect of solvent concentration on the rate of live oil production and live oil properties in the Vapex process. A new apparatus was built and testing procedure was developed to

obtain experimental data. The relationship between solvent concentration, temperature and live oil properties (viscosity and density) was also be examined.

2.0 Literature Review

This section will focus on the following areas: initial development of the Vapex process, viscosity reduction, solvent selection and the de-asphalting process.

2.1 *Initial Development of the Vapex Process*

The Vapex process was first developed by Butler and Mokrys (1989) as a solvent analogue to steam assisted gravity drainage (SAGD). In SAGD, steam injected into a horizontal well situated above a second parallel well. When the steam contacts the cold bitumen, heat is transferred from the steam to the bitumen causing the steam to condense and the bitumen's temperature to increase. Since viscosity is a strong function of temperature the added heat decreases the bitumen viscosity. When sufficient heat has been added and the reduced viscosity of bitumen permits flow, gravity forces causes oil flow downwards towards the lower production well. The flowing oil produced is referred to as live oil. With the continuous addition of steam and removal of live oil, a steam chamber forms and spreads both vertically and laterally in the reservoir.

Butler and Mokrys hypothesized that steam could be replaced with a solvent which would dilute the oil resulting in a decrease in viscosity. Initial experiments were conducted with Athabasca and Suncor bitumen and liquid toluene as the solvent in Hele-Shaw cells (glass plates, separated by thin spacers, sealed on three edges). The following equation was developed from a steady state mass balance in the diffusion layer to estimate the rate of recovery:

$$Q = \sqrt{2kg\phi\Delta S_o N_s h} \quad (2-1)$$

where N_s is the so called Vapex parameter, calculated using the expression:

$$N_s = \int_{c_{\min}}^{c_{\max}} \frac{\Delta\rho D_s (1 - c_s)}{\mu c_s} dc_s \quad (2-2)$$

Equation (2-1) represents the rate of recovery per unit length of the horizontal well from experiments where half of the solvent chamber is developed due to the location of the injector directly above the producer. It does not take into account the effects of deasphalting. Butler and Mokrys concluded that the rate of recovery using a liquid solvent was too low to be economical. In comparison to SAGD, they estimated this process would achieve only 1% of the production rate due to a slow rate of diffusion and smaller density difference between liquid solvent and bitumen compared to steam and bitumen. They repeated the experiments using propane in the vapour phase finding that the liquid phase experiments produced at 20% slower than vapour phase experiments. However, when sand-pack models were used in place of Hele-Shaw cells, the production rate exceeded the rate estimated by Equation (2-1). The mass transfer is thought to be enhanced by convective dispersion and increased interfacial contact due to the porous media and maintenance of a high driving force due to surface renewal.

Das and Butler (1998) found production rates in porous media were almost 10 times higher than those predicted by the Hele-Shaw experiments and scale up equations. They hypothesized that this discrepancy was due to: 1) increased interfacial contact area, 2) increased mass transfer due to capillary imbibition and 3) surface renewal and film drainage. Equation (2-1) was based on the interfacial area for diffusion in a Hele-Shaw cell. Figure 2-1 shows the cross sectional area and interfacial contact area for (a) Hele-Shaw cell, (b) bundle of capillary tubes and (c) packed sand grains. In a Hele-Shaw cell the interfacial area is approximately a trough with a radius of half the plate spacing, thus the ratio of interfacial area to cross-sectional area is:

$$\frac{\textit{interfacial area}}{\textit{cross - sectional area}} = \frac{\pi RL}{2RL} = \frac{\pi}{2} \approx 1.57 \quad (2-3)$$

For a bundle of capillary tubes, the interfacial area of capillary interface divided by the cross-sectional area across plane AB (from Figure 2-1) is:

$$\frac{\text{interfacial area}}{\text{cross-sectional area}} = \frac{2\pi \sum_i r_i^2}{\pi \sum_i r_i^2} = 2 \quad (2-4)$$

Thus, for the same cross-sectional area, the ratio of interfacial area for a bundle of capillary tubes to that of a Hele-Shaw cell is $4/\pi$.

The interfacial area for a sand-pack depends on the position of the interface as well as the distribution of the sand grains. Visually Figure 2-1c shows that the interfacial area can be much larger than the capillary bundle, indicating that the Hele-Shaw cell significantly underestimates the area available for mass transfer.

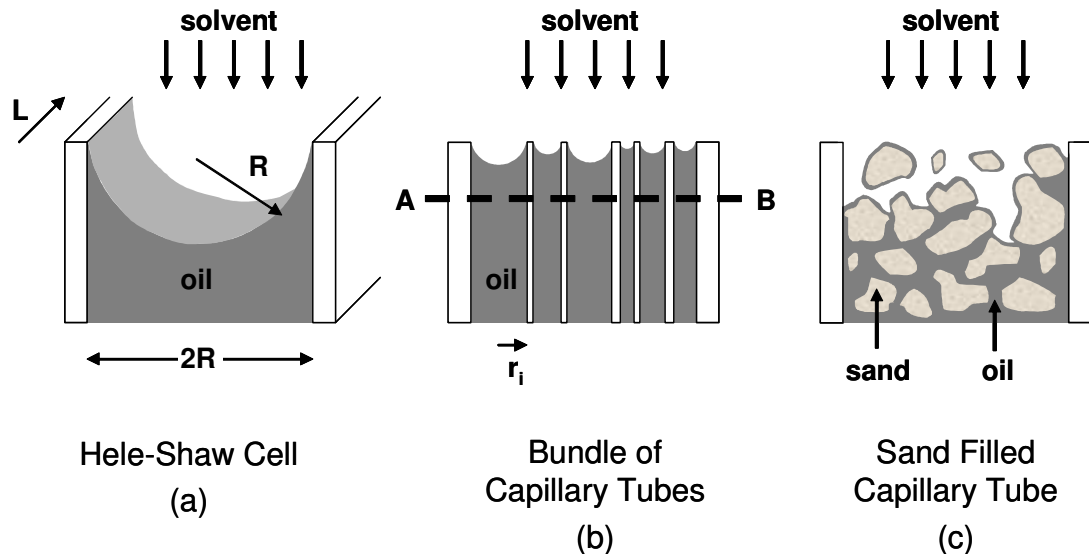


Figure 2-1 - Interfacial Contact Area in Porous Media (after Das and Butler, 1998)

As solvent diffuses into bitumen, both the surface tension and viscosity are reduced. Capillary imbibition draws live oil away from the interface exposing essentially pure bitumen to solvent vapour. The renewal of the interface maintains a high concentration

gradient, and thus a high driving force for mass transfer. In the Hele-Shaw cell, dilute oil flows along the interface surface as the capillary effect is much smaller due to the relatively wide plate spacing. The interface does not undergo the same renewal process as in porous media.

Equation (2-2) was modified by including an apparent diffusion coefficient, D_a as follows:

$$D_a = D\phi^\Omega \quad (2-5)$$

where Ω is the dimensionless cementation factor included to account for tortuous flow paths. Effective diffusivity was then defined for porous media to account for the reduced fluid flow area, A_f , compared to interfacial area, A_d . The effective diffusivity is meant to account for both molecular diffusion and mechanical dispersion.

$$D_{eff} = \left(\frac{A_d}{A_f} \right) D_a \quad (2-6)$$

Applying Equations (2-5) and (2-6) to (2-1) and (2-2), and doubling (2-1) to include the entire solvent chamber produces the following:

$$Q = 2\sqrt{2kg\phi^\Omega \Delta S_o N_s h} \quad (2-7)$$

$$N_s = \int_{c_{min}}^{c_{max}} \frac{\Delta\rho D_{eff} (1 - c_s)}{\mu_s c_s} dc_s \quad (2-8)$$

Yasdani and Maini (2004) wanted to verify the dependence of flow rate on the square root of height as developed in Equation (2-7). Their apparatus differs from previous trough model studies in that the sand pack is located in the annulus space between two concentric tubes. This model allowed them to increase the model height without exceeding pressure limitations. Models were made to mimic the dimensions of rectangular models used in previous work. This apparatus included four thermocouples

and a helical copper tube in the centre of the inner cylinder to maintain constant temperature. Three different packing materials and two types of heavy oil were used for the experiments. The solvent used in all experiments was butane, injected at the top of the model, at a constant pressure that was just below the vapour pressure at the experiment temperature. The production port was located directly beneath the injection port at the bottom of the model. Butane was separated from collected live oil and production rates reflect the dead oil volumes.

Yasdani and Maini (2004) have shown that the results obtained with packings in an annulus are consistent with previous experiments in rectangular models. They also performed experiments with Dina oil at 9°C and Elk Point heavy oil at 21.6°C at which the solvent-free viscosity of the two oils is approximately equal, 18,648 mPa•s and 18,656 mPa•s respectively. Though the oils have different properties (density, viscosity at room temperature, composition) the production rate was not significantly different. Yasdani and Maini (2004) concluded that the modified equation proposed by Butler and Das (1998), given as Equation (2-7) here, underestimates the rate of oil production that can be expected at the field scale. They showed that the drainage rate is not proportional to the square root of drainage height, as given in Equation (2-7), but is of a higher order. Thus, scaled laboratory models will drastically underestimate the rate of production from the field. Plotting $Q/\sqrt{k\phi^\Omega}$ versus \sqrt{h} shows a non-linear relationship that can be fit with either a quadratic or cubic function. The following equation was developed by Yasdani and Maini (2004) to scale experimental rates to expected field rates:

$$\frac{Q_{field}}{Q_{model}} = \left(\frac{h_{field}}{h_{model}} \right)^\lambda \frac{\left(\sqrt{k\phi^\Omega} \right)_{field}}{\left(\sqrt{k\phi^\Omega} \right)_{model}} \quad (2-9)$$

where the exponent λ is in the range of 1.10 to 1.30. An exact value for λ requires further experimental work.

2.2 *Viscosity Reduction*

The most important function of the solvent is to reduce the viscosity of the bitumen. Mass transfer of the solvent into bitumen occurs by both diffusion and convection in a zone in which oil is dilute enough to move, known as the boundary or diffusion layer. The concentration of vapour in bitumen will be at a maximum value at the solvent-bitumen interface. Beyond the boundary layer, the bulk bitumen has a negligible solvent concentration and is unable to flow. Along this interface, a live oil film flows with gravity. In porous media, pore-scale phenomena complicate both mass transfer and gravity drainage (Chatzis 2002).

2.2.1 Solvent Concentration Profile

The distribution of solvent in the liquid and gas phases as a function of position can be seen in Figure 2-2. With a pure solvent, the solvent concentration in the solvent chamber is constant and at its maximum value, $c_{s,max}$. However, in the presence of a non-condensable gas, the solvent concentration in the solvent chamber is a function of horizontal position (y_s decreases as z increases). In the bitumen, beyond the boundary layer-bitumen interface, the solvent concentration is negligible. The minimum oil viscosity will occur at the edge of the boundary layer, $z=i$. As the oil's viscosity is decreased, so is its resistance to flow. Thus, the maximum live oil velocity occurs where viscosity is a minimum.

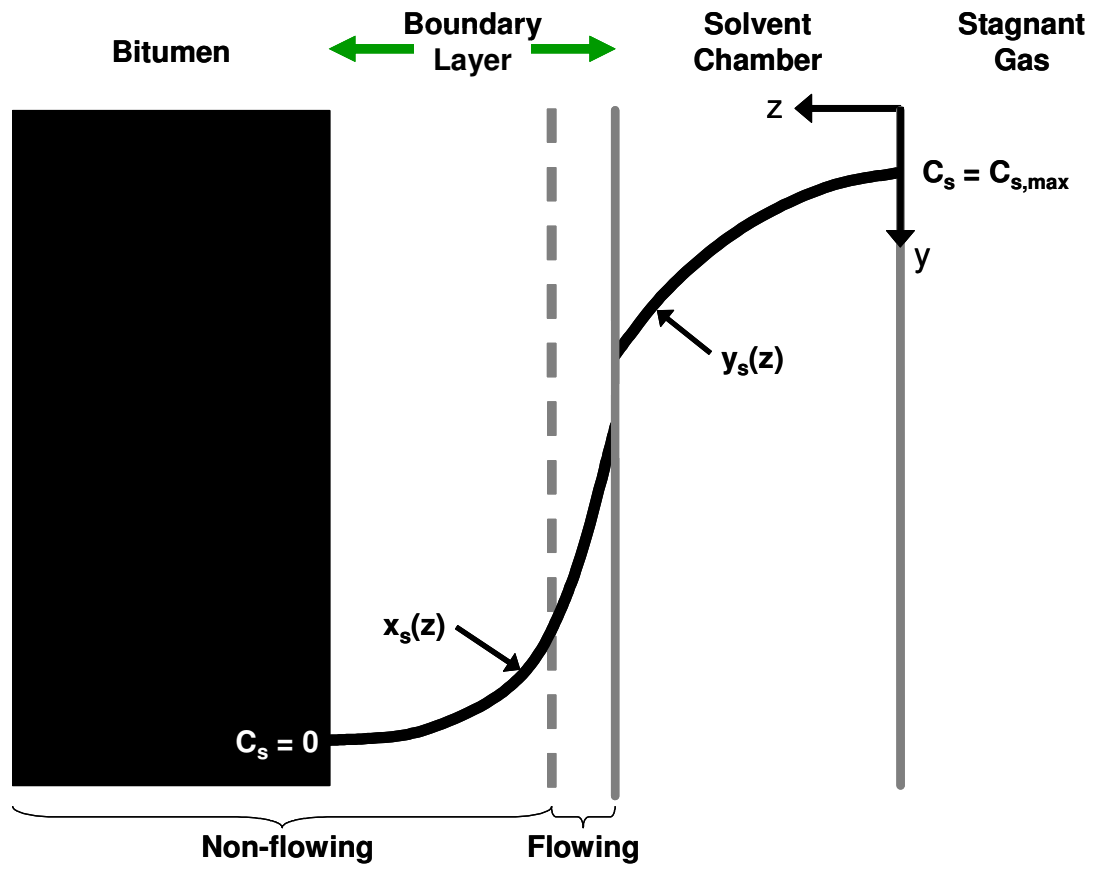


Figure 2-2 – Distribution of Solvent in Liquid and Gas Phases

The surface area for mass transfer is relatively large as gas absorption can occur in pore bodies, pore throats and corners of solvent invaded pores where oil films remain, as seen in Figure 2-3. A pore will drain in the same direction as the pore directly beneath it if a continuous oil film exists. If the pore beneath is filled with vapour, the oil will drain counter-currently to the direction of solvent invasion.

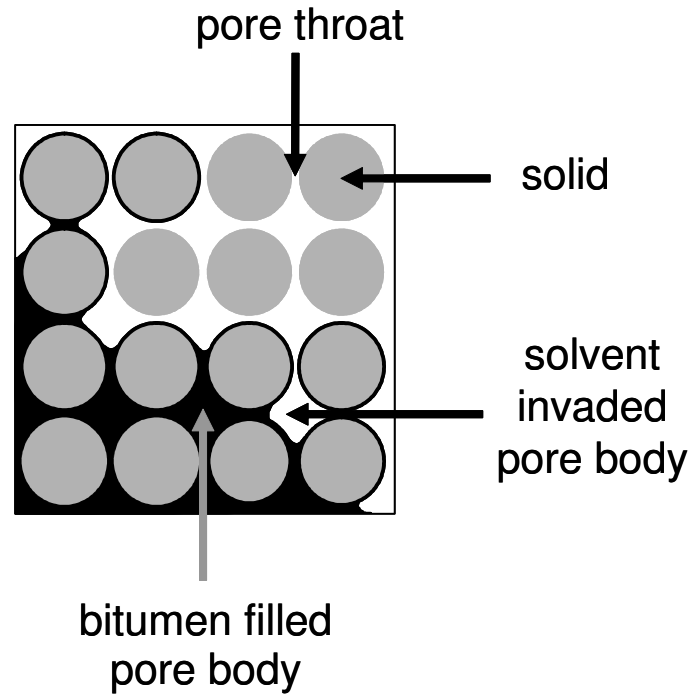


Figure 2-3 - Magnified View of a Pore Network Including Pore Throats, Pore Bodies, Bitumen and Solvent

The Vapex process can be described as a multiphase binary system in which a gaseous solvent diffuses into pseudo-solid bitumen causing the bitumen to become fluid, and thus allowing it to flow along the interface. The interface renewal maintains a high concentration gradient and thus a high driving force for the system.

Jin (1999) and Ramakrishnan (2003) measured the effect of solvent concentration on the viscosity of bitumen, as shown in Figure 2-4. Both found that viscosity was a power law function of solvent concentration though they used different solvents, butane and propane respectively. It should also be noted that each researcher used different types of bitumen.

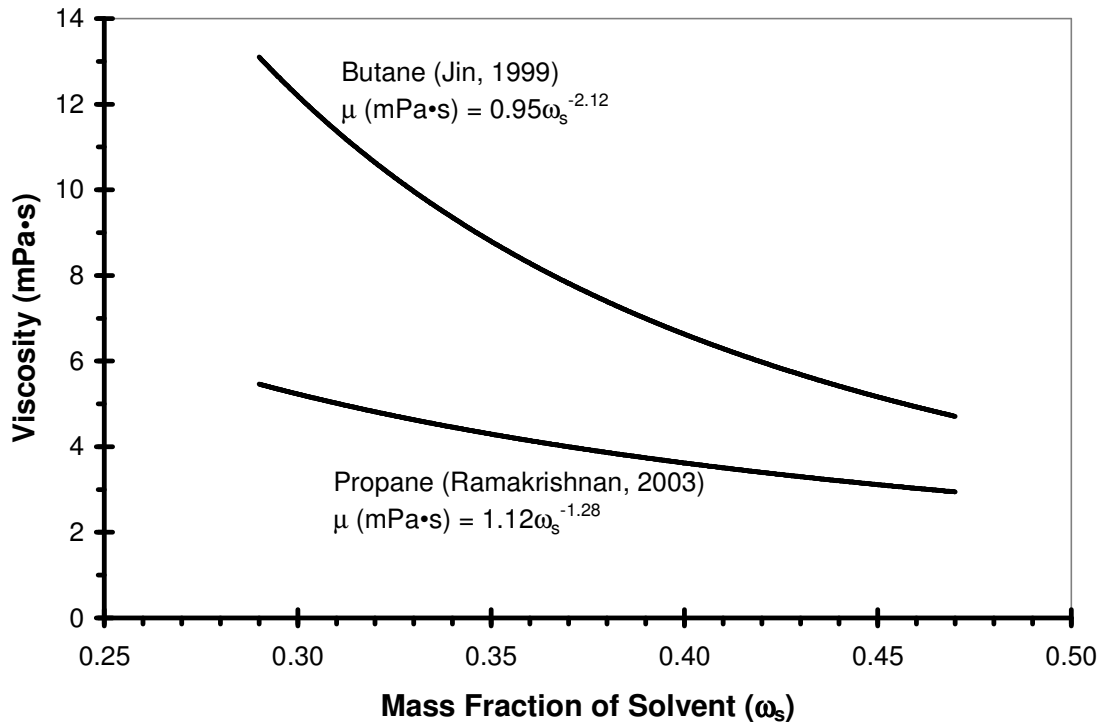


Figure 2-4 - Effect of Solvent Mass Fraction on Bitumen Viscosity

James (2003) summarized experiments by Oduntan (2001), Ramakrishnan (2003) and Butler & Mokrys (1993, 1998) as shown in Table 2-I. This table indicates that the use of either propane or butane as a solvent results in a live oil with approximately 40% solvent (by mass) and a viscosity four orders of magnitude lower than the stock oil.

Table 2-I - Live Oil Properties

Author	Reservoir Type	Solvent	Viscosity (mPa•s)		ω_s (%)
			Bitumen	Live Oil	
Oduntan	Homogeneous	Butane	40,550	2 – 3	0.37
Oduntan	Heterogeneous	Butane	40,550	2 – 3	0.40 – 0.43
James	Homogeneous	Butane	85,000	2 – 3	0.27 – 0.32
Ramakrishnan	Homogeneous	Propane	85,000	4 – 6	0.35 – 0.40
Butler & Mokrys (1993)	Homogeneous	Propane	10,000	2,000*	
Butler & Mokrys (1998)	Homogeneous	Propane	126,000	1,900*	

* Note, Butler & Mokrys measures live oil on a solvent free basis.

2.3 Solvent Selection

The keys aspects of solvent selection include:

1. Solvent should remain a vapour in the solvent chamber,
2. Solvent should cause upgrading (asphaltene precipitation), and
3. Solvent should have the maximum solubility in oil.

2.3.1 Maintaining the Solvent as a Gas Phase

There are several benefits to maintaining the solvent as a gas, including: minimizing solvent requirements, maintaining higher rate of diffusion and maintaining high density difference for gravity drainage conditions. When live oil drains from a pore, the oil volume will be replaced with the injected fluid, solvent for Vapex and water for SAGD. When propane is used as the solvent in Vapex, Das and Butler (1995) estimate that before blowdown, the net cumulative solvent required is 0.02 kg of vapour or 0.5 kg of liquid. Thus, propane vapour would fill 25 times the volume of an equal mass of propane liquid, at the same temperature and pressure. The total solvent required is reduced by recycling produced solvent and a blowdown at the end of production.

The two key mechanisms in Vapex are mass transfer and gravity drainage. In Vapex, the solvent is transferred to bitumen through diffusion. Thus, a higher rate of diffusion leads to a higher production rate. The diffusion coefficient for vapour-liquid diffusion is about four orders of magnitude larger than liquid-liquid diffusion and the diffusional flux is about one order of magnitude larger. The driving force for the second process, gravity drainage, is differences in density. There is a greater density difference between solvent vapour and bitumen than liquid solvent and bitumen. The difference in density allows the solvent vapour to quickly rise in the chamber while the live oil flows downwards to the production well. A solvent vapour attains maximum solubility at or near its vapour pressure (for a given temperature). Condensation is prevented if the reservoir pressure is below the solvent's vapour pressure. Butane is often used in Vapex experiments, however it has a relatively low dew point pressure of 150 kPa at 10°C (Felder and Rousseau, 1986) and would condense in most reservoirs. However, at a given temperature, condensation can be prevented with the addition of a non-condensable gas (NCG). The addition of a non-condensable gas, however has two disadvantages. Firstly, the solvent molecules will also need to diffuse through the NCG to reach the bitumen. Secondly, mass transfer may be impaired due to a reduction in concentration caused by a build-up of NCG in the solvent chamber.

Das and Butler (1995) describes a process, "Butex" that co-injects liquid butane with a high pressure carrier gas. When the mixture reaches the reservoir, some of the liquid solvent will evaporate and be swept towards the bitumen-vapour interface by the carrier gas. Depending on the selection of the carrier gas, it could also participate in bitumen extraction. Butane was selected as the solvent as in previous work by Das and Butler (1994) found butane results in less deasphalting than propane and thus would reduce the chance of wellbore plugging. Butex experiments were carried out in a cell (inner dimensions 70.6 x 20.5 x 3.18 cm) built to withstand 200 psig. The apparatus set up is shown in Figure 2-5. The cell contained a clear plate for visual observation, six thermocouples and 10 ports to allow for variations of injector and production locations. The cell is first packed with sand and then flooded with water. Finally, the water is displaced with bitumen. During the experiment, liquid solvent was injected at a set rate, and nitrogen is pumped in to maintain a set operating pressure. Carrier gas flow was

ensured by continuous production of gas. Live oil is collected and the volume measured. When samples are removed, the solvent vapour is allowed to escape until the mass of the sample has stabilized. Das and Butler (1995) tested two injector/producer configurations: upward leaching (bottom injection) and sideways leaching (top injection). Six experiments (denoted with prefix ‘U’) were performed with the injector located near to oil/water interface, extracting oil as the solvent rose in the cell. The final two experiments located the injector at the top of the cell (experiments denoted with prefix ‘S’). All experiments used butane and nitrogen as the injected solvent except S2 which used propane and nitrogen. Experimental conditions and results are given in Table 2-II.

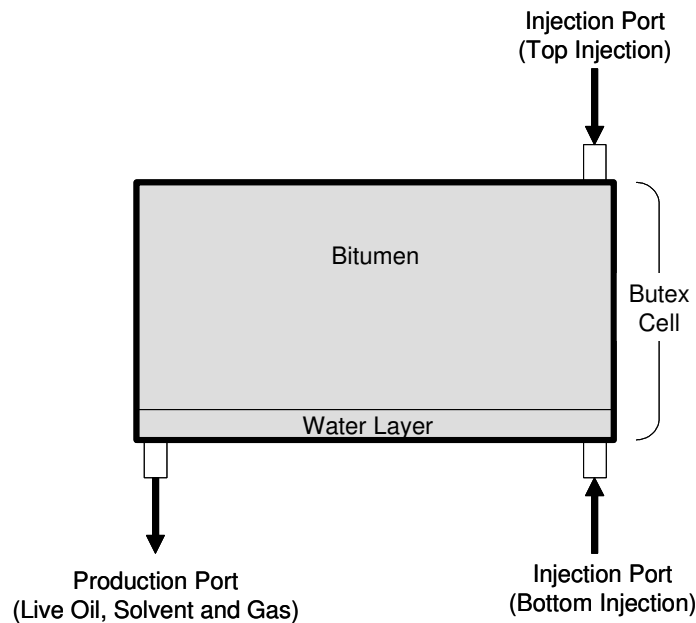


Figure 2-5 - Butex Experimental Apparatus Used by Das and Butler (1995)

The production rates given in Table 2-II are the amount of solvent free oil produced with time. Most experiments start with a high rate of production, which decreases later on as production continues and the height of the oil bank falls. Experiments U2 and U4 were run under similar conditions except that the rate of butane injection in experiment U4 is

approximately 60% of that in U2. The initial and final rates of production in U2 (46.9 g/h and 36 g/h respectively) are significantly higher than those in U4 (28.2 g/h and 18.5 g/h respectively).

Examining oil samples taken during experiment U2, Das and Butler found that the viscosity of the produced oil decreased significantly from the original value of 9,350 mPa•s at 20°C, as shown in Figure 2-6. Though asphaltene precipitation was not mentioned, the decrease in viscosity indicates that some upgrading of the heavy oil has occurred.

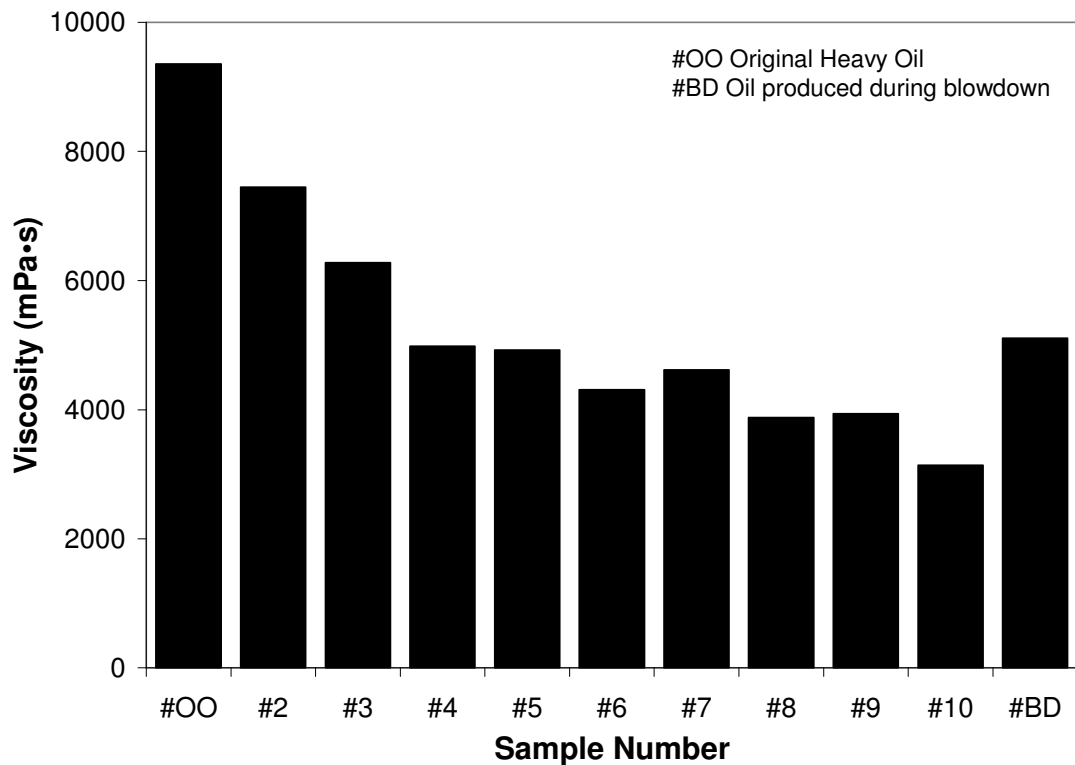


Figure 2-6 - Viscosity of Original and Produced Oil in Experiment U2 (after Das and Butler, 1995)

Table 2-II - Experimental Condition and Results for Butex (Das and Butler, 1995)

Expt No.	k (μm^2)	ϕ	Crude*	S_{a} (%PV)	Solvent	Solvent Injection Rate (g/h)	Nitrogen Injection Rate (l/h)	Pressure (MPa)	Ave. Temp ($^{\circ}\text{C}$)	Production Rate (g/h)
U1	43.5	0.31	PR	0.80	butane	(a) 25 (b) 5	1.2	0.814	21.5	(a) 13.3 (b) 8.0
U2	194.4	0.31	LM	0.89	butane	19.4	1.6	0.779	22.0	(a) 46.9 (b) 36.0
U3	191.5	0.35	LM	0.86	butane	12.5	3.0	0.779	21.7	28.2
U4	191.1	0.33	LM	0.85	butane	11.4	3.4	0.779	21.2	(a) 28.2 (b) 18.5
U5	186.8	0.33	CL	0.88	butane	12.0	3.7	0.779	21.6	9.5
U6	192.4	0.32	LM	0.91	butane	24.8	2.3	0.434	21.6	40.5
S1	195.8	0.37	LM	0.79	butane	9.5	1.5	0.779	21.8	22.4
S2	194.0	0.33	LM	0.93	propane	15.0	1.0	0.959	21.5	(a) 50.0 (b) 25.0

* PR – Peace River bitumen ($\mu=138,300$ mPa•s at 20°C), LM – Lloydminster Tangleflags heavy oil ($\mu=9,350$ mPa•s at 20°C), CL – Cold Lake bitumen ($\mu=65,000$ mPa•s at 20°C)

(a) and (b) represent different phases of production

Asphaltenes remained affixed to the flow visualization cell walls in wave-like patterns, and live oil was observed to drain below the deposits instead of through them. Compared to Hele-Shaw cells, the Butex process occurred ten times faster in a porous medium (Das, 1998) since in porous media, there is increased interfacial contact area which leads to increased mass transfer. Das (1998) found that Vapex production rates were proportional to the square root of permeability.

2.3.2 Asphaltenes

Crude oil is a mixture of hydrocarbons of different molecular weights and volatilities. Asphaltenes are defined as the component of crude oil that is soluble in n-heptane or n-pentane but insoluble in toluene (Sheu & Storm, 1995). Asphaltenes are complex molecules with a high molecular weight, ranging from 1,000 to 2,000,000 g/mole (UIC, 2002). Molecular weight has been difficult to determine as asphaltenes tend to form molecular aggregates and are affected by temperature, solvent used and asphaltene concentration (Speight, 1991). Asphaltenes are the heaviest fractions found in crude oil, and in bitumen they can account for as much as 16 to 22% by weight. Though the exact structure of an asphaltene molecule is unknown, they are hydrocarbons, contain aromatic rings and oxygen, nitrogen and sulphur and heavy metals, especially vanadium, nickel and iron (O, N, S, V, Ni, and Fe respectively). Asphaltene composition varies with location, elemental composition can be determined by exposing the crude to excess (> 40% by volume) n-pentane (Speight, 1991). In Canada's heavy oil reserves (based on 25 samples shown in Table 2-III) asphaltenes contain on average: 45.25% carbon, 52.45% hydrogen, 0.74% nitrogen, 0.68% oxygen and 0.87% sulphur.

Table 2-III - Atomic Composition of Asphaltenes in Canada Precipitated with n-Pentane

Sample #	Atomic Composition (%)				
	C	H	N	O	S
1	43.66	52.57	0.47	1.62	1.68
2	43.85	52.46	0.57	1.57	1.55
3	46.94	51.72	0.73	0.56	0.06
4	41.28	57.69	0.53	0.39	0.11
5	38.72	60.05	0.27	0.85	0.10
6	44.77	52.66	0.56	0.41	1.60
7	44.62	52.93	0.74	0.16	1.55
8	44.77	51.65	1.24	0.84	1.50
9	45.75	51.31	1.33	0.42	1.20
10	46.35	52.81	0.31	0.20	0.33
11	46.72	50.32	1.02	0.68	1.27
12	46.06	51.28	0.71	0.79	1.16
13	45.92	51.09	1.10	0.54	1.34
14	44.69	52.75	0.65	0.65	1.26
15	44.90	52.82	0.70	0.20	1.38
16	46.27	51.50	0.75	0.45	1.03
17	49.55	47.95	0.90	0.39	1.20
18	48.13	49.65	0.92	0.34	0.97
19	43.01	55.79	0.42	0.63	0.15
20	44.03	53.65	0.62	1.44	0.25
21	46.88	50.74	0.66	0.53	1.19
22	47.38	50.01	1.15	0.51	0.95
23	48.38	49.74	1.04	0.74	0.10
24	47.52	50.30	0.61	1.28	0.29
25	43.91	54.39	0.74	0.80	0.15
<i>Average</i>	<i>45.25</i>	<i>52.45</i>	<i>0.74</i>	<i>0.68</i>	<i>0.87</i>
<i>St. Deviation</i>	<i>2.32</i>	<i>2.60</i>	<i>0.28</i>	<i>0.41</i>	<i>0.58</i>

Source: Speight, 1991

Asphaltenes are insoluble in non-polar solvents with a surface tension less than 25 dyne/cm at 25°C (Speight, 2004). Solvents such as n-heptane and n-pentane are commonly used to remove asphaltenes from crude. The amount of precipitation depends on the solvent used, temperature, solvent concentration and contact time. A solubility parameter for non-polar solvents relating internal pressure of the solvent to its solvent power, can be defined as the ratio of surface tension, γ to the cubic root of molar volume, V (Hildebrand, 1919) as shown in Equation (2-10).

$$\beta = \frac{\gamma}{V^{1/3}} \quad (2-10)$$

The solubility parameter, β describes the ability of a solvent to dissolve asphaltenes, thus the higher the solubility parameter the lower the amount of asphaltenes precipitated. For normal hydrocarbons (pentane through decane), the solubility parameter increases with the number of carbon atoms. Figure 2-7 (data from Mitchell and Speight, 1973) shows a comparison of precipitate yields and solubility parameters using various solvents and Athabasca bitumen. Bitumen was first mixed with an equal volume of benzene, then the solution was diluted with 40 volumes of solvent.

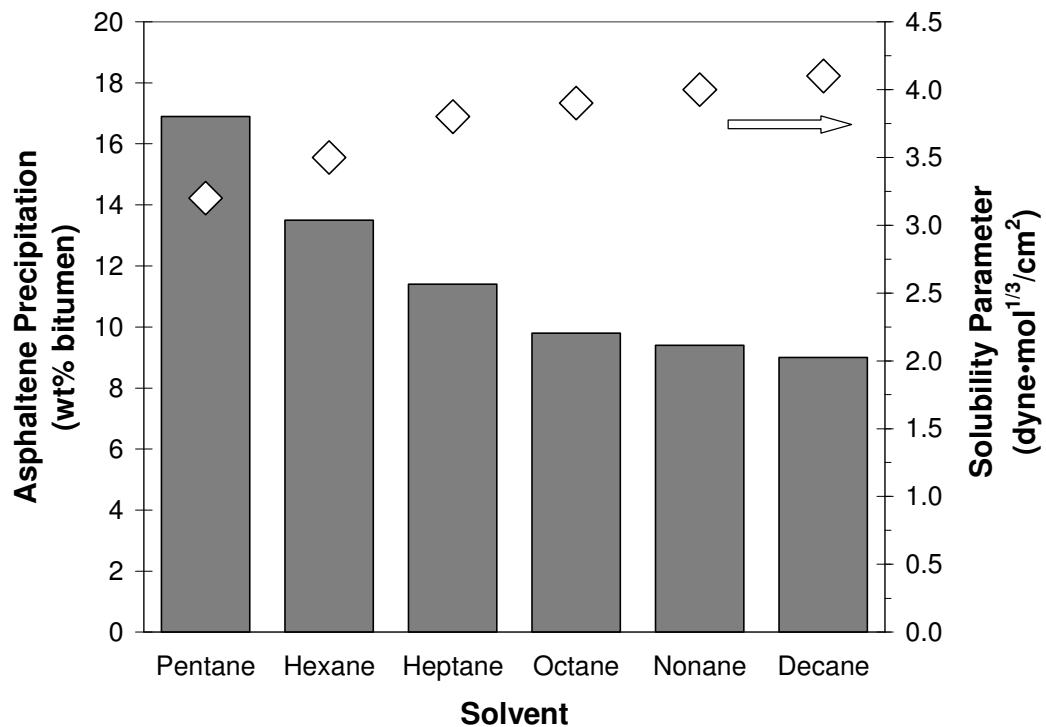


Figure 2-7 - Yield of Asphaltene Precipitate and Solubility Parameter For Various Normal Hydrocarbon Solvents

As temperature increases, so does the amount of asphaltenes precipitated from solution (when solvent is supplied in excess). Using Athabasca bitumen Speight (1991) found that

if temperature is increased from 21°C to 35°C while maintaining the same solvent-bitumen ratio, asphaltene precipitate increased from 17% to 22.5%. As temperature increases, the surface tension decreases, thus so does the solubility parameter defined by Equation (2-10).

The volume of solvent added in asphaltene precipitation tests also has an effect on the amount of asphaltene precipitation. As the ratio of solvent to bitumen increases, precipitation increases until all of the asphaltenes have been removed. The solvent-bitumen ratio depends on the solvent used. Speight (2004) lists numerous standard methods for asphaltene precipitation using n-pentane or n-heptane as given in Table 2-IV. However, to ensure a stable asphaltene yield, Speight (2004) suggests using more than 30 mL precipitant per gram of feedstock and 8-10 hours of contact time. The procedure used enabled the determination of both the precipitation yield and the type of molecules precipitated. Unlike pentane and heptane, propane will cause both asphaltenes and resins to precipitate from crude oil.

The amount of asphaltenes precipitated increases with time until a maximum is reached. At room temperature with Athabasca bitumen and n-pentane, this occurs after approximately 8 hours. A certain length of time is required as settling of asphaltenes from solution is affected by particle size of precipitated asphaltenes.

Table 2-IV - Standard Methods for Asphaltene Precipitation (Speight, 2004)

Method	Precipitant	Volume precipitant per g of sample (mL)
ASTM D-893	n-pentane	10
ASTM D-2006	n-pentane	50
ASTM D-2007	n-pentane	10
ASTM D-3279	n-heptane	100
ASTM D-4124	n-heptane	100
IP 143	n-heptane	30
Syncrude Method	n-pentane	30

2.3.3 De-Asphalting in Vapex

High asphaltene concentration is undesirable as precipitation causes well bore plugging and pipeline decomposition. Additionally, when crude containing asphaltenes is exposed to water, emulsions form because asphaltenes are the most polar fraction of crude oil (Islam, 1995). Emulsions are difficult to separate in the presence of water in distillation. Increased temperature during refining increases the conversion of crude feedstock into lighter and more valuable fractions, however the amount of fouling also increases. When heated above 300°C, asphaltenes decompose into carbon and volatile compounds. Carbon and heavy metals then deposit onto equipment causing fouling which results in reduced flow, increased pressure, reduced heat transfer, increased maintenance and the need to replace catalyst beds (Dickakian, 2001). Thus, it is advantageous to reduce the concentration of asphaltenes in the crude feedstock.

When a light hydrocarbon diffuses into bitumen, the composition and phase behaviour of the oil is altered. As a result the physical change can lead to precipitation of asphaltenes from solution once a critical solvent concentration is reached. Butler and Jiang (2000)

observed that the critical concentration is 20 to 30 wt% for propane for the onset of asphaltene precipitation. In the work of Ramakrishnan (2003), no significant asphaltene precipitation was reported although the propane content in live oil was greater than 30 wt%.

In Vapex, since the solvent concentration in bitumen is highest at the solvent-bitumen interface, asphaltenes will tend to precipitate at this interface. An example of asphaltene precipitation in a Hele-Shaw cell is shown in Figure 2-8. In this example, as the interface moves away, the precipitate can be seen in a fringe pattern with the micro-layer perpendicular to the fringe.

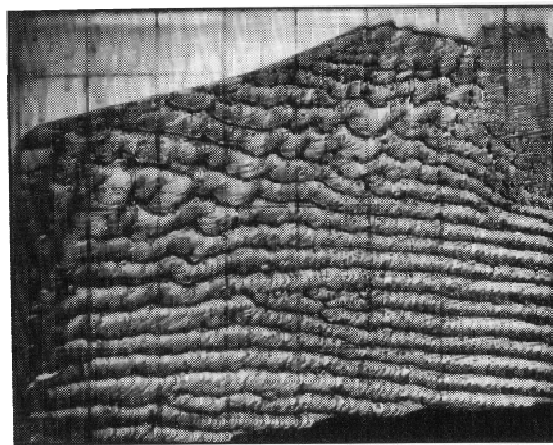


Figure 2-8 - Asphaltene Deposition in a Hele-Shaw Cell (Das and Butler, 1994)

It was expected that the precipitation of asphaltenes would lead to blockage of the pores and impede the flow of live oil. In the Hele-Shaw cell, the flow rate of the oil did not seem to be affected by the precipitation of the asphaltenes. Instead, the solvent vapour appeared to bypass the precipitate and continue to diffuse into the dead oil.

In a porous material it is expected that asphaltene precipitation will reduce the live oil production rate to some extent. Since clay and silica minerals tend to adsorb asphaltenes,

the precipitate will remain in the pores, reducing permeability by up to 20%. Solvent vapour will still be able to by-pass the asphaltenes to continue contacting bitumen.

In addition to preventing problems during transportation and refining, the removal of asphaltenes from bitumen has been seen to drastically reduce viscosity. Experimenting with Peace River bitumen, Das and Butler (1994) found that the crude initially has 19.5% asphaltenes and viscosity of 123,000 mPa•s, but has a viscosity of 3,500 mPa•s when all of the asphaltenes were removed. The viscosity of Cold Lake bitumen was reduced from 65,000 mPa•s to 4,000 mPa•s when the asphaltene content was reduced from 17.6% to zero. The precipitation of asphaltenes further reduces the viscosity of the bitumen thus increasing the oil flow rate. Thus, even after the solvent is removed from the oil (for recycling), the oil's viscosity remains lower than that of the dead oil due to the removal of asphaltenes. The effect of asphaltene content on the viscosity of Cold Lake and Peace River bitumen is shown in Figure 2-9 (Das, 1995). The viscosity reduction by asphaltene removal may allow the oil to flow through pipelines to refineries without the addition of lighter fractions. Along with the asphaltenes, unwanted components such as heavy metals that are bonded to the asphaltenes are also left in the reservoir. Overall, removal of asphaltenes leads to a product with a higher market value.

Asphaltene precipitation has been observed by numerous researchers (Yasdani and Maini (2004), Das (1995), Das and Butler (1998), Oduntan (2001)). The in-situ precipitation of asphaltenes in the experiments carried out at the University of Waterloo was observed at the production end of the system where the solvent concentration is at its maximum. Das and Butler (1998) observed asphaltene deposition when the operating pressure was close to the solvent's vapour pressure at the experimental temperature.

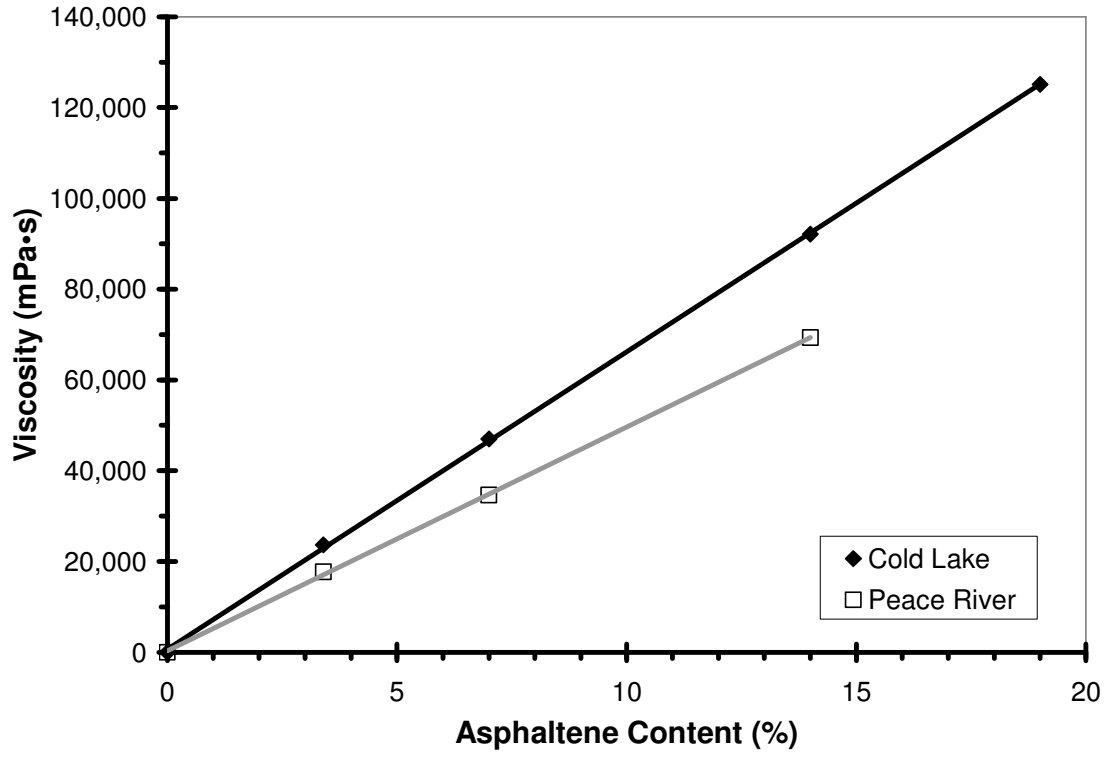


Figure 2-9 - Effect of Asphaltene Content on the Viscosity of Bitumen (after Das, 1995)

3.0 Solvent Diffusion

3.1 *Diffusion Through a Stagnant Gas*

In Vapex, the addition of a non-condensable gas to the solvent vapour will help prevent the solvent from condensing under reservoir conditions. However, the solvent will also have to diffuse through the gas to reach the bitumen, reducing the rate of mass transfer. We will consider the non-condensable gas to be air in this work.

The diffusion of air into bitumen is negligible, thus air is considered a stagnant gas. Thus, in the solvent chamber, the solvent vapour must diffuse through a blanket of stagnant air in the porous medium before contacting the bitumen. Once solvent vapour reaches the bitumen-vapour interface, it will diffuse into the liquid phase bitumen. The accumulation of solvent in bitumen will continue to increase until the viscosity is reduced sufficiently for flow under the action of gravity and capillary forces. The live oil then flows downward, eventually exiting the model. The capillary pressure variation along the interface reflects the different interface curvatures established for different pore sizes and geometries.

A diagram of the apparatus used in the experiments in this work is shown in Figure 3-1. Liquid solvent is present at the bottom of the apparatus in equilibrium with solvent vapour and non-condensable gas. The concentration of solvent is constant in the x and y directions, but varies with position z inside the porous media. As the interface recedes into the porous media, the diffusion length increases as pentane must also move a longer distance through the pore network. The pressure and temperature are assumed constant over the model. The non-condensable gas is assumed to be stagnant as it is insoluble in the live oil. Ideal mixture behaviour is assumed.

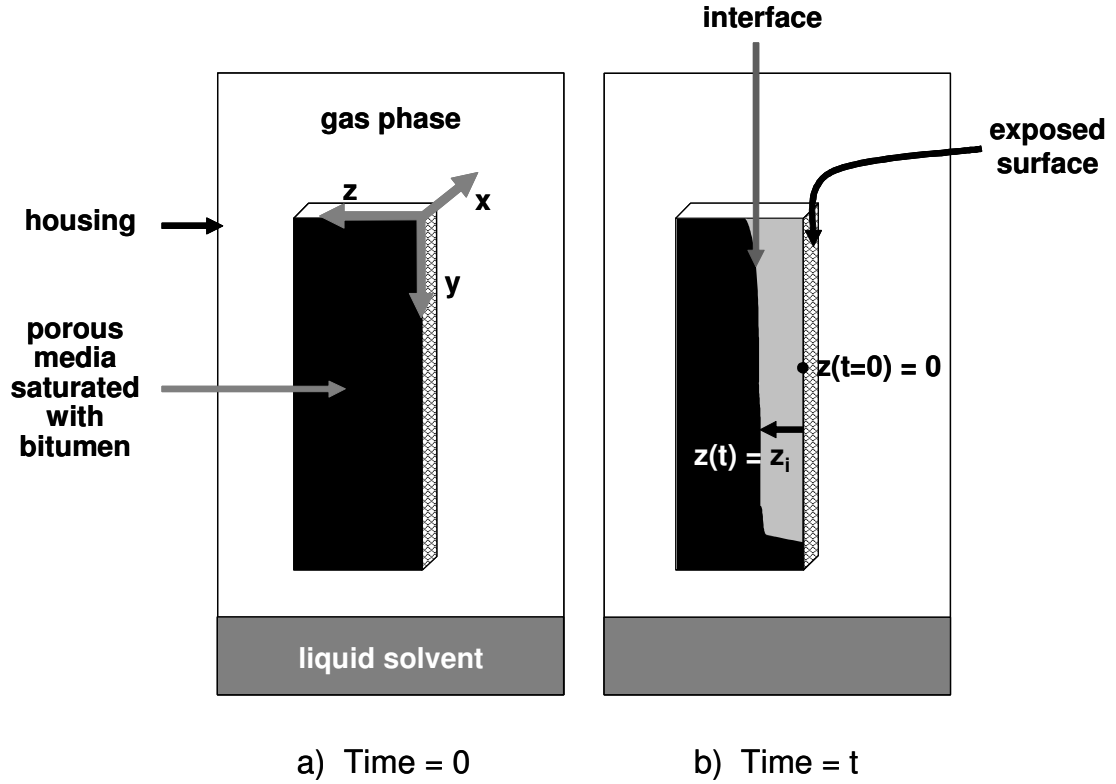


Figure 3-1 - Diagram of System including Co-ordinates

The molar flux of a species describes the molecular transfer of the species through a unit cross-section area in a unit time. Molar flux of species s , N_s , in a rectangular coordinate system is given by (Hines and Maddox, 1985):

$$\frac{\partial c_s}{\partial t} + \left(\frac{\partial N_{sx}}{\partial x} + \frac{\partial N_{sy}}{\partial y} + \frac{\partial N_{sz}}{\partial z} \right) = \dot{R}_s^v \quad (3-1)$$

where c_s is the molar concentration of species s , and \dot{R}_s^v is the molar rate of production of species s in a control volume element. Since there is no chemical reaction and solvent diffusion is assumed to occur only in the z -direction, once steady state is reached, Equation (3-1) can be simplified to:

$$\frac{dN_{sz}}{dz} = 0 \quad (3-2)$$

For a binary system, the total molar flux of gaseous s is:

$$N_s = M J_s + y_s (N_s + N_a) \quad (3-3)$$

Fick's First Law of diffusion for constant total concentration and constant diffusivity coefficients is:

$$M J_s = -cD_{sa} \frac{dy_s}{dz} \quad (3-4)$$

where D_{sa} is the diffusivity of solvent vapour in air.

Substituting Equation (3-4) into Equation (3-3):

$$N_{sz} = -cD_{sa} \frac{dy_s}{dz} + y_s (N_{sz} + N_{az}) \quad (3-5)$$

The diffusion of air into bitumen is negligible thus Equation (3-5) simplifies to:

$$N_{sz} = \frac{cD_{sa}}{1 - y_s} \frac{dy_s}{dz} \quad (3-6)$$

Taking the derivative of Equation (3-6) and substituting in Equation (3-2) yields:

$$\frac{d}{dz} \left(\frac{cD_{sa}}{1 - y_s} \frac{dy_s}{dz} \right) = 0 \quad (3-7)$$

If the diffusion coefficient and total concentration are assumed constant in the z-direction, Equation (3-7) becomes:

$$\frac{d}{dz} \left(\frac{1}{1-y_s} \frac{dy_s}{dz} \right) = 0 \quad (3-8)$$

Integrating Equation (3-8):

$$\int d \left(\frac{1}{1-y_s} \frac{dy_s}{dz} \right) = 0$$

$$\frac{1}{1-y_s} \frac{dy_s}{dz} = k_1 \quad (3-9)$$

Integrating Equation (3-9):

$$\int \frac{1}{1-y_s} dy_s = k_1 \int dz$$

$$-\ln(1-y_s) = k_1 z + k_2 \quad (3-10)$$

Boundary conditions can be used to solve for constants k_1 and k_2 in Equation (3-10). Applying boundary conditions $y_s=y_{s1}$ at position $z=z_1$ and $y_s=y_{s2}$ at $z=z_2$ yields Equations (3-11) and (3-12).

$$-\ln(1-y_{s1}) = k_1 z_1 + k_2 \quad (3-11)$$

$$-\ln(1-y_{s2}) = k_1 z_2 + k_2 \quad (3-12)$$

Evaluating constants k_1 and k_2 yields:

$$k_1 = \frac{\ln \left(\frac{1-y_{s2}}{1-y_{s1}} \right)}{z_1 - z_2} \quad (3-13)$$

and

$$k_2 = -\ln(1 - y_{s1}) - \left(\frac{\ln\left(\frac{1 - y_{s2}}{1 - y_{s1}}\right)}{z_1 - z_2} \right) z_1 \quad (3-14)$$

Substituting Equations (3-13) and (3-14) into (3-10) results in the profile of vapour composition in the z-direction:

$$\ln\left(\frac{1 - y_s}{1 - y_{s1}}\right) = \left[\ln\left(\frac{1 - y_{s2}}{1 - y_{s1}}\right) \right] \left[\frac{z - z_1}{z_2 - z_1} \right] \quad (3-15)$$

$$N_{sz}|_{z=z_1} = \frac{-cD_{sa}}{1 - y_{s1}} \frac{dy_s}{dz} \Big|_{z=z_1} \quad (3-16)$$

Substituting Equation (3-9) and Equation (3-13) into Equation (3-16):

$$N_{sz}|_{z=z_1} = \frac{-cD_{sa}}{1 - y_{s1}} (1 - y_{s1}) \left(\frac{-\ln\left(\frac{1 - y_{s2}}{1 - y_{s1}}\right)}{z_2 - z_1} \right) \quad (3-17)$$

Simplifying the above equation, we get:

$$N_{sz}|_{z=z_1} = \frac{cD_{sa}}{z_2 - z_1} \left[\ln\left(\frac{1 - y_{s2}}{1 - y_{s1}}\right) \right] \quad (3-18)$$

For binary systems containing air and solvent, $y_{ai} = 1 - y_{si}$ and Equation (3-18) becomes:

$$N_{sz}|_{z=z_1} = \frac{cD_{sa}}{z_2 - z_1} \left[\ln\left(\frac{y_{a2}}{y_{a1}}\right) \right] \quad (3-19)$$

Defining a log mean mole fraction:

$$(y_a)_M = \frac{y_{a2} - y_{a1}}{\ln\left(\frac{y_{a2}}{y_{a1}}\right)} \quad (3-20)$$

$$\text{or } \ln\left(\frac{y_{a2}}{y_{a1}}\right) = \frac{y_{a2} - y_{a1}}{(y_a)_M}$$

Substituting Equation (3-20) into Equation (3-19) gives:

$$N_{sz} \Big|_{z=z_1} = \frac{cD_{sa}}{z_2 - z_1} \left(\frac{y_{a2} - y_{a1}}{(y_a)_M} \right) \quad (3-21)$$

At any location in the system, the total pressure of a system is the sum of the component partial pressures:

$$P = \bar{P}_{s1} + \bar{P}_{a1} = \bar{P}_{s2} + \bar{P}_{a2} \quad (3-22)$$

where subscripts 1 and 2 denote locations within the system.

Since the vapour is assumed to be in equilibrium over pure solvent, Dalton's law gives:

$$P_s = y_s P \quad (3-23)$$

$$P_a = y_a P \quad (3-24)$$

For ideal gases:

$$c = \frac{n}{V} = \frac{P}{RT} \quad (3-25)$$

Substituting Equations (3-24) and (3-25) into Equation (3-21) and defining a log mean pressure $(P_a)_M$, the flux expression using pressure differences becomes:

$$N_{sz}|_{z=z_1} = \frac{PD_{sa}}{RT(z_2 - z_1)} \left(\frac{\bar{P}_{a2} - \bar{P}_{a1}}{(P_a)_M} \right) \quad (3-26)$$

This equation describes the flux of a solvent, s through stagnant air. At the bitumen-vapour interface, the flux of solvent into bitumen is related to that defined by Equation (3-26).

3.2 Experimental Determination of Diffusion Coefficient

For diffusion into a semi-infinite stagnant medium with constant diffusivity, D, the concentration at position z and time t, C(z,t) is given by (Crank, 1975):

$$\frac{C}{C_o} = 1 - \operatorname{erf} \left(\frac{z}{\sqrt{4Dt}} \right) \quad (3-27)$$

where C_o is the concentration at the interface and D is the effective diffusion coefficient. Therefore, in a semi-infinite medium with $C_o=0$, the diffusion distance is proportional to the square root of time if the surface concentration is constant. In Vapex, the surface will maintain a constant concentration of solvent as the live oil draining over the interface has been found to contain approximately 40 wt% of solvent [Oduntan (2001), Ramakrishnan (2003)].

At the edge of the diffusion layer (next to the bitumen), the concentration of solvent in bitumen is negligible, thus Equation (3-27) becomes:

$$1 = \operatorname{erf} \left(\frac{z}{\sqrt{4Dt}} \right) \quad (3-28)$$

This enables the determination of depth of diffusion into a stagnant liquid for given D and t conditions. The molar flow rate of pentane in live oil is related to the flux of pentane into bitumen, $N_s(t)$ over the interfacial surface area, A_s shown by:

$$Q_s(t) = N_s(t)A_s = \frac{x_s^v \rho_s}{M_s} \frac{dV_{total,cum}}{dt} \quad (3-29)$$

Experimental data can be used to calculate the volume fraction of pentane in the live oil and the production rate of the system.

The equation describing the diffusive flux of solvent was developed as Equation (3-26). In this system, z describes the distance between the model edge exposed to solvent ($z=0$) and the interface ($z=z_i$), thus the equation describing the flux of solvent through the porous media is given by:

$$N_s(t) = \frac{PD_{sa}}{RT(\Delta z)} \left(\frac{\bar{P}_{ai} - \bar{P}_{a0}}{(P_a)_M} \right) \quad (3-30)$$

Equation (3-30) assumes concentration independent diffusivity.

Equating Equation (3-29) to Equation (3-30) in a porous media:

$$N_s(t) = \frac{PD_{sa,eff}}{RT(\Delta z)} \left(\frac{\bar{P}_{ai} - \bar{P}_{a0}}{(P_a)_M} \right) = \frac{x_s^v \rho_s}{A_s M_s} \left(\frac{dV_{total,cum}}{dt} \right) \quad (3-31)$$

Solving Equation (3-31) for effective diffusivity gives:

$$D_{sa,eff} = \frac{x_s^v \rho_s}{A_s M_s} \left(\frac{dV_{total,cum}}{dt} \right) \frac{RT(\Delta z)(P_a)_M}{P(\bar{P}_{ai} - \bar{P}_{a0})} \quad (3-32)$$

Oduntan (2001), Ramakrishnan (2003) and James (2003) found the experimental production rate of live oil was constant. Grouping constant terms in Equation (3-32) results in:

$$D_{sa,eff} = K \left(\frac{dV_{total,cum}}{dt} \right) \Delta z \quad (3-33)$$

where:

$$K = \frac{x_s^V \rho_s}{2A_s M_s} \frac{RT(P_a)_M}{P(\bar{P}_{ai} - \bar{P}_{a0})} \quad (3-34)$$

In an air-pentane (two component) system, the partial pressure of air is given by:

$$\bar{P}_a = P_{total} - x_s P_s^{vap}(T) \quad (3-35)$$

where x_s is the mole fraction of solvent in the draining live oil near the Vapex interface. For our system, the vapour pressure of pentane is determined at the average model temperature. In the bulk liquid the fraction of pentane is unity thus:

$$\bar{P}_{a0} = P_{total} - P_s^{vap}(T) \quad (3-36)$$

At the bitumen-solvent interface, the fraction of solvent in the liquid phase is estimated by the average mole fraction of pentane in the live oil samples. Thus, the partial pressure of air at the interface is:

$$\bar{P}_{ai} = P_{total} - x_s P_s^{vap}(T) \quad (3-37)$$

In porous media, the diffusion path is not a straight line. The diffusion path in porous media is accounted for by the tortuosity factor, τ . The molecular diffusivity can be related to an effective diffusivity that would occur in a porous media as follows:

$$D_{sa,eff} = D_{sa} \frac{\phi}{\tau} \quad (3-38)$$

3.3 Diffusion Coefficients

3.3.1 Diffusion of Pentane into Air

The diffusivity of non-polar gas pairs can be determined using the Hirschfelder Equation (Hines and Maddox, 1985):

$$D_{AB} = \frac{1.858 \times 10^{-27} T^{3/2}}{P \sigma_{AB}^2 \Omega_D} \left(\frac{1}{M_A} + \frac{1}{M_B} \right)^{1/2} \quad (3-39)$$

where D_{AB} has units of m^2/s , T has units of Kelvin, P is the absolute pressure in atm, σ_{AB} is the collision diameter in meters and Ω_D is the collision integral. For pentane diffusing into air at 295 K:

$$D_{sa} = \frac{1.858 \times 10^{-27} (295 \text{ K})^{3/2}}{(1 \text{ atm})(4.7475 \times 10^{-10} \text{ m})^2 (1.1105)} \left(\frac{1}{72 \text{ kg/kmol}} + \frac{1}{28.8 \text{ kg/kmol}} \right)^{1/2} \quad (3-40)$$

$$D_{sa} = 8.29 \times 10^{-6} \text{ m}^2 / \text{s} = 0.0829 \text{ cm}^2 / \text{s}$$

Effective diffusivity can be calculated assuming a porosity of 40% and a tortuosity factor of 1.5:

$$D_{sa,eff} = \frac{D_{so} (0.40)}{1.5} \quad (3-41)$$

$$D_{sa,eff} = 0.022 \text{ cm}^2 / \text{s}$$

3.3.2 Diffusion of Pentane into Liquid Bitumen

The Wilke-Chang Equation, shown as Equation (3-42), can be used to estimate the diffusivity of a dilute, non-electrolyte solution (Hines and Maddox, 1985).

$$D_{AB}^{\circ} = \frac{1.17 \times 10^{-13} T \sqrt{\xi_B M_B}}{V_A^{0.6} \mu} \quad (3-42)$$

where D_{AB}° has units of m^2/s , T has units of Kelvin, ξ_B is the associate factor for solvent B, M_B is the molecular weight of B, V_A is the molar volume of solute A at the normal boiling point and μ is viscosity in $mPa \cdot s$.

For pentane diffusing into bitumen at room temperature (298 K), Equation (3-42) becomes:

$$D_{so}^{\circ} = \frac{1.17 \times 10^{-13} (295 K) \sqrt{(1)(400 \text{ kg/kmol})}}{\left(\frac{72 \text{ kg/kmol}}{630 \text{ kg/m}^3} \right)^{0.6} (23000 \text{ mPa} \cdot s)} \quad (3-43)$$

$$D_{so}^{\circ} = 1.11 \times 10^{-13} \text{ m}^2/s = 1.11 \times 10^{-9} \text{ cm}^2/s$$

Similarly, for bitumen diffusing into pentane at room temperature, Equation (3-42) becomes:

$$D_{os}^{\circ} = \frac{1.17 \times 10^{-13} (295 K) \sqrt{(1)(72 \text{ kg/kmol})}}{\left(\frac{400 \text{ kg/kmol}}{980 \text{ kg/m}^3} \right)^{0.6} (0.42 \text{ mPa} \cdot s)} \quad (3-44)$$

$$D_{os}^{\circ} = 1.19 \times 10^{-9} \text{ m}^2/s = 1.19 \times 10^{-5} \text{ cm}^2/s$$

The diffusivity of pentane into a non-dilute, ideal pentane-bitumen solution can be determined from the Vignes Equations (Hines and Maddox, 1985):

$$D_{so} = (D_{so}^{\circ})^{x_o} (D_{os}^{\circ})^{x_s} \quad (3-45)$$

It should be noted that, in Vapex, the solvent refers to the vaporized hydrocarbon that is diffusing into bitumen. Using standard terminology, the vapour would be referred to as the solute.

4.0 Materials and Methods

This research examined several areas of the Vapex process including:

1. Interface advancement over a curved surface,
2. Vapour extraction of heavy oil using unconsolidated media in trough models,
3. Visualization of vapour extraction using a 2-D pore network micromodel,
4. Investigation of the variation of live oil viscosity with temperature and pentane fraction and asphaltene content of bitumen
5. Flow visualization of interface advancement during vapour extraction using pentane and other simulated conditions.

4.1 *Interface Advancement Over a Curved Surface*

A physical model simulating drainage of a liquid over a curved interface was constructed. The model was used to examine the effects of a liquid (water) flowing over an interface between a viscous liquid (corn syrup) and air. As the water flows over the interface it dilutes the corn syrup, allowing it to flow along with the water over the interface in the porous media.

The apparatus consisted of a curved acrylic model (outer radius 67.5 cm) as shown in Figure 4-1. The trough space (internal WxH: 2 cm x 7 cm) was packed with a mixture of corn syrup and glass beads. The top of the trough space was exposed to air through a wire mesh covered slit that ran along the outside curve of the model. Water entered the top of the model at a low flow rate, measured every hour. Photos were taken at one hour intervals in a set location. Every hour the volume of produced fluid was recorded and analyzed with a refractometer to determine the concentration of corn syrup in the produced fluid. The experiment was carried out under ambient conditions.

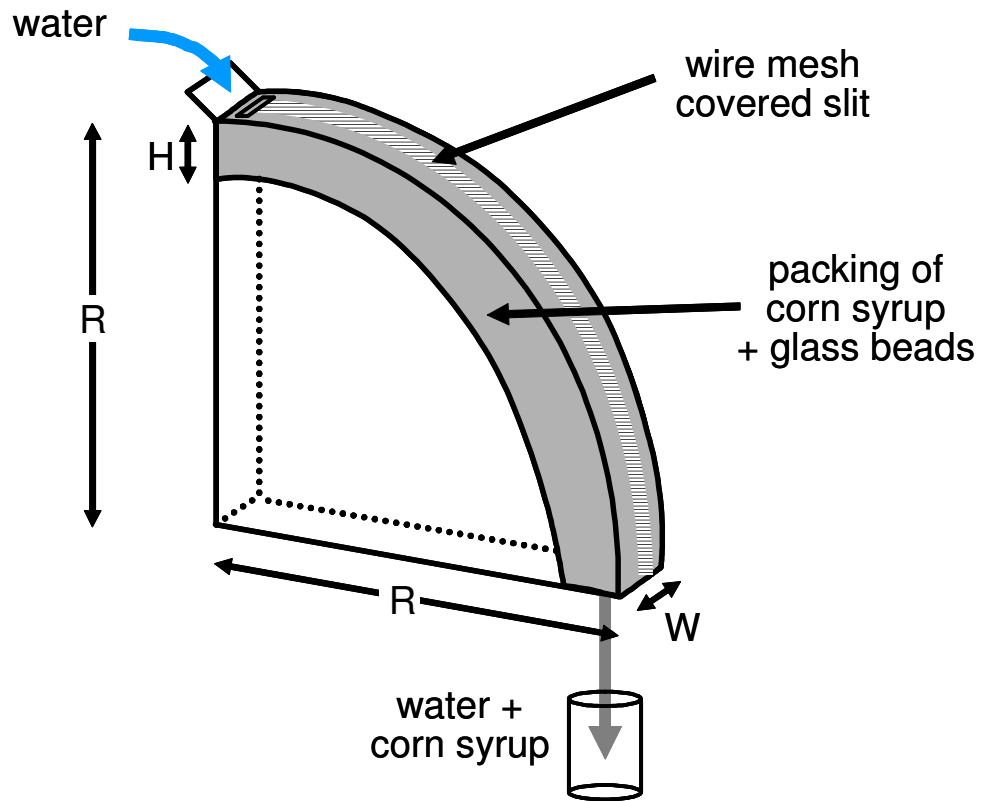


Figure 4-1 - Curved Interface Model

4.2 *Bitumen and Solvent Properties*

All experiments were carried out using Cold Lake bitumen and either Reagent grade or HPLC grade pentane. Properties of these materials are given in Table 4-I.

Table 4-I - Properties of Bitumen and Solvents

Property	Bitumen	Reagent Grade Pentane	HPLC Grade Pentane
<i>Purity (%)</i>	n/a	> 98	> 99
<i>Asphaltene Content (%)</i>	18.26	n/a	n/a
<i>Molecular Weight (g/mol)</i>	400	72.15	72.15
<i>Density* (kg/m³)</i>	0.98	0.63	0.63
<i>Viscosity* (mPa•s)</i>	23,200	0.42	0.42

* approximate value at T = 22°C

4.2.1 Vapex Extraction Using Various Porous Media

The complete apparatus, shown in Figure 4-2, consists of: acrylic housing (exterior dimensions 20.3 cm x 10.6 cm x 52.7 cm) including an 1/8-inch o-ring and lid, graduated cylinder to collect draining oil (2.54 cm ID x 33 cm), a water bath, five thermocouples (T), manometer (P), acrylic trough (interior dimensions 44 cm x 10.5 cm x 0.95 cm), vapour sample port, as well as fittings, valves and tubing. A computer and data acquisition system recorded and displayed information from the apparatus thermocouples (pentane, water bath, model top, model bottom and ambient).

Trough models were packed with glass beads saturated with bitumen ($\mu \approx 23,000$ mPa•s at 22°C) using a procedure developed by Oduntan et al (2001). The glass beads used in this study had an average diameter of 590 μm . After the trough was placed inside the housing and the housing sealed, liquid pentane was added to the apparatus through a port in the top of the housing (not shown in Figure 4-2). Prior to adding pentane, the vapour space in the housing consisted of air at ambient temperature.

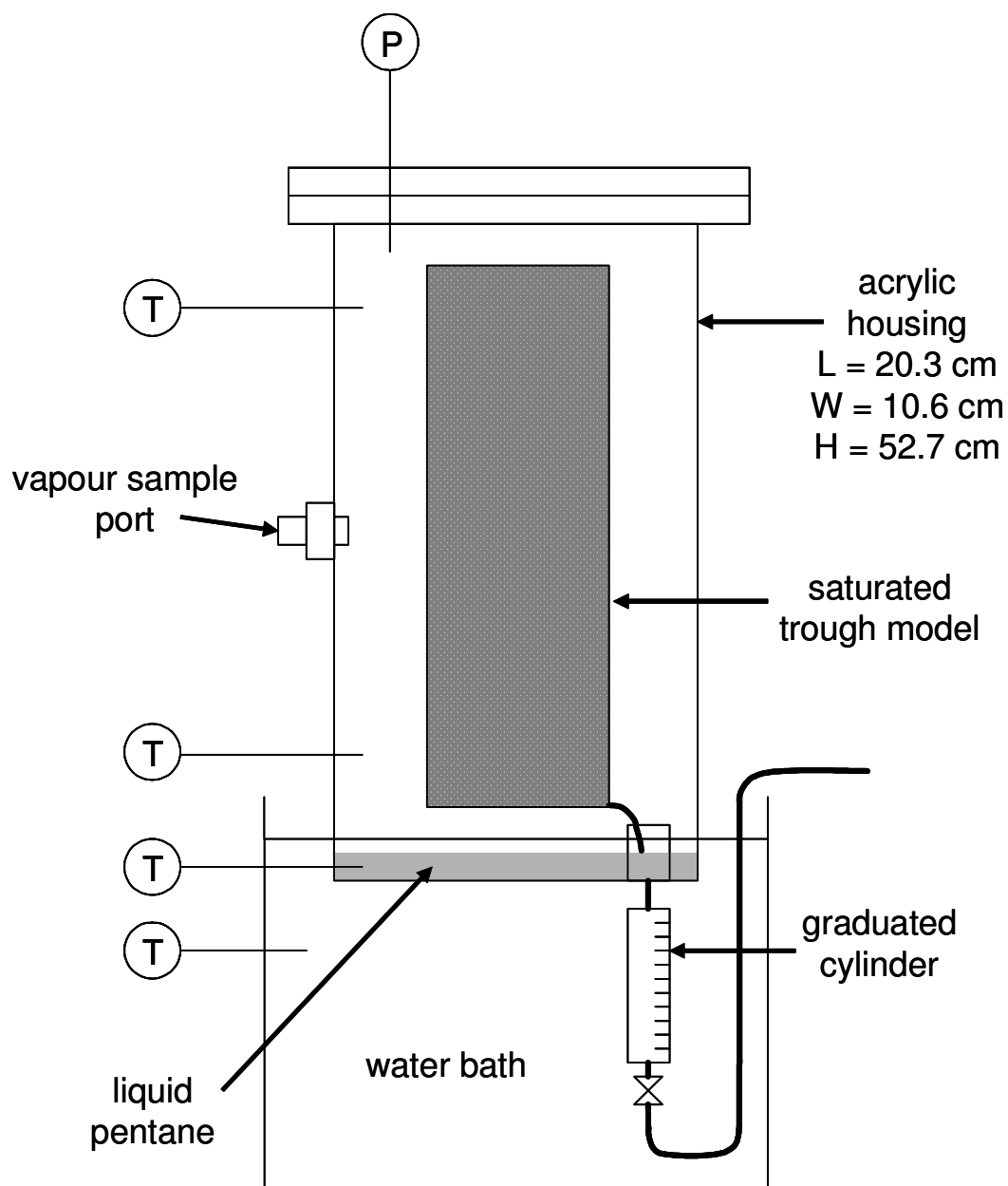


Figure 4-2 - Experimental Apparatus and Set Up

The vapour pressure of component j, P_j^{vap} , is related to temperature according to Antoine's equation:

$$P_j^{vap}(T) = 10^{\left[A - \frac{B}{T+C}\right]} \quad (4-1)$$

where P_j^{vap} has units of mmHg, temperature has units of °C, and A, B and C are parameters unique for component j. For n-pentane, A=6.85221, B=1064.63 and C=232.000 (Felder & Rousseau, 1986). Increasing the temperature of liquid pentane in the housing increases the vapour pressure of pentane which leads to an increase in the fraction of pentane vapour in the system.

The relationship between vapour fraction of pentane and vapour pressure of pentane is shown in equation (4-2).

$$y_j = \frac{P_j^{vap}}{P} \quad (4-2)$$

where P is the absolute pressure in the system.

Experimental run time began when all of the pentane has been added to the apparatus. In examining experiments performed by various authors (Butler, Das, Mokrys, Jiang, Yasdani, Boustani, Maini, Karmaker and co-authors) it should be noted that solvent is injected at a given rate and the produced oil and its properties was reported on a solvent free basis. Experiments performed at the Porous Media Group, University of Waterloo provide excess solvent so that the reservoir may freely uptake the solvent and reported production values and live oil properties contain dissolved solvent. Excess solvent ensures that the solvent is always available and the maintenance of a high concentration gradient.


Approximately every two hours the Vapex/bitumen interface position, volume of produced oil, temperatures and gauge pressure were recorded manually. Temperature data were recorded every ten minutes using the data acquisition system. Ambient pressure was obtained from the University of Waterloo weather station (updated every 15 minutes). When approximately 25 mL of live oil had been recovered in the collection cylinder, the live oil sample was removed via a length of tubing fitted with a two-way valve. A 60 mL syringe was attached to the valve using 1/4-inch plastic tubing, the valve was opened and the plunger slowly drawn back. Collected samples were placed into labelled vials, and oil samples were analyzed at ambient temperature (approximately 24°C) to determine live oil viscosity, density and pentane fraction.

4.2.2 Data Acquisition System

Temperature data were recorded every ten minutes for the duration of experiments with the use of a computer and data acquisition system. Temperature data were taken from five thermocouples³ located in the pentane liquid, water bath, housing near the trough model top and bottom, and outside the system (ambient). Thermocouples were connected to a control board which was connected to the computer via 9-pin cabling. LabVIEW 6.0 software was used to convert the electronic signals to temperature readings. The LabVIEW user interface is shown in Figure 4-3 and the logic diagram in Figure 4-4.

The positive and negative end of each thermocouple wire is attached to positive and negative terminals of a channel on the control board. The “Board Number” indicates the location that the control board is attached to the computer. Selection of “Low” and “High” channels indicate the range of channels that the thermocouple wires are attached to and informs the LabVIEW program the number of inputs to sample. Typically, the five thermocouples were attached to channels 0 through 4.

³ Teflon® Neoflon PFA wrapped, AWG-24 solid thermocouple wire from Omega Engineering Inc, accurate to $\pm 0.5^{\circ}\text{C}$

The metronome shown on the far right side of Figure 4-4 represents the loop delay sub virtual instrument (VI). When the millisecond timer is a multiple of the specified millisecond multiple, the loop executes by sampling each channel once. Here the millisecond multiple is 60,000 milliseconds (10 minutes), so LabView will sample the thermocouples when the timer reaches 60,000 ms, 120,000 ms, 180,000 ms, et cetera. Upon execution of the loop, run time and data from the input channels is sampled and placed into an array. The array contains single precision floating point integers, denoted by . The array is appended to a data file if this option is selection on the User Interface. Appending the data allows the current array to be added to the end of the previous array so that data is not over-written and in the case of a power-failure, all data prior to the failure will be saved. The data file will be given the name supplied by the user on the User Interface. The loop continues until the program is manually stopped at the end of the experiment.

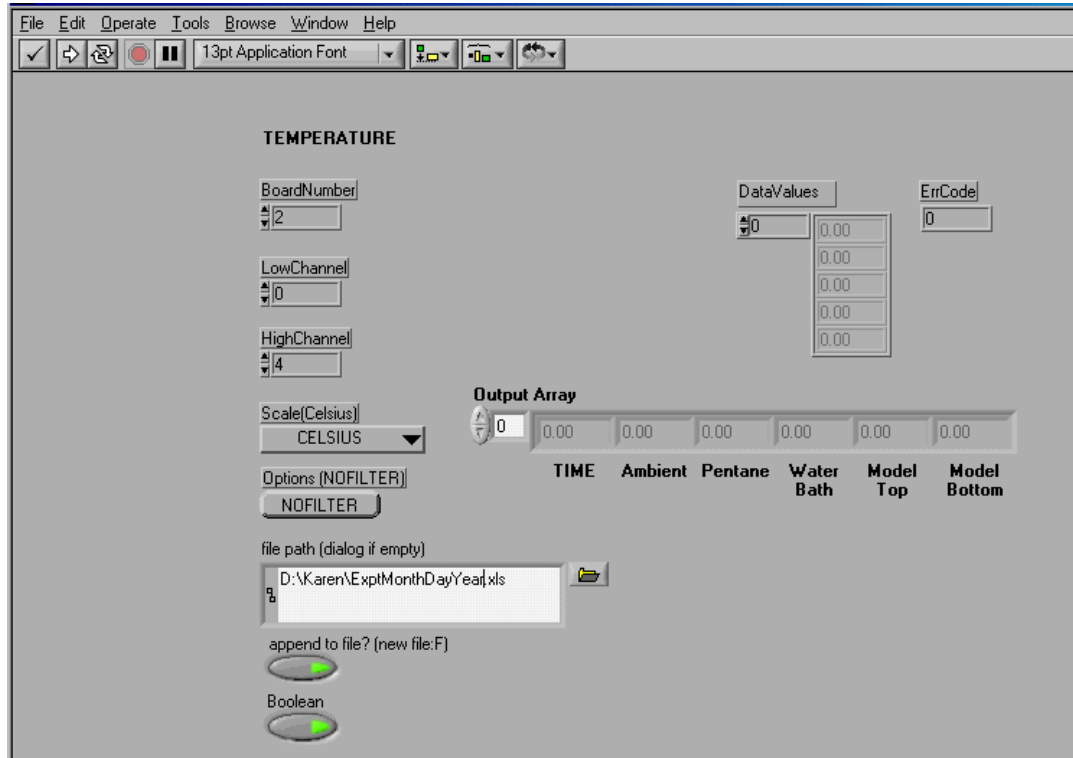


Figure 4-3 - LabView User Interface

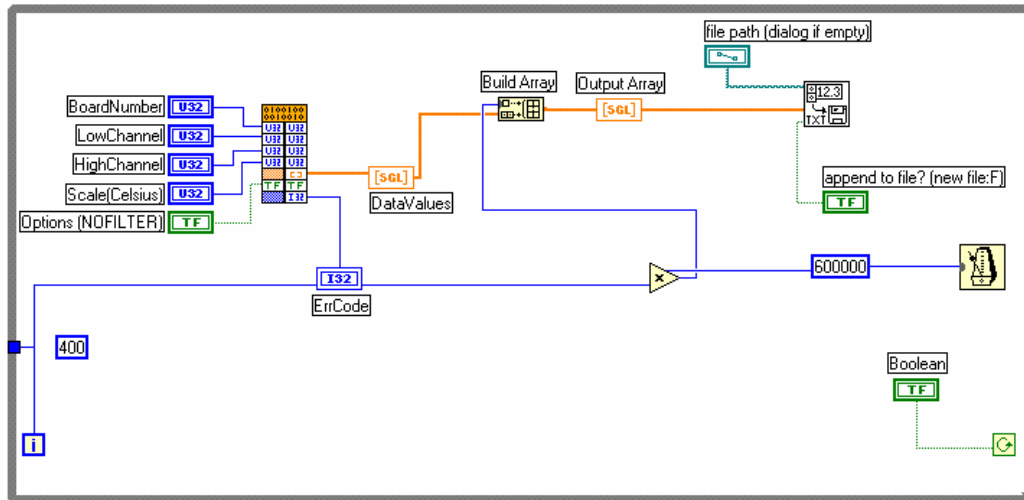


Figure 4-4 - LabView Logic Diagram

4.2.3 Vapour Extraction with 2-D Pore Network Micromodels

A two-dimensional pore network micromodel was used to examine the Vapex process on the pore scale. Micromodels consist of a pore network that has been etched onto glass, as shown in Figure 2-3.

The pore network pattern and characteristics shown in Figure 4-5 is referred to as OC-4. The model is 305 mm (149 pores) long by 91 mm (45 pores) wide⁴ and has a permeability of 90 Darcy. The model differed from previous experiments by James and Chatzis (2004) in that the glass along the right side of the model was removed, resulting in an exposed edge of pores running the length of the model. Prior to saturation the exposed edges of the micromodel were sealed using rubber gasket and clamps. A syringe filled with heated bitumen was used to inject bitumen into the micromodel through a port in the top part of the model. Injection continued until all of the pores were saturated with bitumen. After

⁴ For experiment #7, the model length was reduced to 230 mm (103 pores).

the model was saturated with bitumen, it was returned to room temperature and the rubber gasket was removed.

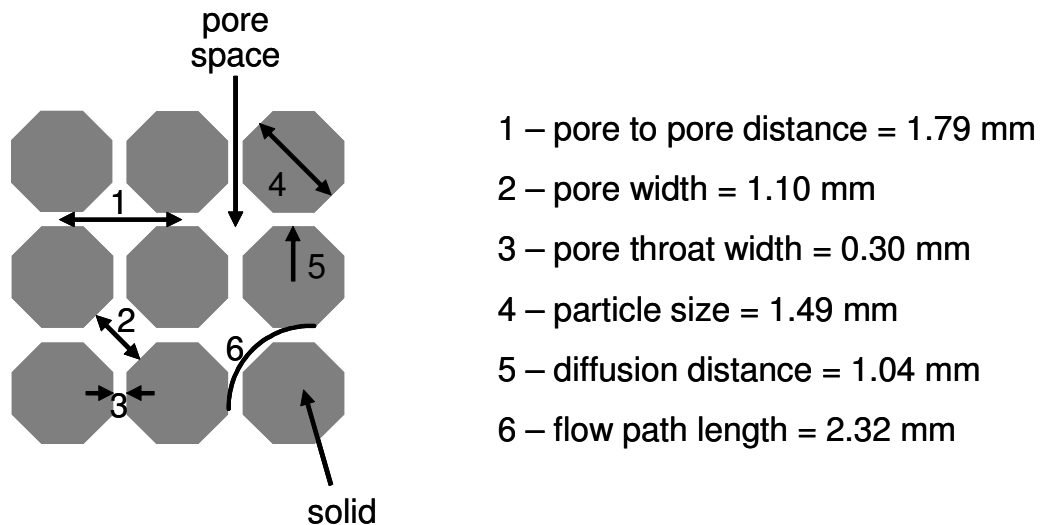


Figure 4-5 - Micromodel Characteristics of Model OC-4 (after James and Chatzis, 2004)

The Vapex experiment using bitumen in the micromodel was carried out in a similar manner as the trough model experiments. The micromodel was placed, upright, in the apparatus shown in Figure 4-2, however, due to the small volume of oil contained in the model, the live oil production was not collected. A data acquisition system recorded temperature gathered from five thermocouples (pentane, water bath, model top and model bottom and ambient) in ten-minute intervals and a manometer was used to monitor gauge pressure of the system.

The experiment began once the housing was sealed and pentane had been added to the system. Approximately every hour the position of the solvent-bitumen interface was recorded with a digital video camera. The interface is highly visible as the bitumen appears black, while the pores and throats that have been invaded appear white (due to the background colour). Figure 2-3 illustrates the typical interfaces between bitumen,

solvent and pore bodies as they appear during the experiment. A plot of the number of invaded pores versus time indicates the rate of interface advancement with time. Differentiating this curve with respect to time yields the velocity of interface advancement at any time.

4.2.4 Viscosity Variation with Temperature and Pentane Content

The relationship between the viscosity of bitumen-solvent solutions at different temperatures was studied as follows:

1. A solution was produced by mixing a small amount of bitumen with a large volume of liquid pentane. The solution was allowed to sit for approximately 15 hours, allowing the asphaltenes to precipitate out of solution. The solution was then filtered through a fine mesh screen and Whatman #4 Qualitative filter paper to remove the asphaltenes. Experiments were performed with the resulting filtrate.
2. Using a large waterbath, filtrate viscosity was measured for a given temperature as described in Section 4.3.1. After removing the solution, density and pentane content of the solution were determined using the methods outlined in Sections 4.3.2 and 4.3.3 .
3. The stock filtrate solution was then placed in an oven for two to ten minutes at 95°C to reduce the concentration of pentane in the solution by evaporation. This method was repeated approximately four times for each stock solution. A new stock solution was prepared to test the viscosity variation with solvent content at a different waterbath temperature.

4.3 Analysis of Experimental Data

4.3.1 Solution Viscosity

Solution viscosity at a given temperature was determined using a Cannon-Fenske routine viscometer, shown in Figure 4-6, held vertical in a retort stand. The solution to be tested was injected into tube 'L.' The viscometer was then allowed to sit at the test temperature for approximately 30 minutes before proceeding to acclimatize the solution and viscometer. After 30 minutes had elapsed, a syringe was used to push air into the viscometer forcing the oil into the bulb above line 'E'. The time (in seconds) taken for the sample liquid in the viscometer to flow freely between lines 'E' and 'F' was measured in three trials. The average time to drain a known volume and the viscometer constant, G , are used to calculate kinematic viscosity, ν :

$$\nu = Gt \quad (4-3)$$

Dynamic viscosity, μ , is calculated using equation (4-4):

$$\mu = \nu\rho \quad (4-4)$$

4.3.2 Live Oil Density

Live oil density was determined at room temperature. A 10 mL volumetric flask and an analytical balance were used to determine the mass of a sample of known volume. Density is simply the ratio of mass to volume.

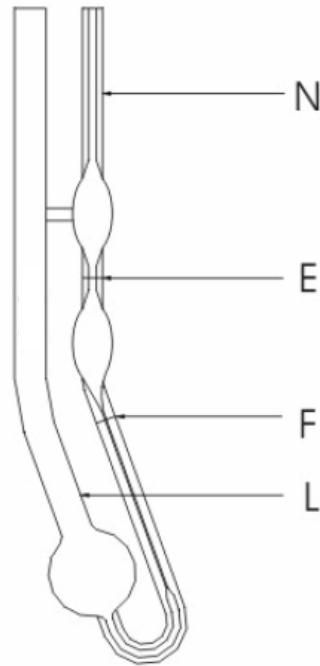


Figure 4-6 - Cannon-Fenske routine viscometer (Cannon Instruments, 2004).

4.3.3 Determination of Solvent Fraction in Filtrate/Live Oil

Approximately 2mL of oil (live oil for Vapex experiments or filtrate for Viscosity-Temperature-Solvent Fraction experiments) was placed in an aluminium dish of known mass. The mass of the dish plus the oil was determined using an analytical balance (accurate to $\pm 5 \times 10^{-6}$ g). The sample was then placed in a convection oven at 95°C for one hour. The addition of heat caused the dissolved solvent to be released from solution by evaporation. The change in mass caused by the release of solvent determines the solvent mass fraction, ω_s , given by Equation (4-5):

$$\omega_s = 1 - \frac{m_{Ho}}{m_o} \quad (4-5)$$

where m_{Ho} is the mass of bitumen after evaporation of solvent and m_o is the mass of live oil containing solvent.

4.3.4 Asphaltene Content

Asphaltene content was determined by mixing a known mass of bitumen, m_{o1} , with a large (known) mass of liquid pentane at ambient conditions. The asphaltenes were allowed to precipitate from solution for several hours. The solution was then filtered, and the particulate matter was dried in an oven. The mass of the dry particulate, m_{o2} , was compared to the mass of the original bitumen sample, m_{o1} , to determine the asphaltene mass percent.

$$wt\% \text{ Ashpaltenes} = \left(\frac{m_{o2}}{m_{o1}} \right) * 100\% \quad (4-6)$$

4.3.5 Residual Oil Saturation

Residual oil saturation, S_{or} , is the volume fraction of oil remaining in a reservoir after production ceases. Upon completion of a trough experiment, the model was removed from the housing and the wire mesh was removed, exposing the extracted bitumen. Sections of beads were carefully removed from the model and placed in a beaker of known mass. Figure 4-7 indicates the location of the sample sections for each experiment. The mass of the beaker, beads and residual oil was determined using an analytical balance. The oil and beads were then placed in a funnel lined with filter paper. Toluene was used to rinse the beaker and the beads until all of the oil was removed. The beads and filter paper were returned to the beaker and placed inside a convection oven at approximately 100°C until all of the toluene had evaporated.

Once dry, the filter paper was carefully removed and the mass of the beaker and beads determined. A graduated cylinder was used to determine the volume of beads. Residual saturation, S_{or} , measured as a percentage of initial oil in place (IOIP), was determined using Equation (4-7):

$$S_{or} (\% IOIP) = \left(\frac{m_o / \rho_o}{V_b \phi} \right) * 100 \quad (4-7)$$

where m_o is the mass of residual oil, ρ_o is the density of bitumen, V_b is bulk volume of solids and ϕ is porosity.

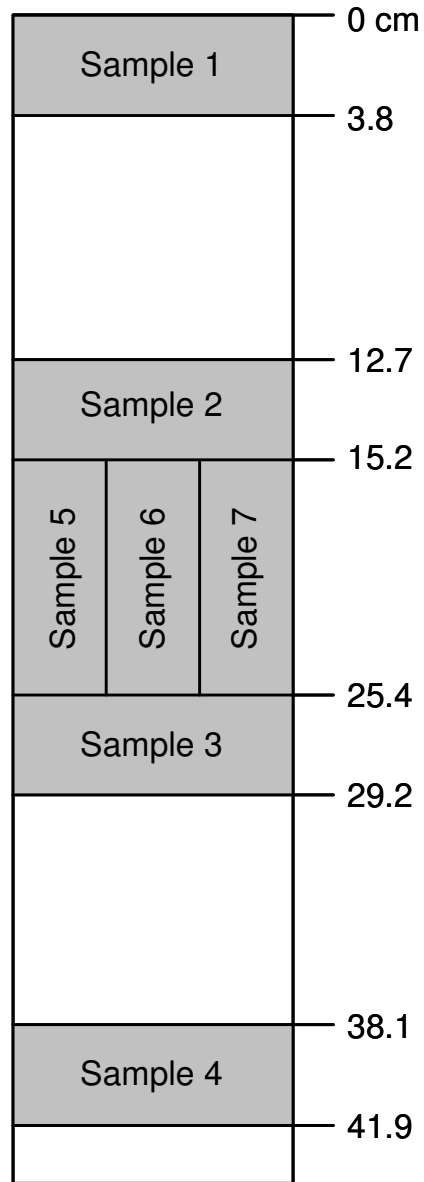


Figure 4-7 - Residual Oil Sample Locations

5.0 Results and Discussion

5.1 *Movement of an Interface over a Curved Surface*

The curved interface model was packed with a mixture of glass beads and corn syrup, and water entered the model at an average rate of 0.65 ml/s. As water came in contact with the corn syrup in the porous media it would dissolve in the water and be carried by the flowing water. Photographs were taken at one location throughout the duration of the experiment. At this location, the distance from the upper edge of the model to the interface was measured, perpendicular to the curved edge, as shown in Figure 5-1. The produced solution was collected for approximately 30 minutes, at which time the volume was measured. All samples were analyzed with a calibrated refractometer (Appendix A, Figure A1) to determine the mass fraction of corn syrup in the produced solutions.

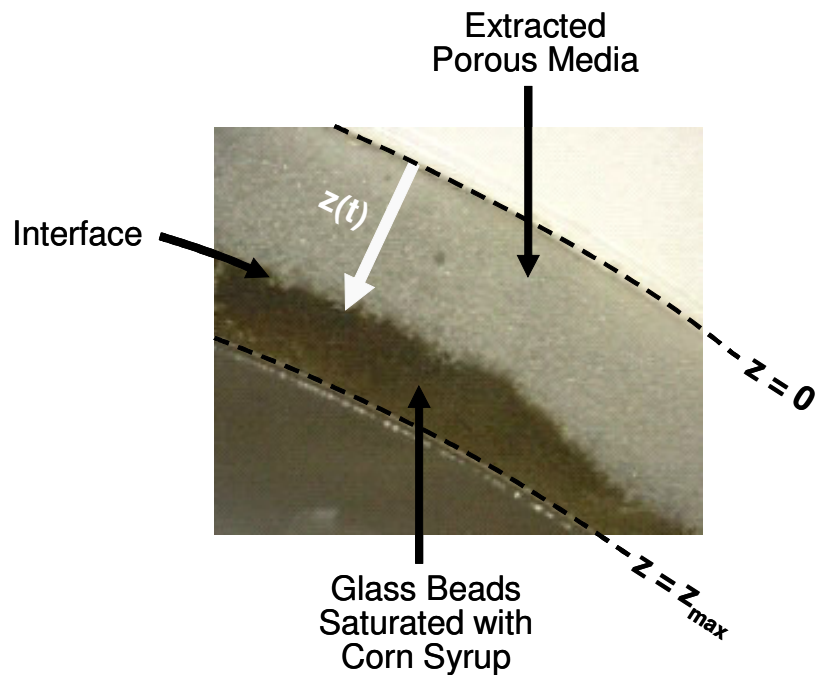


Figure 5-1 - Measurement of Interface Advancement Perpendicular to Fluid Flow

Figure 5-2 shows the water-syrup interface advancement with time at the location where measurements were made. These results show the interface position relative to the surface of the packing increases linearly with time and the velocity of interface advance was 0.0094 cm/min (0.564 cm/h). Thus interface advancement is linear with time for either a curved surface (examined here) or a flat surface as in Vapex experiments by Ramakrishnan (2003), Oduntan (2001), and James and Chatzis (2005).

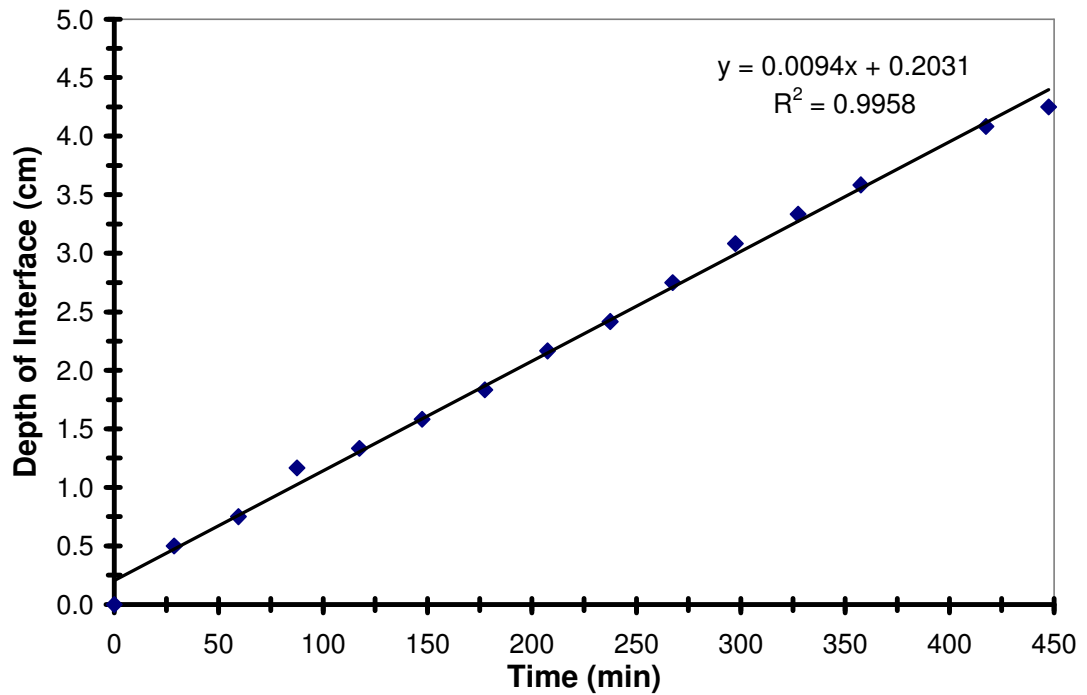


Figure 5-2 - Corn Syrup-Air Interface Position over Time

The mass fraction of corn syrup in produced samples ranged from 0.17 to 0.28 with an average value to 0.219. Knowing the rate of interface advancement, dz/dt and the concentration of corn syrup in the produced fluid ($C/C_0 \approx 0.2$), Equation (3-27) can be used to determine the steady state diffusion coefficient. For the corn syrup experiment at ambient conditions, the effective diffusion coefficient is $1.4 \times 10^{-5} \text{ cm}^2/\text{s}$ (shown in Appendix A, Figure A2). This corresponds to a molecular diffusivity of $5.1 \times 10^{-5} \text{ cm}^2/\text{s}$ for a porosity of 40% and tortuosity factor of 1.5.

5.2 Viscosity of Heavy Oil with Temperature and Solvent Fraction

Experiments were carried out at 22°C, 24°C, 27°C, 29°C and 32°C with pentane fractions in heavy oil ranging from 0-100%.

5.2.1 Effect of Asphaltenes on Stock Heavy Oil

The addition of pentane to bitumen causes a change in equilibrium conditions resulting in the precipitation of asphaltenes from solution. When dried, the asphaltenes appear as a shiny brittle black solid, shown in Figure 5-3.

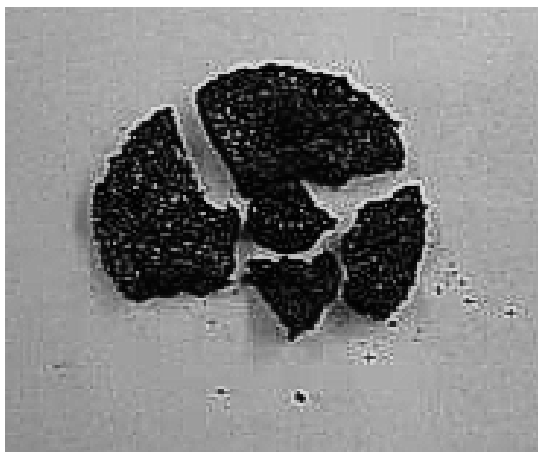


Figure 5-3 - Sample of Precipitated Asphaltenes

Asphaltenes content was determined by combining stock heavy oil with a large volume of pentane at room temperature (approximately ten times by volume). The solution was stirred and allowed to precipitate over night before being filtered with filter paper. The asphaltenes that remained in the flask and on the filter paper were dried at 95°C until no liquid remained.

The stock bitumen was found to contain approximately 18% asphaltenes (by mass) with a dynamic viscosity of 23,176 mPa•s at 22°C. After the asphaltenes were removed from solution, the bitumen was found to have a viscosity of 9,380 mPa•s at 22°C, a 60% reduction in viscosity. This confirms that asphaltene removal alone has a significant impact on bitumen viscosity.

5.2.2 Effects of Temperature and Pentane Concentration on Viscosity of Bitumen

Figure 5-4 shows the effect of increasing pentane concentration on viscosity of de-asphalted bitumen for the five temperatures tested. For a given temperature, increasing pentane concentration from zero to approximately 40 wt%, results in a sharp, logarithmic decrease in solution viscosity. However, increasing pentane concentration beyond 40% has a much less dramatic effect, which can be approximated by a linear relationship.

Similarly, for pentane concentrations less than 40 wt%, the viscosity of the solution is a strong function of temperature. For temperatures between 22°C and 29°C and solutions containing over 40% pentane, the effect of temperature on viscosity is not very strong.

Two trials at 22°C were performed to verify the repeatability of the data. Figure 5-5 shows viscosity data for both trials. The trend can be described by the following function:

$$\mu (cP) = 0.37\omega_s^{-2.69} \quad (5-1)$$

Figure 5-6 compares the effect of increasing solvent mass fraction on solution viscosity with pentane, butane (Jin, 1999) and propane (Ramakrishnan, 2003). The trend observed for pentane-bitumen solutions agrees well with that for butane and propane though different types of bitumen were used.

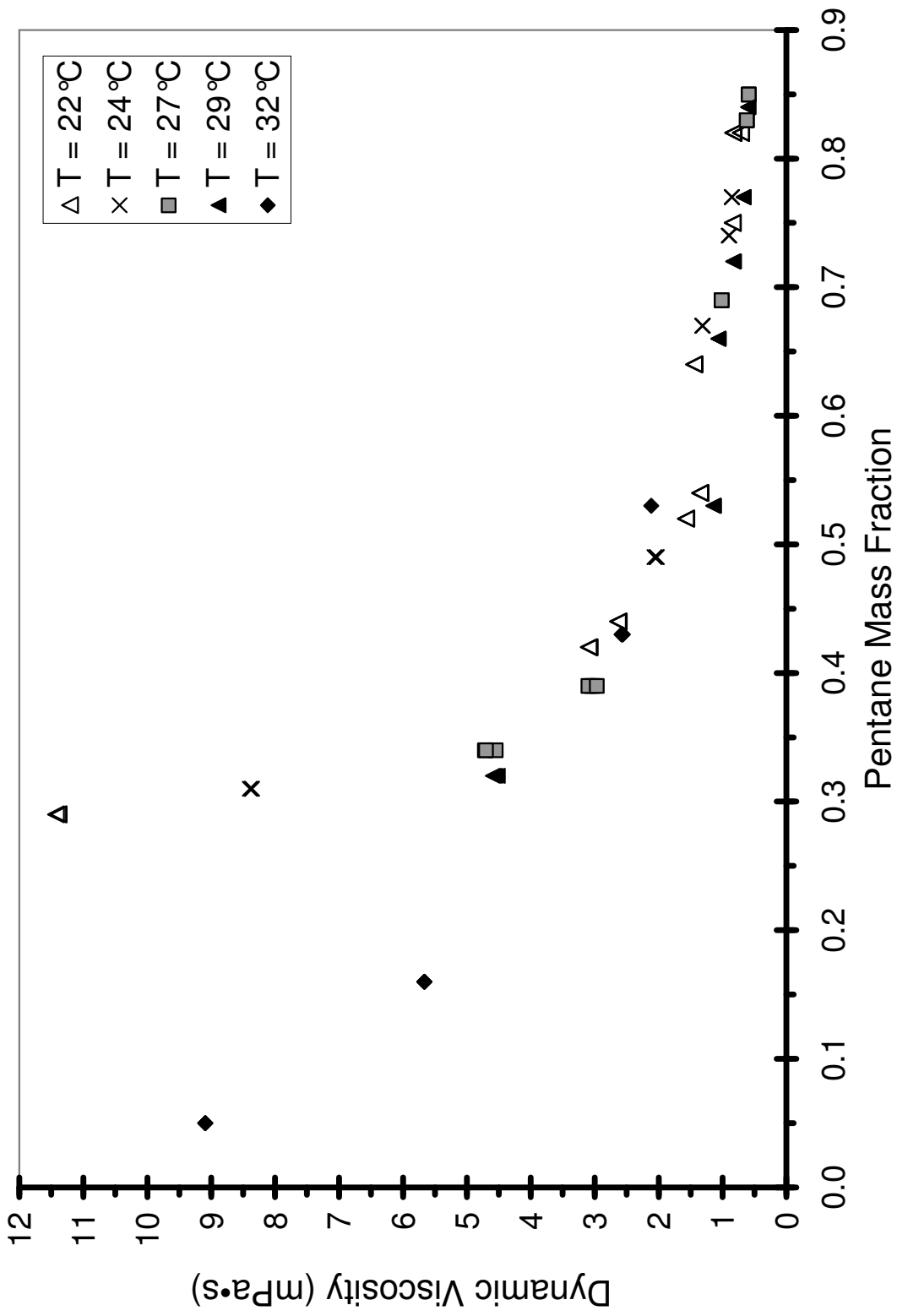


Figure 5-4 - Effect of Increasing Pentane Fraction on Bitumen Solution Viscosity

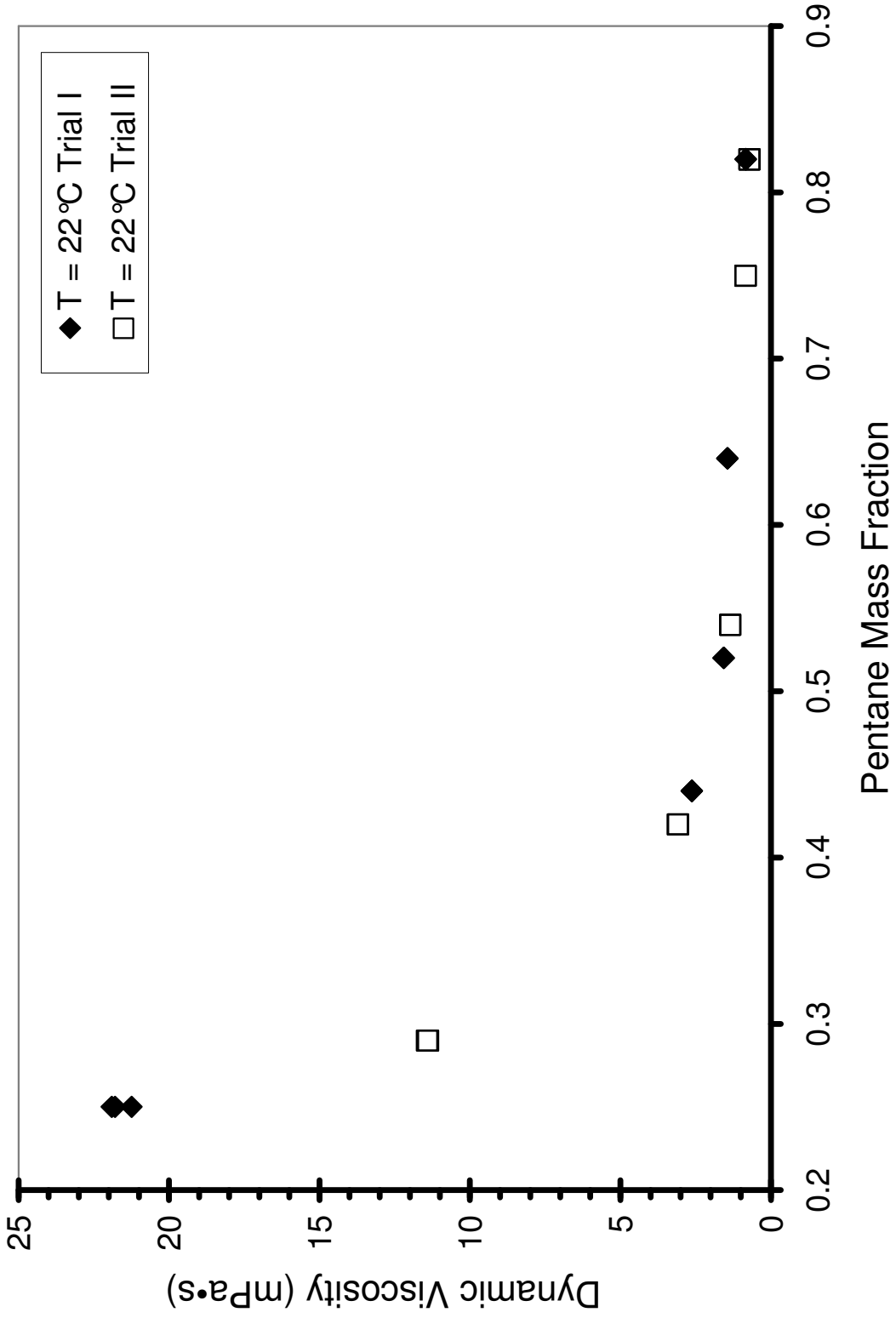


Figure 5-5 - Relationship Between Viscosity of De-asphalted Oil and Pentane Mass Fraction at T = 22°C

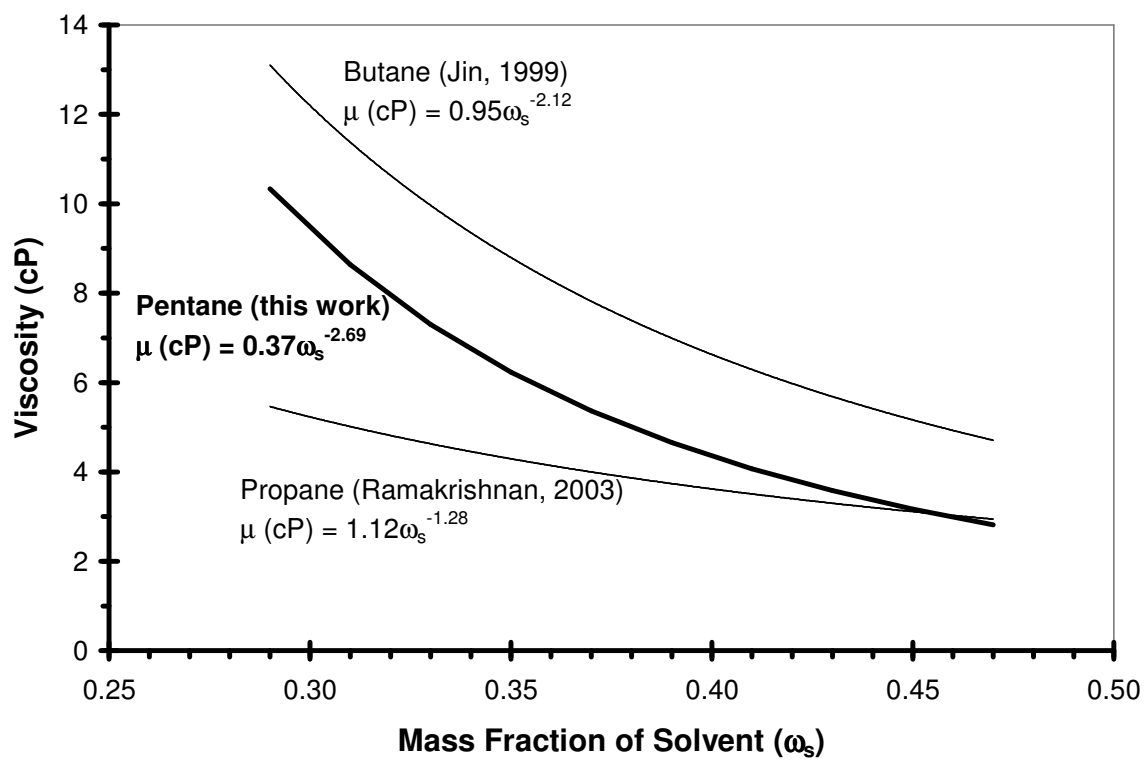


Figure 5-6 - Effect of Solvent Mass Fraction on Bitumen Viscosity by Solvent Type

5.3 Summary of Vapour Extraction Experiments

Seven experiments (including two micromodel experiments) were conducted examining the effect of increased pentane concentration on the production rate and rate of interface advancement on the Vapex process. The experimental conditions are outlined in Table 5-I. Plots of experimental temperatures are given in Appendix C, Figure C30 through C36.

Table 5-I - Summary of Experimental Parameters

Exp't #	Model Type	Average Experiment Temperature (°C)				
		Ambient	Pentane	Water Bath	Model Top	Model Bottom
1	trough	24.58	31.45	35.50	24.53	26.77
2	trough	24.64	29.35	31.58	24.92	26.16
3	trough	25.07	25.78	26.29	25.42	26.14
4	trough	23.02	24.41	25.05	23.78	24.46
5	trough	22.88	28.12	31.43	22.90	24.32
6*	trough	22.82	N/A	N/A	N/A	N/A
7	micro model	23.55	29.79	32.59	23.68	25.81
8	micro model	22.83	29.31	32.56	22.59	25.41

* Experiment was not run to completion.

For all experiments there was a temperature gradient between the top and bottom of the model due to the liquid pentane located below the model having a temperature higher than ambient. In the trough models, the gradient ranged from 0.7°C (Experiment #3 and #4) to 2.2°C (Experiment #1). The temperature gradient in the micromodels varied from 2.1°C (Experiment #7) to 2.8°C (Experiment #8).

5.4 Pore Scale Phenomena

Experiments 7 and 8 (as shown in Table 5-I) were performed in a micromodel in place of the trough models used for the first six experiments. The purpose for conducting these experiments was to examine pore-scale events in the Vapex process. The use of a micromodel demonstrates the movement of oil from pore to pore as the interface advances.

During work hours, the interface position was recorded approximately once per hour, with the use of a digital camera, for a total run time of 97 hours for Experiment #7. The water bath was maintained at an average temperature of 32.59°C, while the average pentane temperature was 29.79°C for this experiment.

After enlarging the photos, the number of invaded pores in each row was counted and recorded for each sample time as described in Section 4.2.3. The model was divided into sections each containing ten rows of pore bodies, and the measurements focus on the average number of invaded pores in rows 1 to 10 (“Row 1”), 41 to 50 (“Row 5”), 91 to 100 (“Row 10”) and 121 to 130 (“Row 13”). Throughout the life of the experiment Row 14 did not drain (with the exception of four to six pores adjacent to the exposed edge), indicating that this is the capillary height for bitumen, measured to be approximately 29 mm (16 pores) from the bottom of the first row of pores.

5.4.1 Movement of Live Oil in Micromodels

Figure 5-7 shows selected frames from the video to illustrate several pore scale events such as trapping and the movement of live oil films. Approximately 50 minutes of video was captured during experiment #8 showing Row 8, Columns 2 (right of line) and 3 (left of line). Examination of the video shows:

1. ***Snap Off***- Figure 5-7 (a)

Snap off is a capillary phenomena that causes one or more pores to remain filled with oil while the surrounding pores drain. Oil has become trapped inside the pore body located two pores from the right hand side and two pores from the bottom edge. This phenomenon can occur if the pore throats surrounding the trapped oil are smaller than others around it and there is not sufficient pressure to overcome the capillary pressure inside the pore.

2. ***Oil Film Movement*** - Figure 5-7 (a-e)

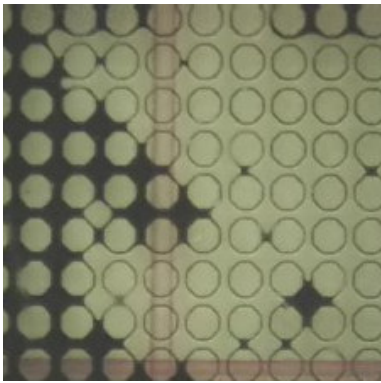
Oil films drain by flowing along the path of least resistance, along the interface. Figure 5-7 (a-e) show oil draining from above, moving both downwards and to the left to meet the live oil film. The film then continues to drain in a downward direction. The net movement of oil in this section is downwards due to gravity.

3. ***Trapping*** - Figure 5-7 (e-i)

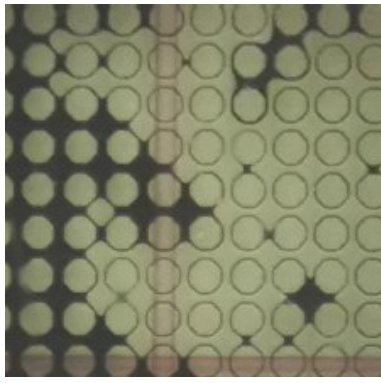
Trapping occurs when an oil film descends into an area that was previously cleared of oil. Oil draining from above results in trapping of solvent vapour in the pore body located three pores to the left of the line and four pores from the top. Solvent trapped will continue to diffuse into the oil surrounding it.

4. ***Oil Film Drainage*** - Figure 5-7 (i-o)

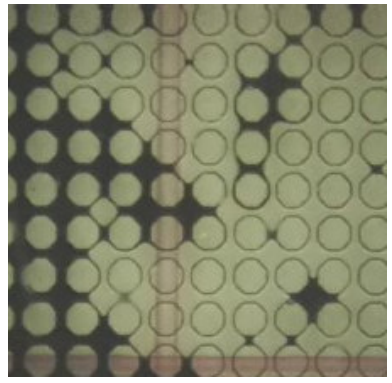
Solvent vapour is beginning to invade the pore located three pores to the left of the line and one pore from the top. Once this pore is invaded, solvent continues to invade pores downward as live oil drains along the interface.



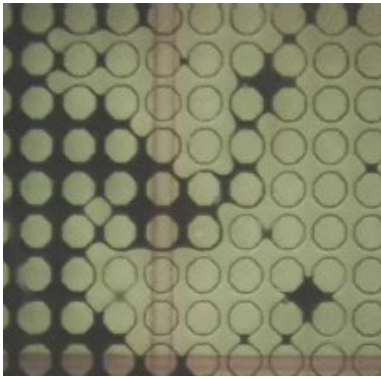
(a)



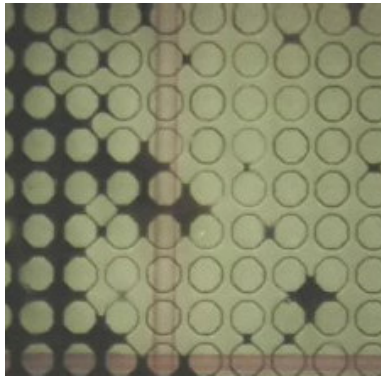
(b)



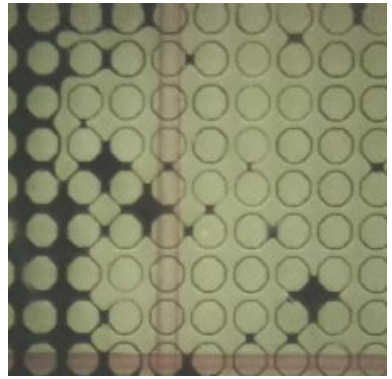
(c)



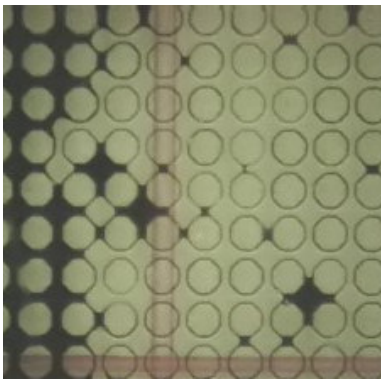
(d)



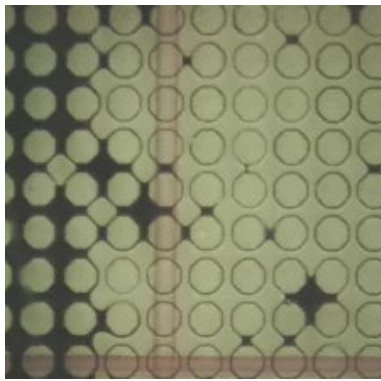
(e)



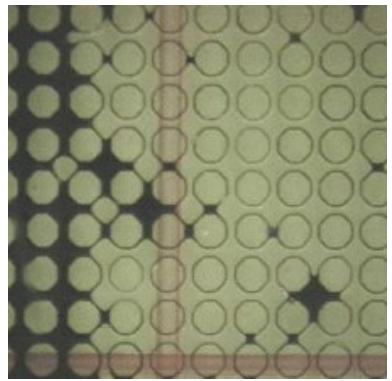
(f)



(g)

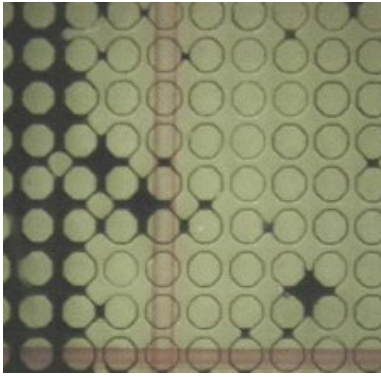


(h)

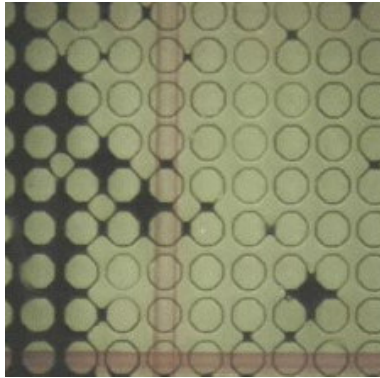


(i)

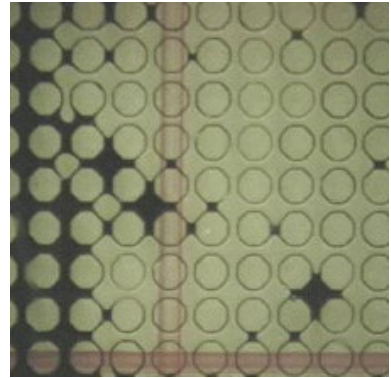
Figure 5-7 - Pore Scale Events



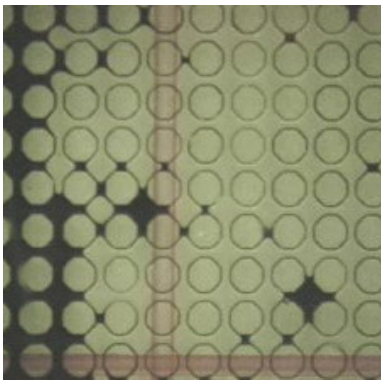
(j)



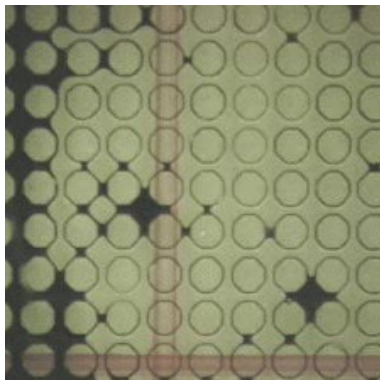
(k)



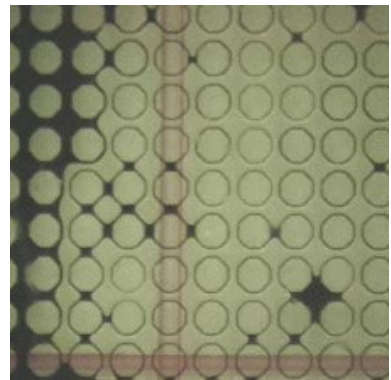
(l)



(m)



(n)



(o)

Figure 5-7 - Pore Scale Events (continued)

5.5 *Interface Advancement*

Interface position was recorded manually for both the trough models and micromodels. In the trough models, as live oil drained from the porous media, the resulting area was noticeably lighter in colour than the remaining bitumen. In the micromodels, the bitumen filled pores were black while the drained pores were nearly colourless.

In the trough model experiments, the shape of the interface was a curve, as indicated in Figure 5-8. This figure shows the interface shape for Experiment #5 at selected time steps, illustrating that the interface advances in two directions: horizontally (away from the mesh screen) and vertically (downwards from the top of the model). For experiment #5 (shown in Figure 5-8) the back of the model is reached while the average interface position (above the capillary height⁵) is 1 cm from the edge exposed to solvent.

Figure 5-8 illustrates that in the middle section of the trough, the interface is nearly vertical. Deviations from vertical are due to heterogeneities in packing which reduce or increase the local porosity compared to the average. An area of reduced porosity will slow interface advancement, while an area of increased porosity will accelerate interface advancement. In Figure 5-8 at t=1440 minutes an area of reduced porosity exists 17-18 cm from the top of the model. At t=4590 minutes, there is increased porosity at approximately 34-38 cm from the top of the model as the interface has advanced significantly farther at this location than in the region directly above. Unless the region of lower porosity exists as a horizontal band, spanning the model width, once the interface has passed the region of lower porosity, the interface shape is able to return to vertical.

As a comparison, Figure 5-9 illustrates the Vapex interface in a micromodel as photographed during Experiment #7 at a run time of 1860 minutes.

⁵ Capillary height for the trough models is approximately 3 cm from the bottom of the model.

A normalized plot of Figure 5-8 is shown as Figure 5-10. Here the vertical distance indicates the distance from the top of the interface relative to the maximum vertical height of undrained bitumen above the capillary height. Relative horizontal distance is a measure of the interface position relative to the model width. A similar plot for micromodel Experiment #7 is shown as Figure 5-11, however the interface position is measured by the number of invaded pores relative to the maximum number of drained vertical pores (above the capillary height) and the number of pores the model is wide.

Comparing Figure 5-10 to Figure 5-11, in the trough model, the interface begins to recede downwards quickly compared to that in the micromodel. Table 5-II compares the amount of time required for the interface to reach the upper left corner of the model, t_b . For the trough experiments, the time required ranged from 6 to 16% of the total time required to drain the model above the capillary height. In comparison, the interface in the micromodel reached the upper left corner of the model after approximately 73% of the total experiment time. Dividing the average interface position at t_b , $z_{i,ave}$ by the model width, W_{model} comparisons can be made between the micromodel and trough model experiments by examining the normalized width of the model that has been drained. When the upper left corner is reached, the average interface position has advanced 10 to 28% of the model width for the trough models, but 86.2 and 87.5% for the micromodels.

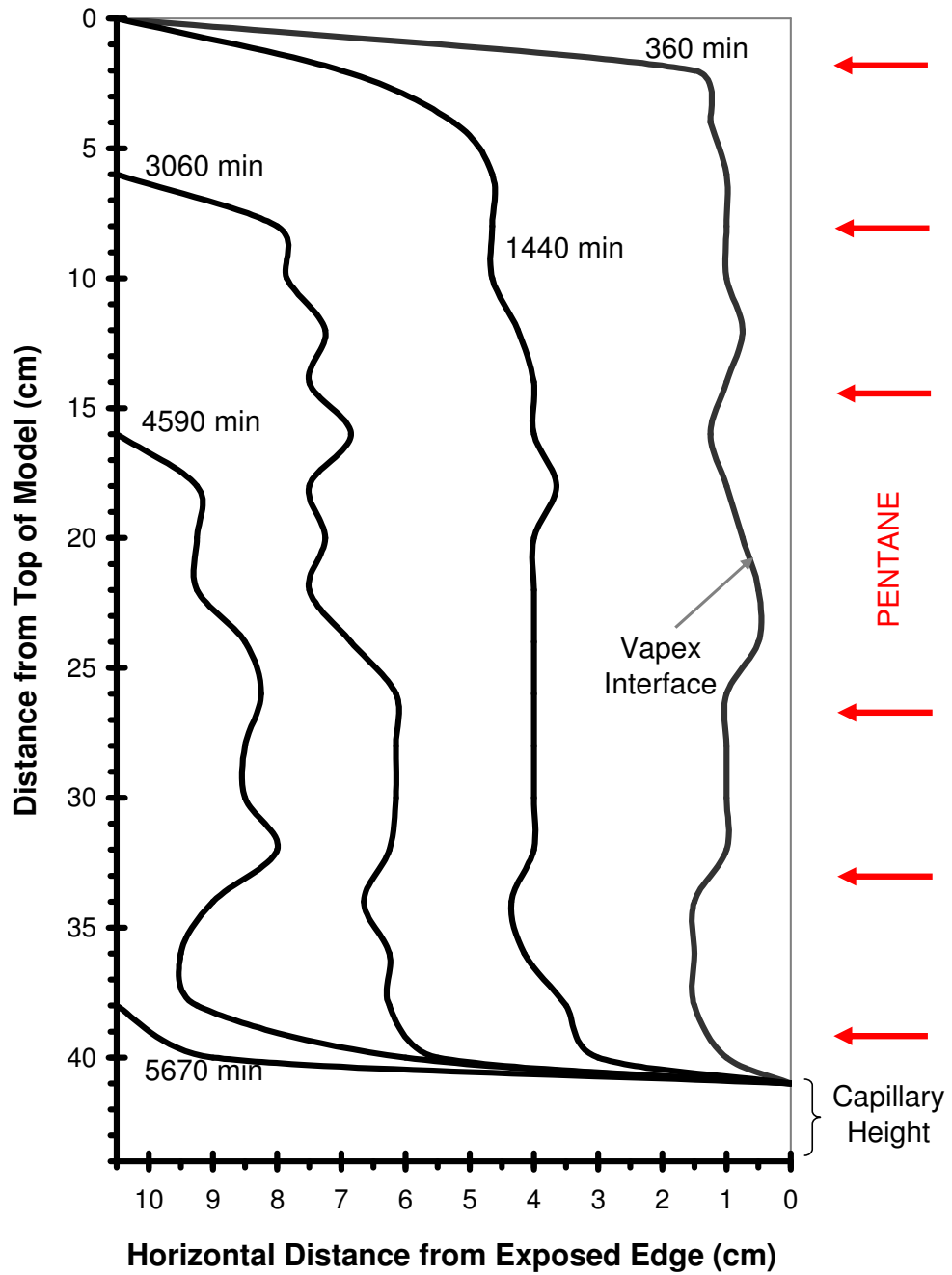


Figure 5-8 - Advancement of Interface in a Trough Model at Selected Times
(Experiment #5)

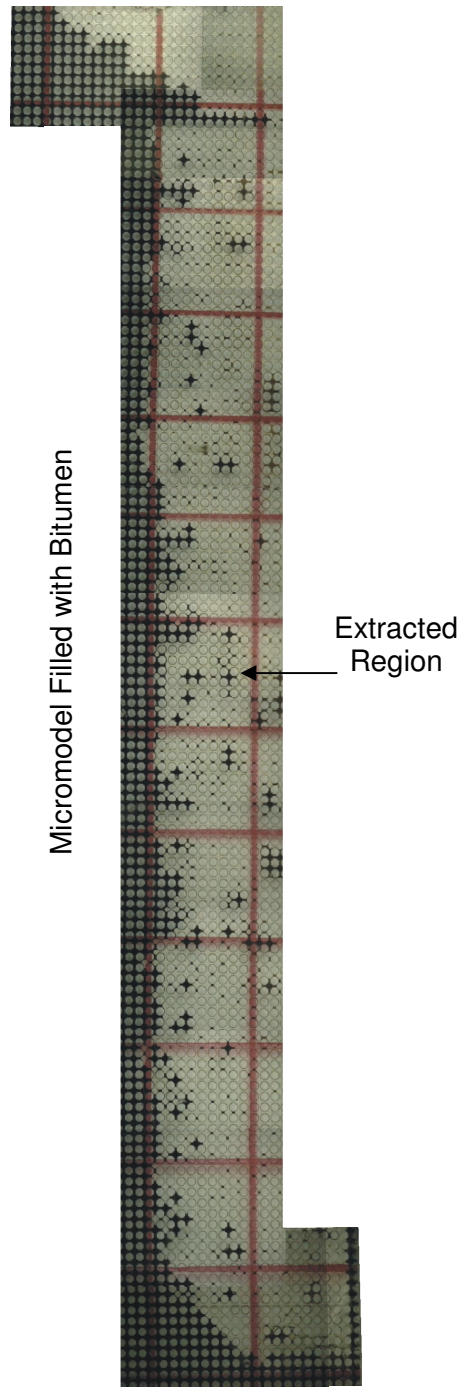


Figure 5-9 – Photo showing the Bitumen/Vapour Capillary Interface in Glass Micromodel (Experiment #7, $t = 1860$ min)

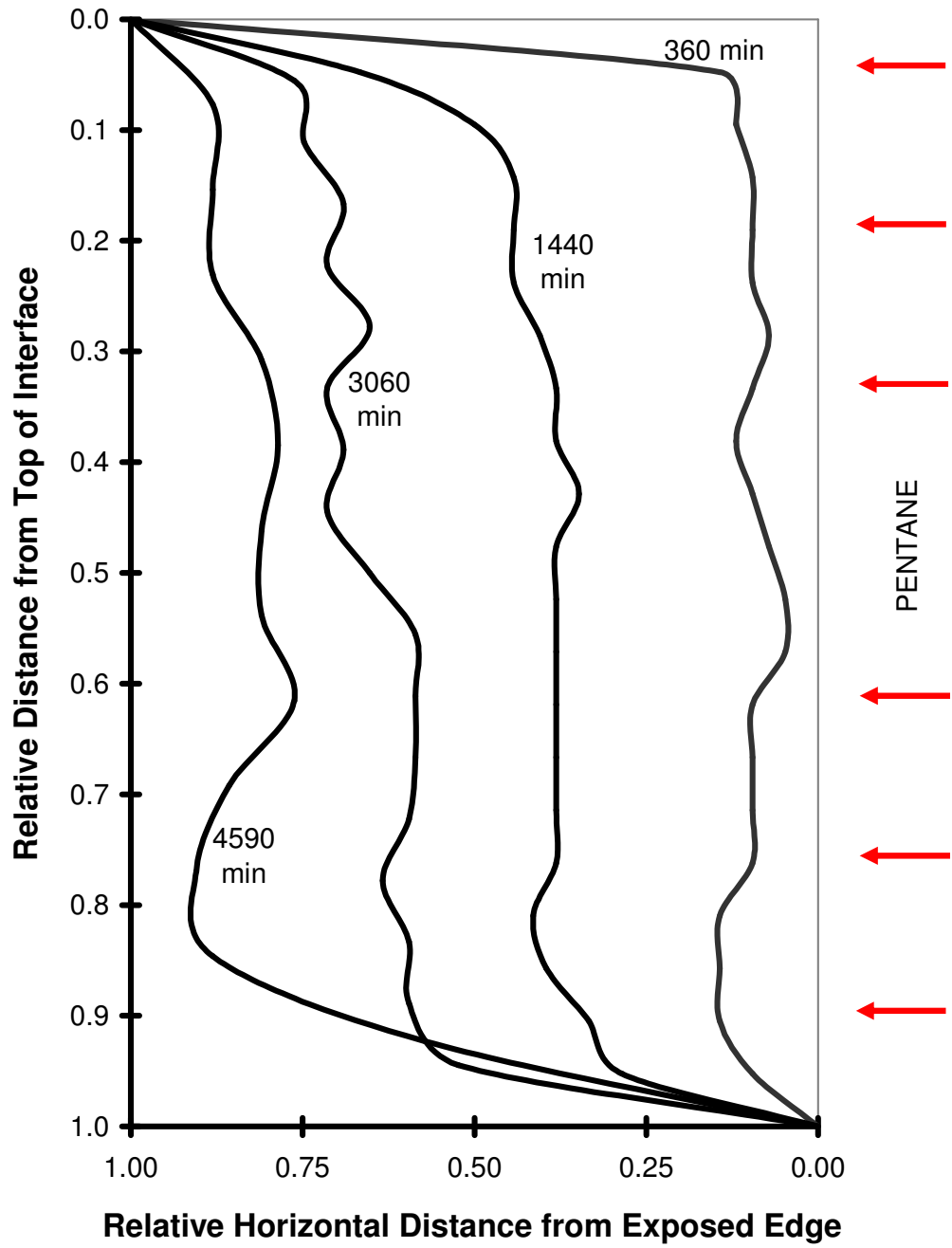


Figure 5-10 - Normalized Advancement of Interface in a Trough Model at Selected Times (Experiment #5)

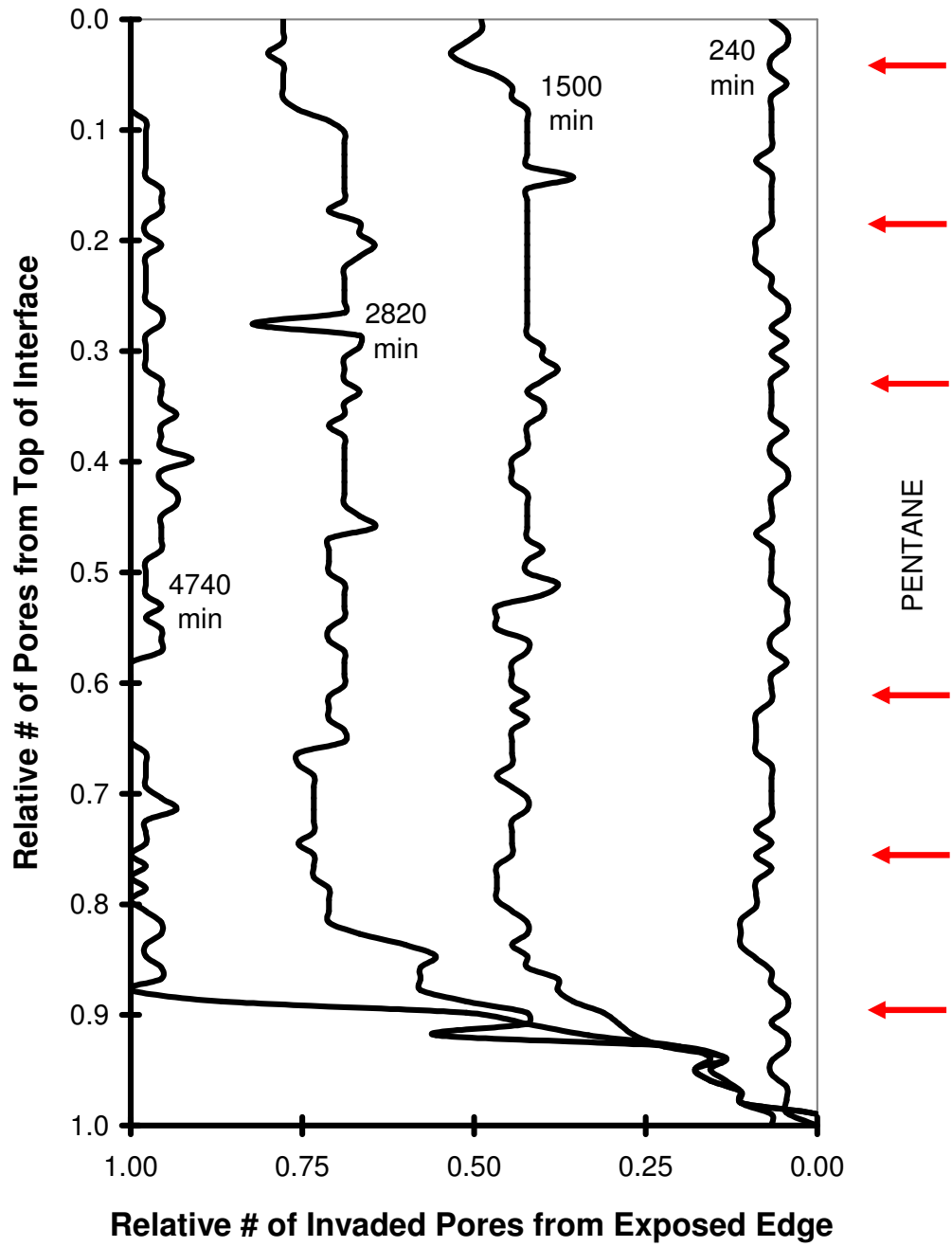


Figure 5-11 - Normalized Advancement of Interface in a Micromodel at Selected Times (Experiment #8)

Table 5-II - Time Required for Interface to Reach the Back of the Model

Exp't #	Model Type	Pentane Temp (°C)	t_b (min)	t_{total} (min)	t_b	$z_{i,ave}(t_b)$
					t_{total} (%)	W_{model} (%)
1	trough	31.45	486	4714	10.2	15.2
2	trough	29.35	785	5025	15.6	28.2
3	trough	25.78	825	5800	14.2	21.7
4	trough	24.41	605	6465	9.4	14.1
5	trough	28.12	360	5755	6.3	10.0
7	micro-model	29.79	4260	5820	73.2	86.2
8	micro-model	29.31	5785	5185	81.9	87.5

*above the capillary height

The difference in interface shape and advancement between the trough models and micromodels is most likely due to the packing of the trough models. Along the solid sides of the trough model, the porosity of the glass bead packing is much higher than that in the bulk packing, as illustrated in Figure 5-12. The higher porosity provides a large flow path for vapour and live oil which results in accelerated advancement of the interface in these regions.

In addition to larger pathways for solvent transport, as oil drains from the model, trapped air is liberated, causing beads and remaining oil to compact downwards providing an open space for gas at the top of the trough. This area provides a larger pathway for the vapour to travel, and increases the contact area for mass transfer along the top of the porous medium. Unlike the trough models, the pore network in the micromodel is fixed, as is the porosity throughout the experiment. In a reservoir, the mass of earth on top of the pay zone will likely prevent shifting of the porous media, thus behaving in a manner similar to the micromodel.

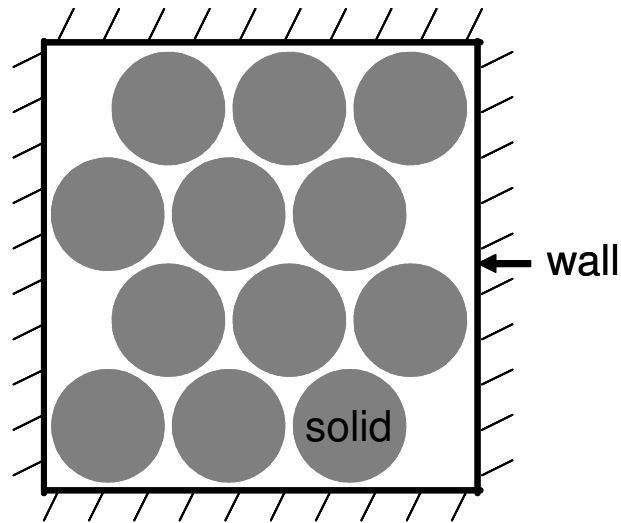


Figure 5-12 - Effects of Lower Porosity on Live Oil Drainage in Trough Models

This effect was examined by stopping Experiment #6 after 420 minutes. The final interface position was recorded and the model removed from the housing. The wire mesh was removed, allowing access to the glass beads. The beads in the solvent swept areas were carefully removed until the bitumen saturated portion was reached. It was noted that the swept area along the sides of the model was farther advanced than the swept area in the centre of the trough. Results are shown in Figure 5-13. Figure 5-14 illustrates the difference between the visual interface location at the model edges and the interface location at the centre of the trough model. Since it is not possible to observe the actual interface position in the model during an experiment, all calculations are based on the visual location of the interface, $z_i(t)$ though this value will overestimate the average interface position along the model width.

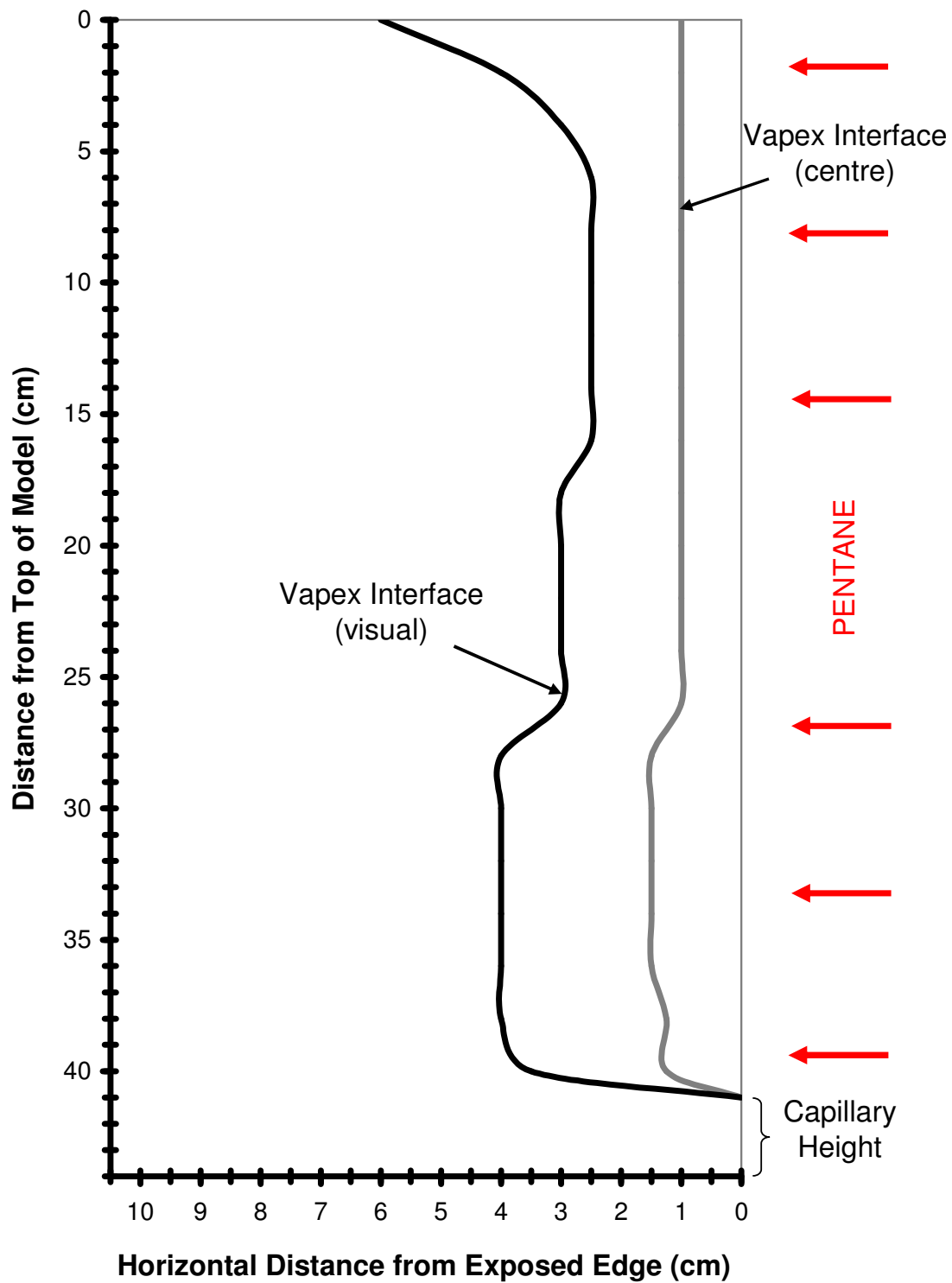


Figure 5-13 - Vapex Interface Visible from Edge and in Model Centre
(Experiment #6)

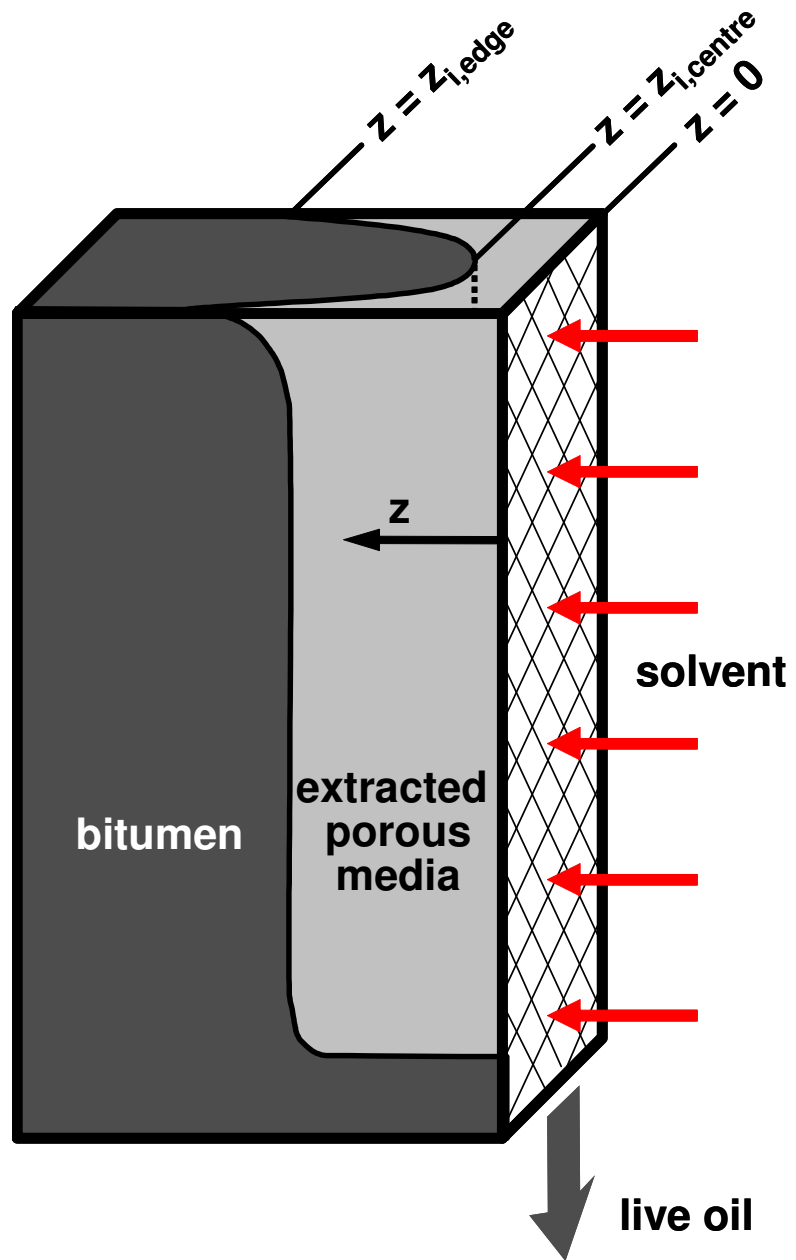


Figure 5-14 - Location of Interface Visible from Outside Model

A plot of average number of invaded pores versus time for Row 1, 5, 10 and 13, Experiment #7 is shown in Appendix C, Figure C38. The number of invaded pores increases with time until the edge of the model is reached (45 pores). As this relationship is non-linear, it is evident that the rate of interface advancement is not constant and in fact decreases with time. In the curved-interface experiment in Section 5.1 and experiments with pure solvents [Ramakrishnan (2003), Oduntan (2001)] the rate of interface advancement was linear with time.

The average number of invaded pores versus the square root of time for Row 1, 5, 10 and 13 is shown in Figure 5-15. This relationship is positive and shows a high degree of linearity. It can also be observed that there is a time delay from experiment start (sealing of the housing, $t=0$) to the start of interface advancement. As the interface moves downwards, pores are exposed to pentane vapour over a greater surface area, increasing the rate of mass transfer, thus Row 1 also shows the highest rate of interface advancement. Row 5 and Row 10 show virtually the same trend, indicating that the interface moves at approximately the same speed below the vertical bitumen-solvent interface until Row 13. The interfaces for Row 13, located directly above the capillary height, advanced at a significantly slower rate than the top row (Row 1) and middle rows (Rows 2-12).

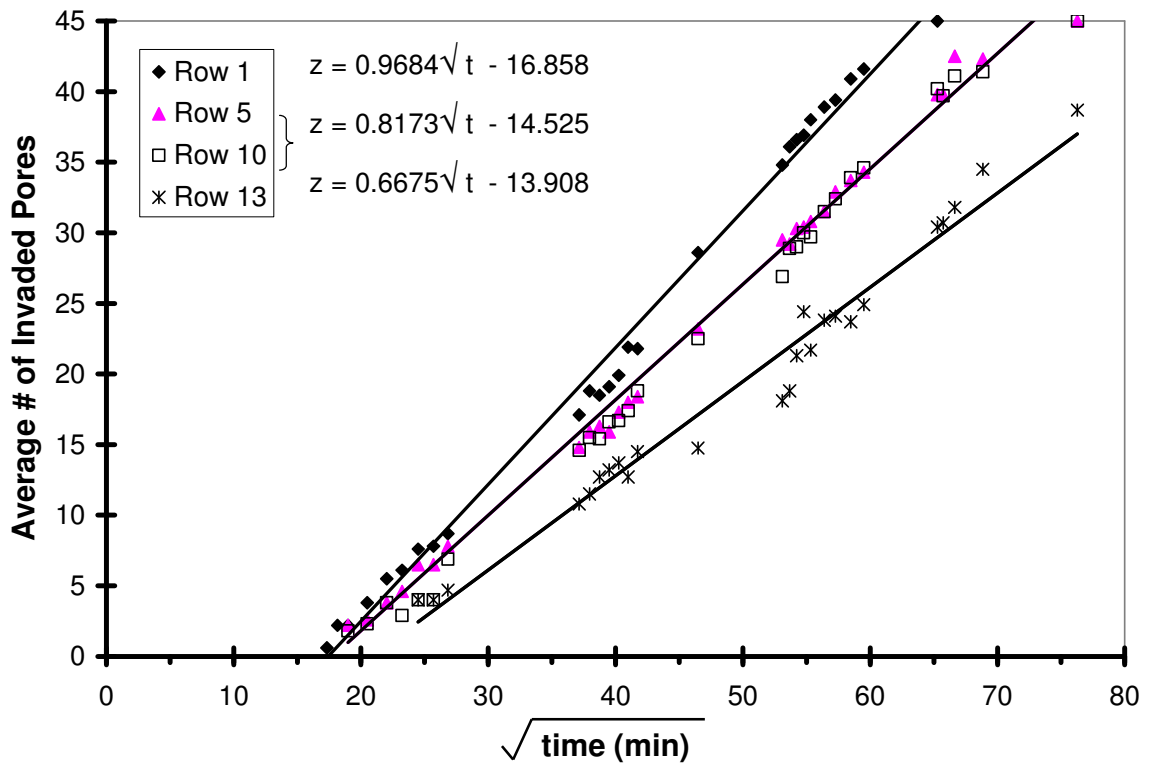


Figure 5-15 - Interface Advancement as a Function of Square Root Time
(Experiment #7)

Normalizing the data shown in Figure 5-15 and shifting the time to correspond to the beginning of interface advancement in each row produces Figure 5-16.

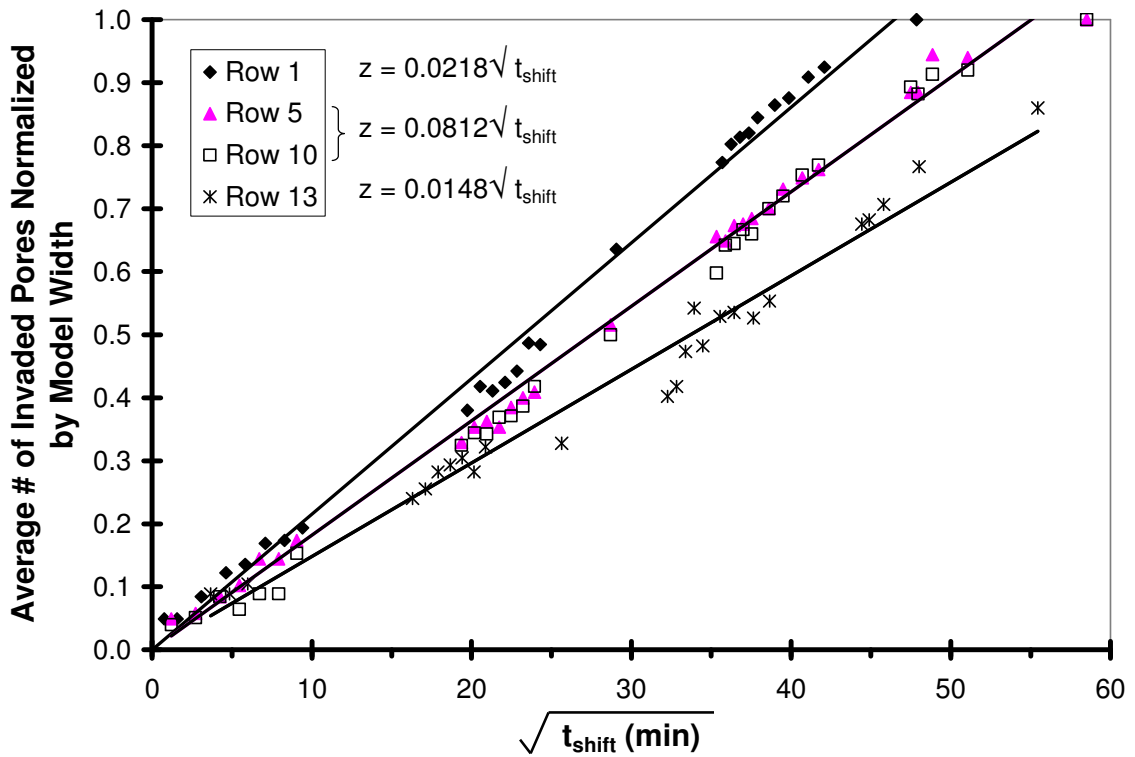


Figure 5-16 – Normalized Interface Advancement as a Function of Square Root Time (Experiment #7)

Figure 5-17 is a plot of interface position versus the square root of time for positions 20 cm and 40 cm below the top of the model in trough model Experiment #5. As in the micromodel, the interface advances much faster at the top than at the bottom. There is a delay in interface advancement from the start of experimental run time. The exact delay is difficult to observe in the physical models as the first 0.5 cm of porous media is blocked by the wire mesh. If time is shifted so that $t=0$ reflects the start of interface advancement for a given location, Figure 5-17 transforms to Figure 5-18.

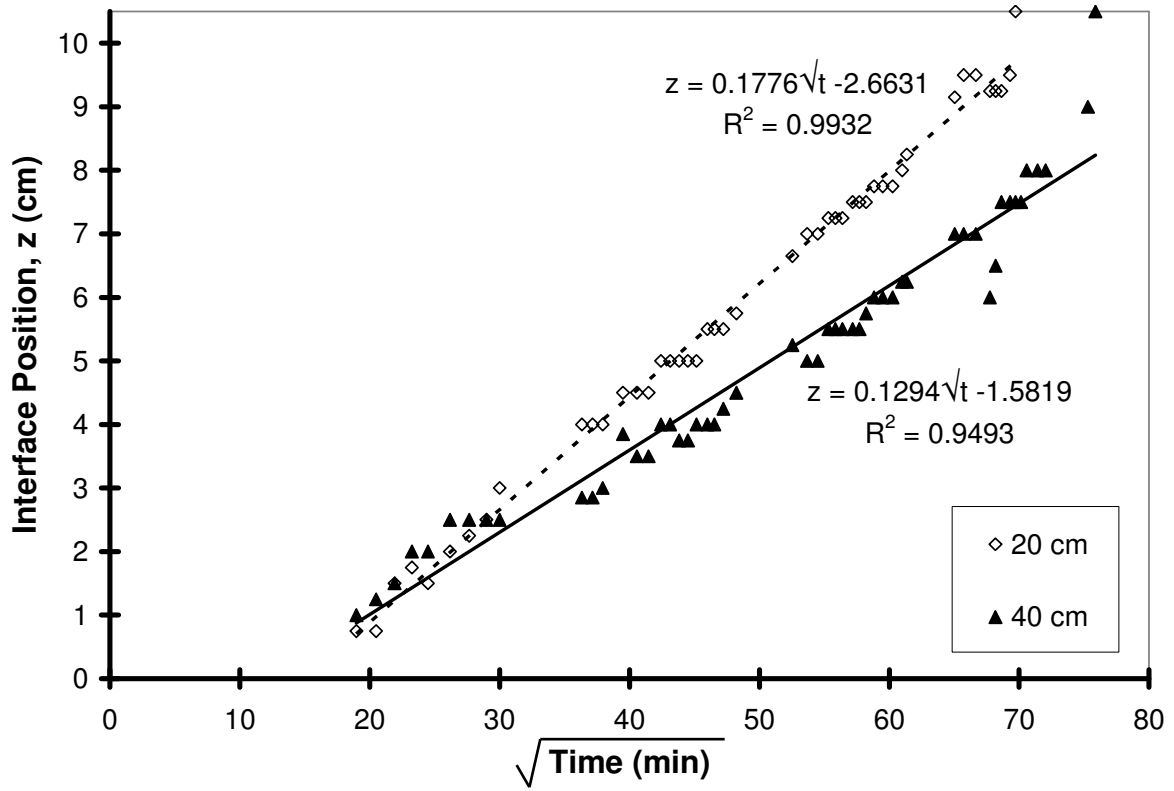


Figure 5-17 - Interface Advancement 20 and 40 cm from Model Top (Experiment #5)

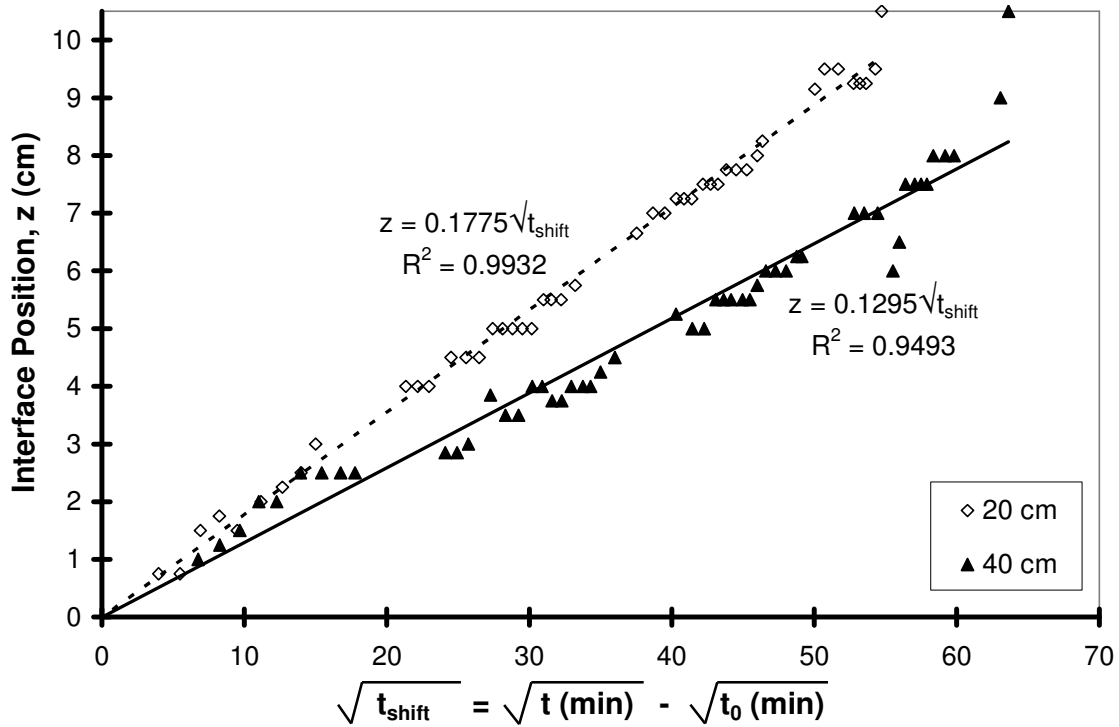


Figure 5-18 - Time Adjusted Interface Advancement 20 and 40 cm from Model Top
(Experiment #5)

5.6 *Live Oil Production*

The economics of the Vapex process depends strongly on the rate that oil is produced. A plot of cumulative live oil production versus time for Experiment #5, shown in Figure 5-19, indicates that the production rate is non-linear.

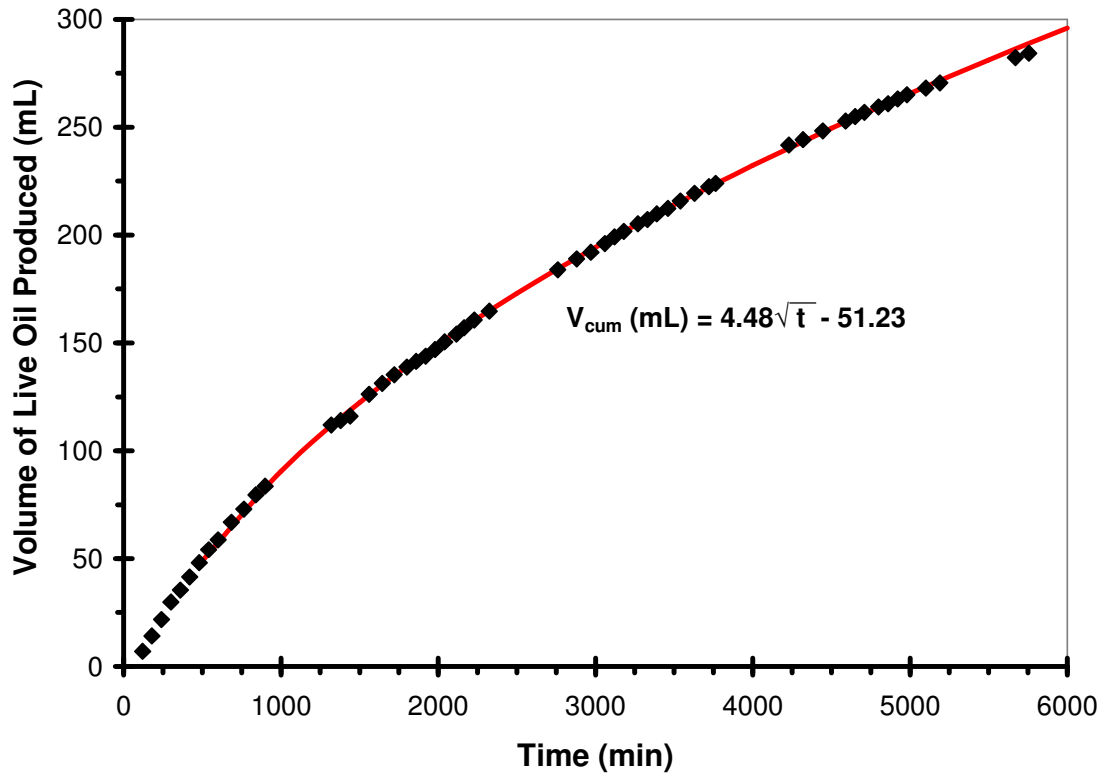


Figure 5-19 - Live Oil Production History (Experiment #5)

Figure 5-20 shows production history for all trough experiments. All experiments show that cumulative oil production is proportional to the square root of time. In general, as the pentane temperature increases the pentane vapour mole fraction increases and the volume of oil produced at a given time also increases. This trend is not followed by Experiment #2 (pentane temperature = 29.35°C) which shows oil production below that for the lowest pentane temperature experiment, possibly due to a reduction in initial oil saturation in the trough compared to the other experiments.

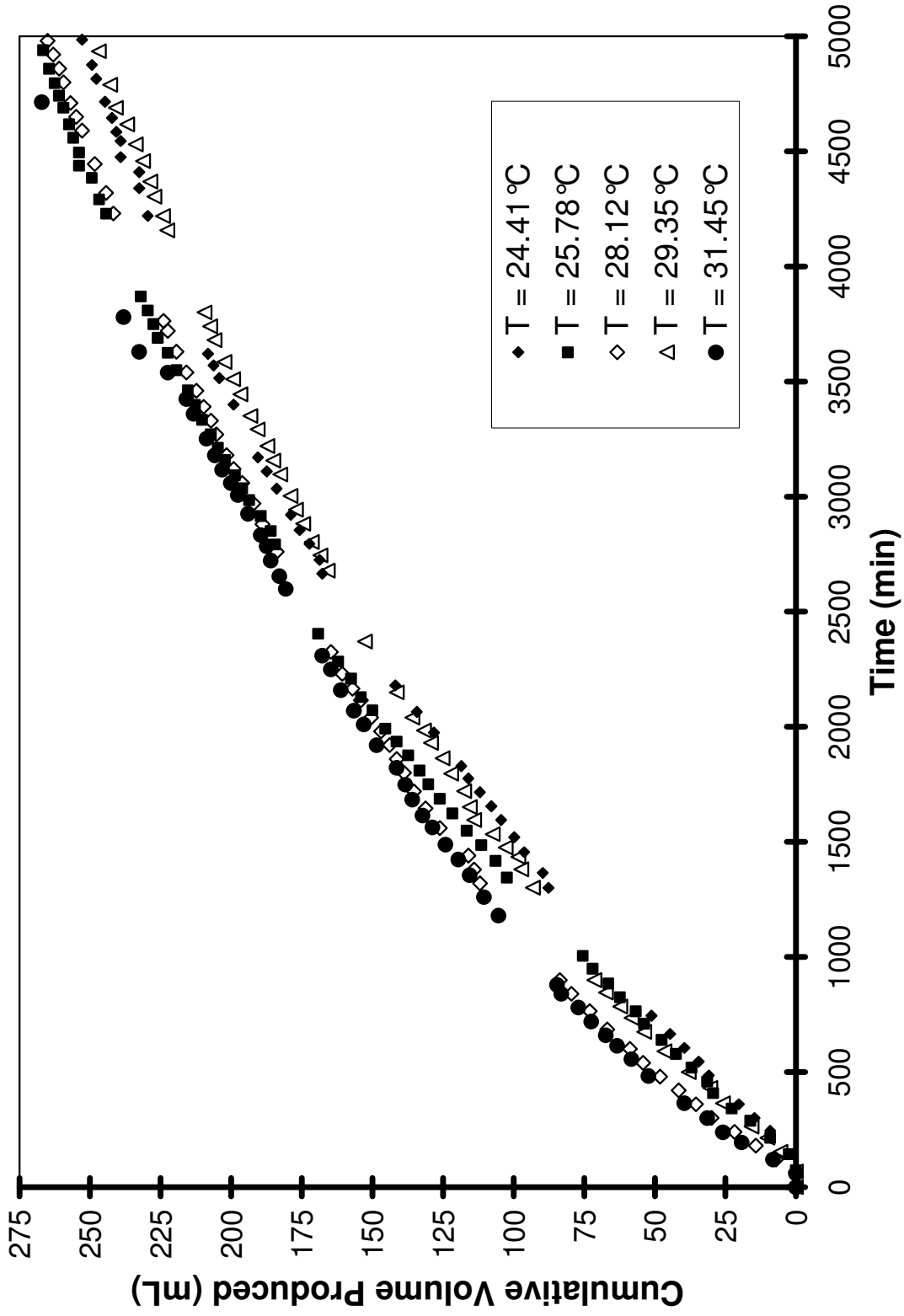


Figure 5-20 - Comparison of Cumulative Production Rates for Trough Experiments

Table 5-III compares the production rate and production volume for a given interface position and also for a given run time. If we examine one interface position, $z=4$ cm, the run time required to reach this position and the cumulative volume produced at this time decreases as pentane temperature increases. However, the production rate is relatively constant with an average value of $0.063 \text{ cm}^3/\text{min}$ ($3.77 \text{ cm}^3/\text{h}$). Similarly, for a given run time of 2500 minutes (approximately 50% of the total run time of all experiments), the interface position and cumulative volume produced (except Experiment #2) increases with pentane temperature. Again, the production rate is relatively constant at $0.046 \text{ cm}^3/\text{min}$ ($2.78 \text{ cm}^3/\text{h}$). This analysis shows that pentane temperature, and thus mole fraction of pentane in the bulk has little effect of the rate of production in the range tested.

Table 5-III - Production Rate at Given z or t

Pentane Temp (°C)	$z = 4 \text{ cm}$			$t = 2500 \text{ min}$		
	t (min)	V_{cum} (cm^3)	dV/dt (cm^3/min)	z (cm)	V_{cum} (cm^3)	dV/dt (cm^3/min)
24.41 (4)	1545.50	273.13	0.061	5.86	156.46	0.048
25.78 (3)	1439.38	263.61	0.065	6.36	169.93	0.049
28.12 (5)	1407.56	219.31	0.060	6.22	172.77	0.045
29.35 (2)	1327.78	222.81	0.060	6.37	157.52	0.044
31.45 (1)	1118.44	202.98	0.068	6.94	177.52	0.046

Increasing temperature decreases both the viscosity of bitumen and the solubility of pentane in bitumen. Since the live oil properties at room temperature (Table 5-IV) show constant pentane fraction and viscosity, the bulk concentration of pentane in the range examined is not the limiting step. Rather, the increase in diffusion distance causes a reduction in production rate as the solvent chamber grows.

5.6.1 Live Oil Properties

The stock bitumen had a viscosity of approximately 23,000 mPa•s at 22°C. All live oil samples collected show a dramatic reduction in viscosity by four orders of magnitude, shown in Table 5-IV. Similarly, the mass fraction of solvent remaining in the live oil samples ranged from 46-48% for all experiments. This agrees with experimental results reported by Oduntan (2001), Ramakrishnan (2003) and James (2003).

Table 5-IV - Average Live Oil Properties for Trough Experiments

Exp't #	Pentane Temp (°C)	$y_s (T_s)$	S_{or} Sample 1 (%PV)	Average Live Oil Property	
				$\mu (T^*)$ (mPa•s)	ω_s
4	24.41	0.75	3.80	5.98	0.48
3	25.78	0.65	4.59	5.51	0.47
5	28.12	0.69	4.40	6.39	0.47
2	29.35	0.79	4.14	4.19	0.46
1	31.45	0.86	5.98	3.93	0.47

* Samples were run at ambient temperature 22-24°C.

Though model temperature varied between the top and bottom of the model, Figure 5-4 shows that for pentane mass fractions exceeding 40 wt%, the experimental model temperature will have little effect on viscosity.

5.6.2 Solvent Diffusion

The surface area for mass transfer was estimated from the interface positions taken at 2 cm vertical intervals. The length of the interface was approximated by taking the sum of all straight lines between the point interface positions, shown in Equation (5-2).

$$L = \sum_{i=1}^{24} \sqrt{(z_i - z_{i-1})^2 + (x_i - x_{i-1})^2} \quad (5-2)$$

A plot of surface area versus time (Appendix C, Figure C37) shows that the interface length, and therefore the surface area, was not constant over the length of the experiment. The surface area first increased sharply until the back edge of the model was reached, and then decreased slowly with time for the majority of the experiment. In a reservoir, it can be expected that surface area would increase until the solvent chamber met a vertical impermeable region or another solvent chamber.

The experimental steady state diffusion coefficient for pentane diffusing into air can be determined using Equations in Section 3.2.

The volumetric flow rate of live oil (solvent and bitumen) as a function of time is known from experimental data to be:

$$V_{total,cum} = B\sqrt{t} - F \quad (5-3)$$

where B and F are experimental fit parameters. Differentiating Equation (5-3) with time results in:

$$\frac{dV_{total,cum}}{dt} = \frac{B}{2\sqrt{t}} \quad (5-4)$$

Substituting Equation (5-4) into Equation (3-29) and re-arranging for flux yields:

$$N_s(t) = \frac{x_s^V \rho_s}{A_s M_s} \left(\frac{B}{2\sqrt{t}} \right) \quad (5-5)$$

Equation (5-5) allows the determination the experimental flux of solvent into bitumen from production data. Constant B is the value of the slope of the line generated by plotting cumulative total production against the square root of time. Constant F represents the square of lag time in production from the start of the experiment. The mass fraction of solvent at the bitumen-solvent interface is estimated by the average measured mass fraction of solvent in the produced live oil samples. The mass fraction is converted to a volume fraction by:

$$x_s^V = \frac{\frac{\omega_s}{M_s}}{\frac{\omega_s}{M_s} + \frac{1 - \omega_s}{M_b}} \quad (5-6)$$

The interfacial area is calculated using the dimensions of the exposed model surface area above capillary height (40 cm x 0.95 cm).

Equating the experimental determined flux in Equation (5-5) to theoretical flux in Equation (3-30):

$$N_s(t) = \frac{PD_{sa,eff}}{RT(\Delta z)} \left(\frac{\bar{P}_{ai} - \bar{P}_{a0}}{(P_a)_M} \right) = \frac{x_s^V \rho_s}{A_s M_s} \left(\frac{B}{2\sqrt{t}} \right) \quad (5-7)$$

Solving Equation (5-7) for effective diffusivity gives:

$$D_{sa,eff} = \frac{x_s^V \rho_s}{A_s M_s} \left(\frac{B}{2\sqrt{t}} \right) \frac{RT(\Delta z)(P_a)_M}{P(\bar{P}_{ai} - \bar{P}_{a0})} \quad (5-8)$$

Grouping together constant terms in Equation (5-8) results in:

$$D_{sa,eff} = K \left(\frac{B}{\sqrt{t}} \right) \Delta z \quad (5-9)$$

where:

$$K = \frac{x_s^V \rho_s}{2A_s M_s} \frac{RT(P_a)_M}{P(\bar{P}_{ai} - \bar{P}_{a0})} \quad (5-10)$$

Experimental results show that the interface position is a positive linear function of the square root of time. The relationship can be described as:

$$z(t) = \psi_1 \sqrt{t} - \psi_2 \quad (5-11)$$

where $z(t)$ is the penetration distance from the model edge to the bitumen-solvent interface at a given time and the constant ψ_1 is related to the diffusivity of solvent into bitumen. Substituting Equation (5-11) into Equation (5-9) yields:

$$D_{sa,eff} = K \left(\frac{B}{\sqrt{t}} \right) (\psi_1 \sqrt{t} - \psi_2) \quad (5-12)$$

$$\text{or } D_{sa,eff} = \alpha_1 - \frac{\alpha_2}{\sqrt{t}}$$

where α_1 and α_2 are constants. For long periods of time, $\frac{\alpha_2}{\sqrt{t}}$ is negligible, thus:

$$D_{sa,eff} = \alpha_1 \quad (5-13)$$

The constant α_1 is a function of the system temperature and pressure. As the temperature or pressure of the system increase the diffusion coefficient should also increase.

The Vapex interface in rectangular porous media models is “S” shaped, thus an average penetration distance of Vapex interface into the model is used. The average is taken over all the height of the model above the capillary height, but below the height where the back wall has been reached.

A summary of experimental trough model results showing diffusivity and relationships between interface position and the square root of time and cumulative oil produced and the square root of time is shown in Table 5-V.

The volume of live oil produced shows a positive linear relationship with the square root of time. Data for Experiment #5 is shown in Figure 5-19. Table 5-V shows that as pentane temperature increases, the slope of the line relating cumulative production and the square root of time remains approximately the same. As vapour pressure increases with temperature, the mole fraction of pentane vapour in the bulk housing and the driving force for mass transfer should also increase.

Table 5-V - Summary of Experimental Relationships for Trough Model Experiments

Pentane Temp* (°C)	Cumulative Volume of Live Oil Collected** (cm ³)	Interface Position at Row 20** (cm)	Effective Diffusivity** (cm ² /s)	Average D_{eff} (cm ² /s)
24.41 (4)	$V_{cum} = 4.81\sqrt{t} - 84.04$	$z = 0.1742\sqrt{t} - 2.8483$	$D_{sa,eff} = \frac{-5.514}{\sqrt{t}} + 0.408$	0.0788
25.78 (3)	$V_{cum} = 4.93\sqrt{t} - 76.57$	$z = 0.1956\sqrt{t} - 3.4209$	$D_{sa,eff} = \frac{-7.852}{\sqrt{t}} + 0.424$	0.0757
28.12 (5)	$V_{cum} = 4.48\sqrt{t} - 51.23$	$z = 0.1776\sqrt{t} - 2.6631$	$D_{sa,eff} = \frac{-5.936}{\sqrt{t}} + 0.432$	0.0844
29.35 (2)	$V_{cum} = 4.40\sqrt{t} - 62.48$	$z = 0.1746\sqrt{t} - 2.3622$	$D_{sa,eff} = \frac{-3.525}{\sqrt{t}} + 0.335$	0.0654
31.45 (1)	$V_{cum} = 4.56\sqrt{t} - 50.48$	$z = 0.1774\sqrt{t} - 1.9328$	$D_{sa,eff} = \frac{-8.278}{\sqrt{t}} + 0.493$	0.0895

*Experiment number is given in brackets.

**Time has units of minutes for all equations.

If the data is shifted so that the experimental time starts when the interface begins to move at Row 20, the data listed in Table 5-V becomes that in Table 5-VI. In all trough model experiments, the interface position is a function of the square root of time, as expected from Equation (3-28).

Table 5-VI - Summary of Experimental Relationships for Trough Model Experiments with Shifted Time[#]

Pentane Temp* (°C)	t ₀ (min)	Interface Position at Row 20** (cm)	Average D _{sa,eff} (cm ² /s)
24.41 (4)	267	$z = 0.1743\sqrt{t_{shift}}$	0.1188
25.78 (3)	306	$z = 0.1956\sqrt{t_{shift}}$	0.1071
28.12 (5)	225	$z = 0.1775\sqrt{t_{shift}}$	0.1213
29.35 (2)	183	$z = 0.1747\sqrt{t_{shift}}$	0.0886
31.45 (1)	119	$z = 0.1774\sqrt{t_{shift}}$	0.1211

$$\# \sqrt{t_{shift}} = \sqrt{t} - \sqrt{t_0}$$

*Experiment number is given in brackets.

**Time has units of minutes for all equations.

Table 5-VI also shows that the average effective diffusivity is not dependent on temperature. Excluding Experiment #2, the average effective diffusivity over all experiments is 0.116 cm²/s. This value approximately five times larger than the effective diffusivity calculated by the Hirschfelder Equation (0.022 cm²/s) in Chapter 3.

Several assumptions were made to calculate the theoretical and experimental diffusion coefficients. The theoretical diffusion coefficient assumes a porosity value of 0.4 (spherical particles) and a tortuosity value of 1.5. The experimental diffusivity was estimated assuming the following:

1. Pentane and bitumen behave as an ideal solution.
2. The concentration of pentane at the interface is equal along the entire length of the interface and equal to the concentration of pentane in produced live oil.
3. No temperature gradient exists along the height of the model.
4. The Vapex interface was located at the position visually observed along the exterior walls of the trough.

If pentane and bitumen do not form an ideal solution, the partial pressure of pentane at the interface will not follow Raoult's law. Rather, an activity coefficient, γ describing the deviation from the vapour pressure predicted by Raoult's law, P_s^* is required as follows (Raff, 2001):

$$P_s = \gamma x_s P_s^* \quad (5-14)$$

Depending on the value of the activity coefficient, the partial pressure of pentane at the interface could be higher or lower than that predicted by Raoult's law.

In Experiment #6, after 420 minutes it was observed that the position of the interface at the edge of the model had advanced an average of 2.2 cm farther than in the centre of the model. Therefore, the visual interface position overestimates the average location of the interface in the model.

Table 5-VII shows the effective diffusivity resulting from reductions in the interface position, Δz and the addition of an activity coefficient. The effective diffusion coefficient is directly related to the interface position. If the interface position is overestimated, the resulting effective diffusion coefficient will also be overestimated. If the live oil solution behaves such that the vapour pressure of pentane is lower than that predicted by Raoult's

law, the effective diffusion coefficient will also be lower than previously. If both effects are combined such that the average interface position is 75% of the visual position recorded and $\gamma=0.75$, then the average effective diffusion coefficient for all experiments (excluding #2) is $0.046 \text{ cm}^2/\text{s}$. This modified effective D_{sa} is approximately twice that predicted by the Hirschfelder Equation.

Table 5-VII - Effective Diffusivity (cm^2/s) Variation Resulting from Errors in Δz and Non-Ideal Solution Behaviour

Parameter Adjustment	Exp't #1	Exp't #2	Exp't #3	Exp't #4	Exp't #5
Original	0.1211	0.0886	0.1071	0.1188	0.1213
$0.9*(\Delta z)$	0.1090	0.0798	0.1025	0.1069	0.1091
$0.75*(\Delta z)$	0.0909	0.0665	0.0855	0.0891	0.0909
$0.5*(\Delta z)$	0.0606	0.0443	0.0570	0.0594	0.0606
$\gamma = 0.90$	0.0860	0.0650	0.0820	0.0846	0.0858
$\gamma = 0.75$	0.0621	0.0481	0.0602	0.0613	0.0618
$\gamma = 0.50$	0.0447	0.0356	0.0441	0.0442	0.0443
$0.75*(\Delta z)$ and $\gamma = 0.75$	0.0466	0.0362	0.0451	0.0460	0.0463

6.0 Conclusions & Recommendations

6.1 Conclusions

1. Bitumen viscosity is a function of both temperature and pentane content. Increasing pentane content up to approximately 40 wt% results in a significant reduction in solution viscosity.
2. The removal of asphaltenes from stock bitumen resulted in a 60% reduction in viscosity from 23,176 mPa•s to 9,380 mPa•s.
3. Pentane is an effective solvent for the Vapex process. Compared to a pure solvent, combining pentane with a non-condensable gas reduces the rate of interface advancement and rate of oil production. In the presence of a non-condensable gas, interface position and cumulative live oil production were found to be linear with the square root of time.
4. Live oil properties were found to be consistent throughout each experiment and between experiments. On average, live oil contained 46-48 wt% pentane and viscosity was reduced from 23,000 mPa•s to 4-6 mPa•s.
5. Based on production data, the average effective diffusion coefficient of pentane into stagnant air is $0.116 \text{ cm}^2/\text{s}$. This is approximately five times larger than the effective molecular diffusion coefficient estimated by the Hirschfelder Equation ($0.022 \text{ cm}^2/\text{s}$).
6. In the range of vapour phase mole fraction of pentane examined, the bulk pentane fraction in air has no effect on live oil production rate. As the solvent chamber grows, diffusion distance increases, resulting in reduced production due to mass transfer control in gas phase.

7. The rate of interface advancement over a curved interface where the porous medium was filled with corn syrup with a film of water flowing over it at steady state proved that the rate of interface advancement by leaching mechanism is constant throughout.

6.2 Recommendations

1. A novel method for saturating and packing trough models will ensure consistent trials without obstructing the first 0.5cm of the model.
2. Additional trials should be performed to investigate lower temperatures, higher pressures and the use of carbon dioxide (CO₂) as the non-condensable gas. The use of CO₂ has environmental benefits and has the ability to reduce bitumen viscosity. Trials should also be repeated with more viscous oil and finer mesh beads.
3. Verification of the bulk vapour phase pentane concentration will provide a more accurate estimation of solvent flux and diffusion.
4. Oil remaining in the model and live oil samples should be analyzed for asphaltene content. This will indicate both the amount of asphaltenes removed and the location of precipitation.
5. The development of a model that incorporates reservoir parameters such as pay zone height, well length, porosity, saturation, permeability, etc. will aid reservoir engineers in determining production characteristics.
6. Pentane-bitumen solution thermodynamics should be investigated to determine the solution's deviation from Raoult's law.

7.0 References

Alberta Energy and Utilities Board, "Statistical Series 2003-98: Alberta's Reserves 2002 Supply/Demand Outlook 2003-2012," Alberta Energy and Utilities Board, Calgary, Alberta, 2003.

Boustani, A. and Maini, B.B., "The Role of Diffusion and Convective Dispersion in Vapour Extraction Process," *Journal of Canadian Petroleum Technology*, Volume 40, No. 4, pp 68-77, April 2001.

Butler, R.M., "Closed-loop Extraction Method for the Recovery of Heavy Oils and Bitumens Underlain by Aquifers: The Vapex Process," *The Fifth Petroleum Conference of the South Saskatchewan Section of the Petroleum Society*, Regina, SK, October 18-20, 1993.

Butler, R.M. and Jiang, Q., "Improved Recovery of Heavy Oil by Vapex with Widely Spaced Horizontal Injectors and Producers," *Journal of Canadian Petroleum Technology*, Volume 39, No. 1, pp 48-56, January 2000.

Butler, R.M. and Mokrys, I.J., "A New Process (VAPEX) for Recovering Heavy Oils Using Hot Water and Hydrocarbon Vapour," *Journal of Canadian Petroleum Technology*, Volume 30, No. 1, pp 97-106, January-February, 1991.

Butler, R.M. and Mokrys, I.J., "Closed-loop Extraction Method for the Recovery of Heavy Oils and Bitumens Underlain by Aquifers: the Vapex Process," *Journal of Canadian Petroleum Technology*, Volume 37, No. 4, pp 41-50, April 1998.

Butler, R.M. and Mokrys, I.J., "Recovery of Heavy Oils Using Vapourized Hydrocarbon Solvents: Further Development of the Vapex Process," *Journal of Canadian Petroleum Technology*, Volume 32, No. 6, pp 56-62, June 1993.

Butler, R.M. and Mokrys, I.J., "Solvent Analog of Steam Assisted Gravity Drainage," AOSTRA Journal of Research, Volume 5, No. 1, pp 17-31, June 1989.

Canadian Association of Petroleum Producers (CAPP), "Canadian Crude Oil... Increasing Energy Security," Calgary, AB, www.capp.ca, accessed March 20, 2004.

Cannon Instruments, "Instructions for the use of the Cannon-Fenske Routine Viscometer," State College, PA, <http://www.cannoninstrument.com/P10-0100%20CFR%20instructions.pdf>, 2004, accessed November 2005.

Chatzis, I., "Pore Scale Mechanisms of Heavy Oil Recovery using the Vapex Process," Proceedings of the International Symposium of the Society of Core Analysts, Monterey, California, September 2002.

Crank, J., The Mathematics of Diffusion, 2nd Edition, Clarendon Press, Oxford, 1975.

Das, S., In Situ Recovery of Heavy Oil and Bitumen Using Vapourized Hydrocarbon Solvents, PhD Dissertation, University of Calgary, Calgary, AB, 1995.

Das, S., "Vapex – A Unique Canadian Technology," Journal of Canadian Petroleum Technology, Volume 41, No. 8, pp 32-34, August 2002.

Das, S.K., "Vapex: An Efficient Process for the Recovery of Heavy Oil and Bitumen," SPE 50941, SPE Journal, pp 232-237, September 1998.

Das, S.K., and Butler, R.M., "Effect of Asphaltene Deposition on the Vapex Process: A Preliminary Investigation Using a Hele-Shaw Cell," Journal of Canadian Petroleum Technology, Volume 33, No. 6, pp 39-45, June 1994.

Das, S. and Butler, R.M., "Extraction of Heavy Oil and Bitumen Using Solvents at Reservoir Pressure," presented at the Sixth Petroleum Conference of the South Saskatchewan Section, The Petroleum Society of CIM, Regina, SK, October 16-18, 1995.

Das, S. and Butler, R.M., "Mechanism of the Vapour Extraction Process for Heavy Oil and Bitumen," *Journal of Petroleum Science and Engineering*, Volume 21, pp 43-59, 1998.

Dickakian, G., "Fouling Problems," *Fouling and Coking Technology*, Inc., Kingswood, Texas, http://www.foulingrefinery.com/pages/fouling_costs.htm, 2001, accessed October 31, 2005.

Felder, R.M. and Rousseau, R.W., Elementary Principles of Chemical Processes, 2nd Edition, John Wiley & Sons, Toronto, ON, 1986.

Hildebrand, J.H., "Solubility III – Relative Values of Internal Pressure and Their Practical Application," *Journal of the American Chemical Society*, Volume 41, No. 7, pp 1067-1080, 1919.

Hines, A.L. and Maddox, R.N., Mass Transfer Fundamentals and Applications, Prentice Hall, New Jersey, 1985.

Islam, M.R., "Potential of Ultrasonic Generators for use in Oil Wells and Heavy Crude Oil/Bitumen Transportation Facilities," Asphaltenes: Fundamentals and Applications, Shue E.Y., and Mullins, O.C., ed, Plenum Press, New York, 1995.

James, L.A., A Closer Look at VAPEX, Masters Thesis, University of Waterloo, Waterloo, ON, 2003.

James, L.A. and Chatzis, I., "Core Analysis Issues in Heavy Oil Recovery Using Vapex," prepared for presentation at the International Symposium of the Society of Core Analysts, Toronto, Ontario, August 21-25, 2005.

James, L.A. and Chatzis, I., "Details of Gravity Drainage of Heavy Oil During Vapour Extraction," prepared for presentation at the International Symposium of the Society of Core Analysts, Abu Dhabi, United Arab Emirates, October 5-9, 2004.

Jin, W., Heavy Oil Recovery Using the Vapex Process, Masters Thesis, University of Waterloo, Waterloo, ON, 1999.

Karmaker, K. and Maini, B.B., “Applicability of Vapour Extraction Process to Problematic Viscous Oil Reservoirs,” Paper SPE 84034 presented at the SPE Annual Technical Conference and Exhibition, Denver, Colorado, October 5-8, 2003.

Mitchell, D.L. and Speight, J.G., “The Solubility of Asphaltenes in Hydrocarbon Solvents,” Fuel, Volume 52, pp 149-152, April 1973.

Oduntan, A.R., Heavy Oil Recovery Using the Vapex Process: Scale-Up and Mass Transfer Issues, Masters Thesis, University of Waterloo, Waterloo, ON, 2001.

Oduntan, A.R., Smith, J.D., Chatzis, I., and Lohi, A., “Heavy Oil Recovery Using the Vapex Process: Scale-Up Issues,” Paper 2001-127 presented at the Petroleum Society’s Canadian International Petroleum Conference, Calgary, AB, June 2001.

Raff, L.M., Principles of Physical Chemistry, Prentice Hall, New Jersey, 2001.

Ramakrishnan, V., In-situ Recovery of Heavy Oil by VAPEX using Propane, Masters Thesis, University of Waterloo, Waterloo, ON, 2003.

RWE Dea AG, “Recovery Methods,” <http://www.rwe-dea.com/en/203.htm>, accessed February 2004.

Sheu, E.Y. and Storm, D.A., “Colloidal Properties of Asphaltenes in Organic Solvents,” Asphaltenes: Fundamentals and Applications, Shue E.Y., and Mullins, O.C., ed, Plenum Press, New York, 1995.

Smalley, C., Heavy Oil and Viscous Oil, chapter from Modern Petroleum Technology, R.A. Dawe, ed, John Wiley & Sons Ltd., 2000.

Speight, J.G., "Petroleum Asphaltenes, Part 1, Asphaltenes, Resins and the Structure of Petroleum," *Oil & Gas Science and Technology*, Volume 59, No. 5, pp 467-477, 2004.

Speight, J.G., *The Chemistry and Technology of Petroleum*, 2nd Edition, Marcel Dekker, Inc., New York, 1991.

Yasdani, A., and Maini, B.B., "Effect of Drainage Height and Grain Size on the Convective Dispersion in the Vapex Process: Experimental Study," Paper SPE 89409 presented at the 2004 SPE/DOE Fourteenth Symposium on Improved Oil Recovery, Tulsa, OK, April 17-21, 2004.

Appendix A - Experimental Data – Curved Interface

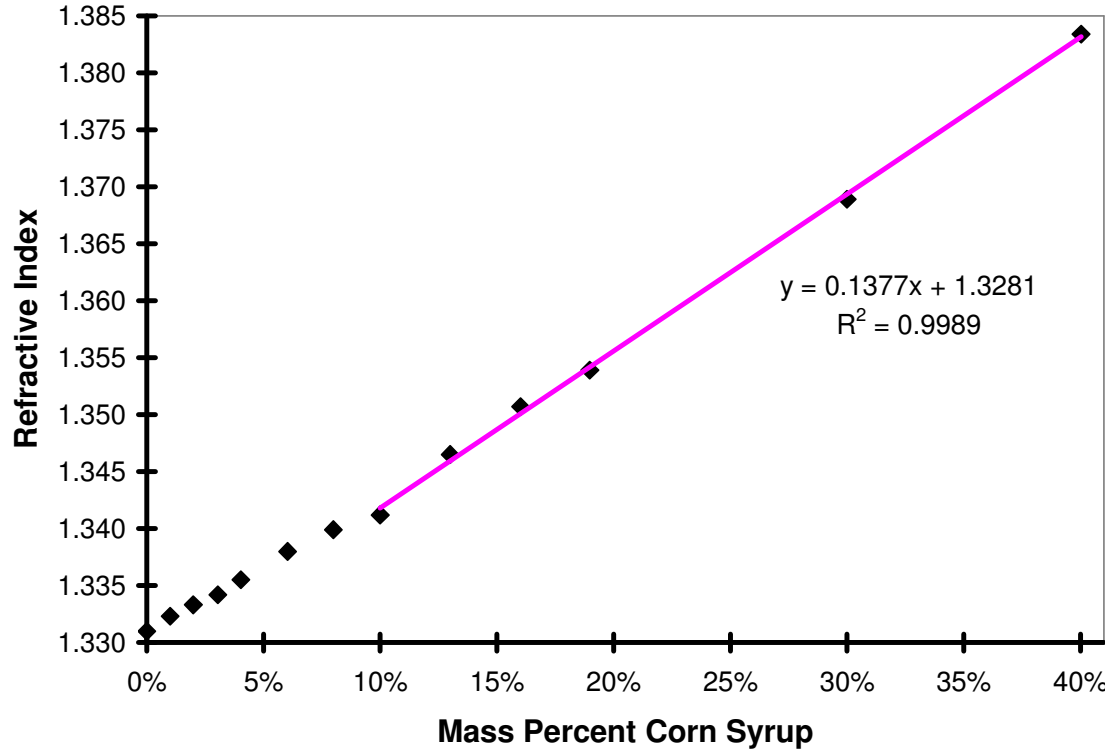


Figure A1 – Calibration Curve Showing Refractive Index for Known Corn Syrup Solution Concentrations

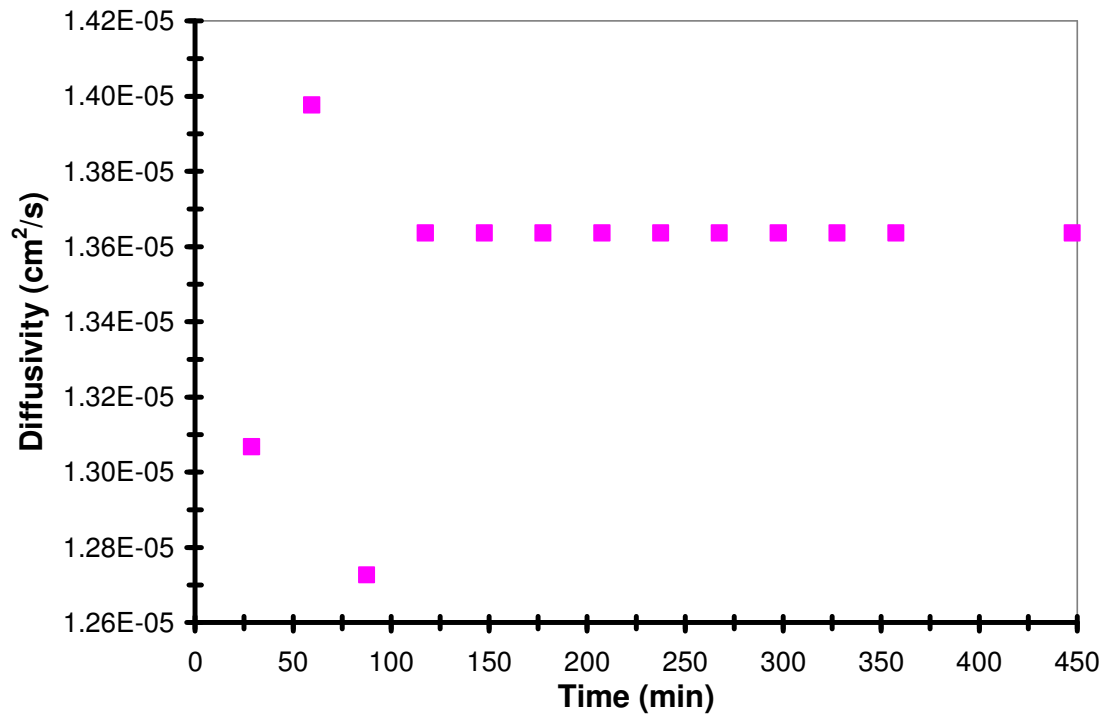


Figure A2 – Diffusivity of Water into Corn Syrup with Time

Appendix B - Experimental Data – Viscosity- Temperature-Pentane Fraction

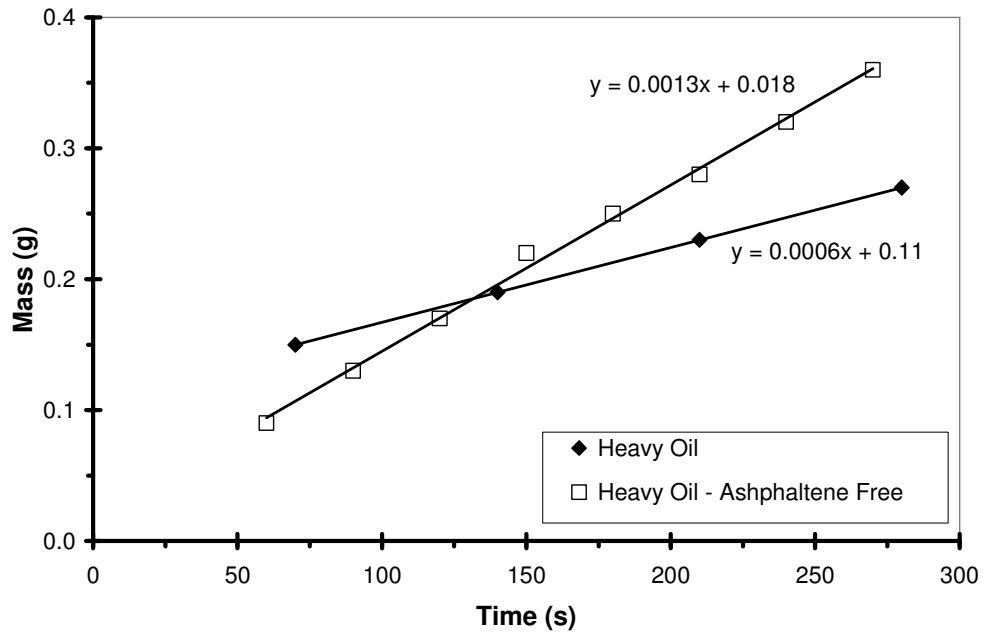


Figure B1 – Flow of Bitumen Through a Capillary Viscometer

Table B.I – Density and Viscosity Measurement of Bitumen

	Original Bitumen	Asphaltene-Free Bitumen
<i>Height of Oil (m)</i>	0.197	0.184
<i>Length of Capillary (m)</i>	0.396	0.396
<i>Capillary Diameter (m)</i>	0.0033	0.0033
<i>Mass Flow Rate (g/s)</i>	0.0006	0.0013
<i>Sample Volume (cm³)</i>	19.5	20.5
<i>Sample Mass (g)</i>	19.11	18.86
<i>Density (g/cm³)</i>	0.98	0.92
ΔP (Pa)	1892	1659
<i>Viscosity (mPa•s)</i>	23,178	9,380

Appendix C - Experimental Data – Vapex Experiments

Sample Calculations for Experiment #5, t=1800 min

Surface Area

$$\begin{aligned}A_{surface} &= L * W \\ &= (40 \text{ cm})(0.95 \text{ cm}) \\ &= 38.1 \text{ cm}^2\end{aligned}$$

Vapour Pressure

$$\begin{aligned}P_j^{vap} (23.84) &= 10^{\left[A - \frac{B}{T+C} \right]} \\ &= 10^{\left[6.85221 - \frac{1064.63}{23.08+232} \right]} \\ &= 476.89 \text{ mmHg} \\ &= 63.58 \text{ kPa}\end{aligned}$$

Vapour Phase Mole Fraction of Solvent in the Bulk

$$\begin{aligned}y_{s0} &= \frac{P_s^{vap} (T)}{P} \\ &= \frac{63.58 \text{ kPa}}{102.47 \text{ kPa}} \\ &= 0.62\end{aligned}$$

Liquid Phase Mole Fraction of Solvent

$$\begin{aligned}\bar{x}_s &= \frac{\frac{\bar{\omega}_s}{M_s}}{\frac{\bar{\omega}_s}{M_s} + \frac{1-\bar{\omega}_s}{M_b}} \\ &= \frac{\frac{0.47}{72 \text{ g/mol}}}{\frac{0.47}{72 \text{ g/mol}} + \frac{1-0.47}{400 \text{ g/mol}}} \\ &= 0.83\end{aligned}$$

Vapour Phase Mole Fraction of Solvent at the Vapex Interface

$$\begin{aligned}y_{si} &= \frac{\bar{x}_s P_s^{vap}(T)}{P} \\ &= \frac{(0.83)(63.58 \text{ kPa})}{102.47 \text{ kPa}} \\ &= 0.52\end{aligned}$$

Partial Pressure of Solvent at the Vapex Interface

$$\begin{aligned}P_{si} &= \bar{x}_s P_s^{vap}(T) \\ &= (0.83)(63.58 \text{ kPa}) \\ &= 52.85 \text{ kPa}\end{aligned}$$

Flux of Solvent

$$\begin{aligned}N_s(t) &= \frac{\bar{x}_s \rho_s}{M_s A_{surface}} \left(\frac{dV}{dt} \right) \\ &= \frac{\bar{x}_s \rho_s}{M_s A_{surface}} \left(\frac{B}{2\sqrt{t-F}} \right) \\ &= \frac{(0.83)(0.63 \text{ g/cm}^3)}{(72 \text{ g/mol})(38.1 \text{ cm}^2)} \left(\frac{4.4826 \text{ cm}^3/\text{min}^{0.5}}{2\sqrt{1800 \text{ min}-11.43 \text{ min}}} \right) \\ &= 1.01 \times 10^{-5} \text{ mol/cm}^2 \text{ min}\end{aligned}$$

Effective Diffusion of Solvent in Porous Media

$$\begin{aligned}
 D_{sa,eff} &= \frac{(N_s(t))RT(\Delta z)}{P} \left(\frac{(P_a)_M}{P_{ai} - P_{a0}} \right) \\
 &= \frac{(1.01 \times 10^{-5} \text{ mol/cm}^2 \text{ min})(8.314 \text{ kPaL/molK})(296.23 \text{ K})(4.91 \text{ cm})}{102.47 \text{ kPa}} \times \\
 &\quad \left(\frac{1000 \text{ cm}^3}{\text{L}} \right) \left(\frac{44.04 \text{ kPa}}{49.62 \text{ kPa} - 38.89 \text{ kPa}} \right) \\
 &= 4.88 \text{ cm}^2/\text{min} = 0.081 \text{ cm}^2/\text{s}
 \end{aligned}$$

Molecular Diffusivity

$$\begin{aligned}
 D_{sa} &= \frac{D_{sa,eff} \tau}{\phi} \\
 &= \frac{(0.081 \text{ cm}^2/\text{s})(1.5)}{0.4} \\
 &= 0.304 \text{ cm}^2/\text{s}
 \end{aligned}$$

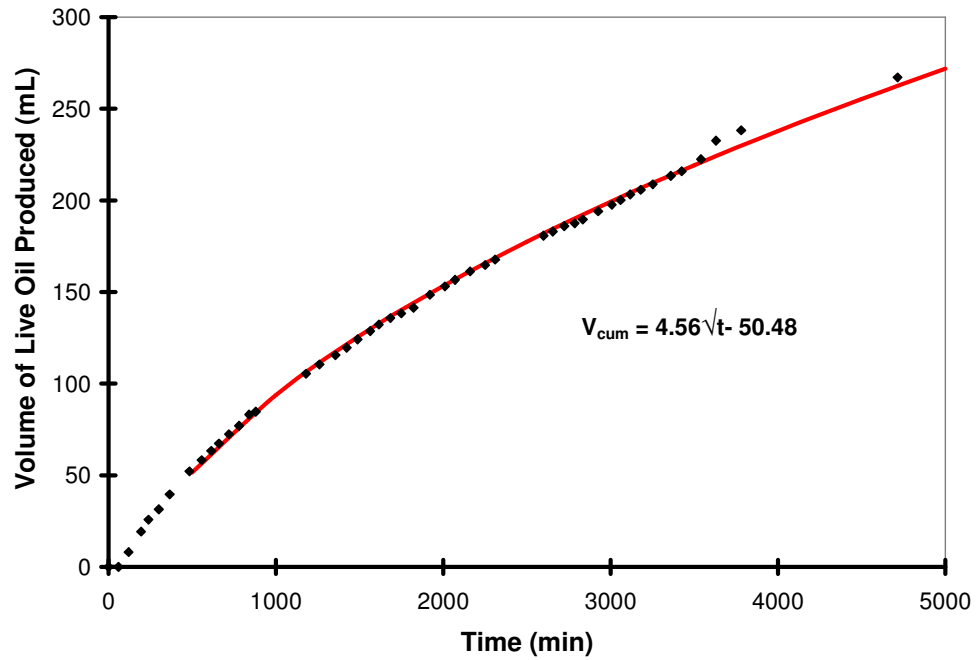


Figure C1 – Live Oil Production History (Experiment #1)

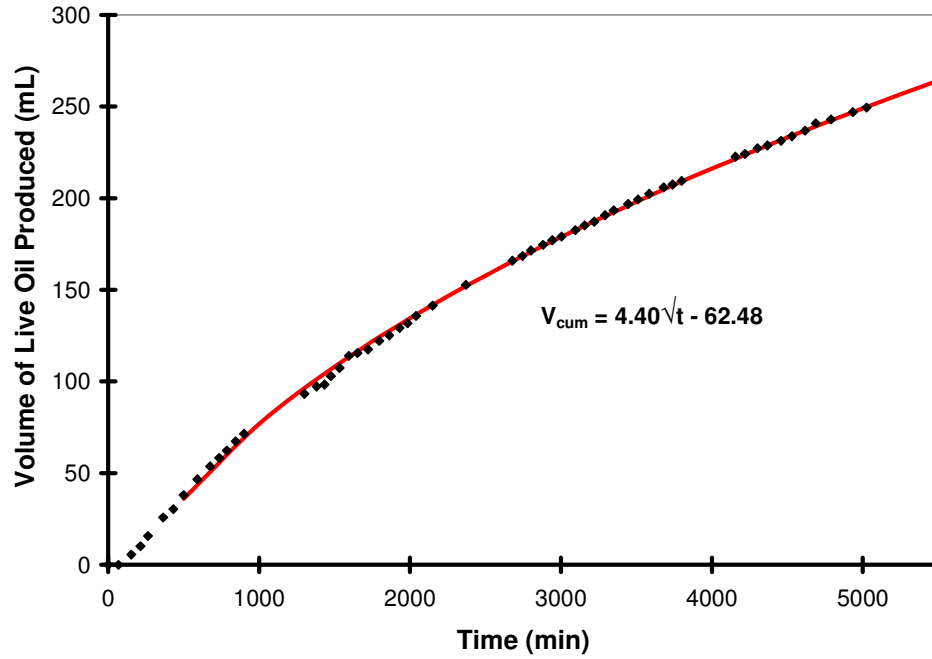


Figure C2 – Live Oil Production History (Experiment #2)

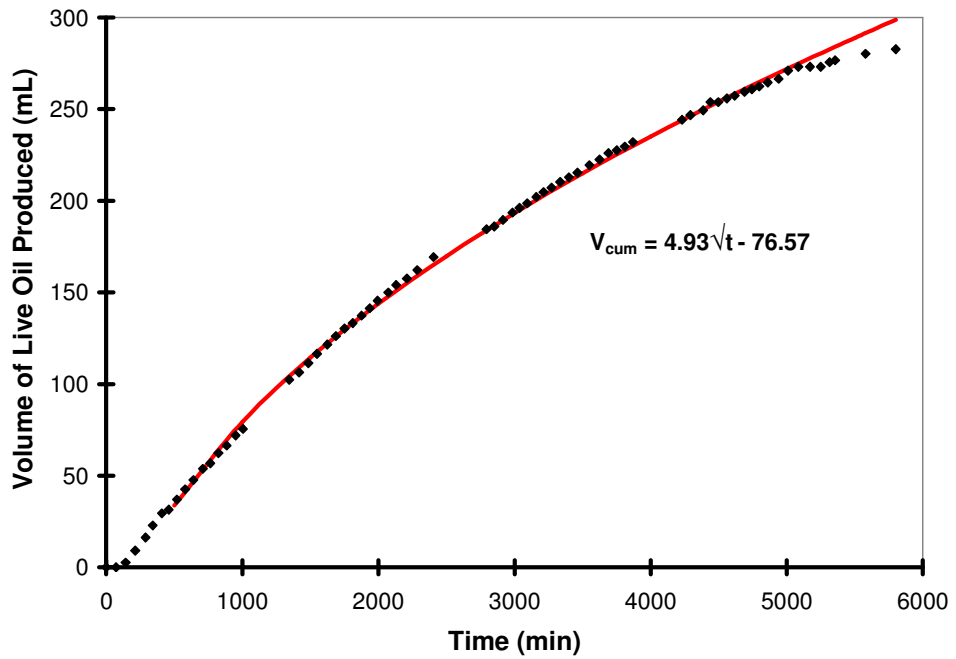


Figure C3 – Live Oil Production History (Experiment #3)

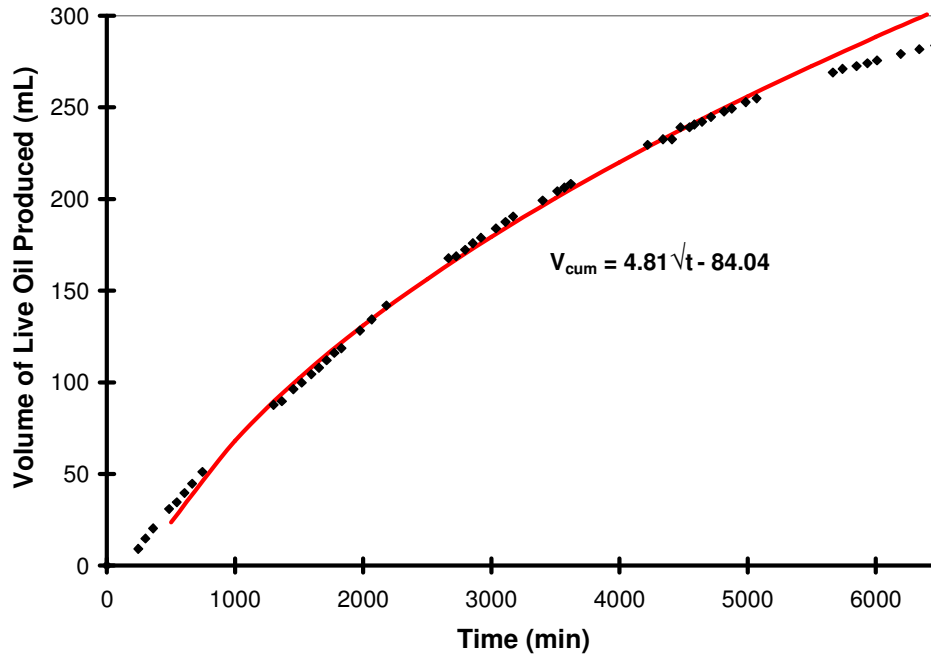


Figure C4 – Live Oil Production History (Experiment #4)

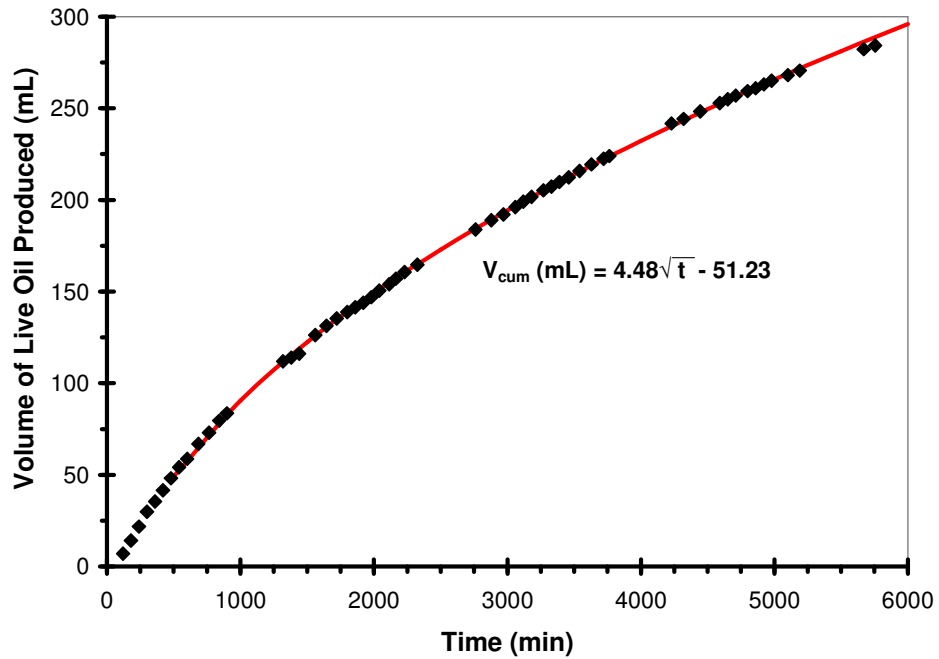


Figure C5 – Live Oil Production History (Experiment #5)

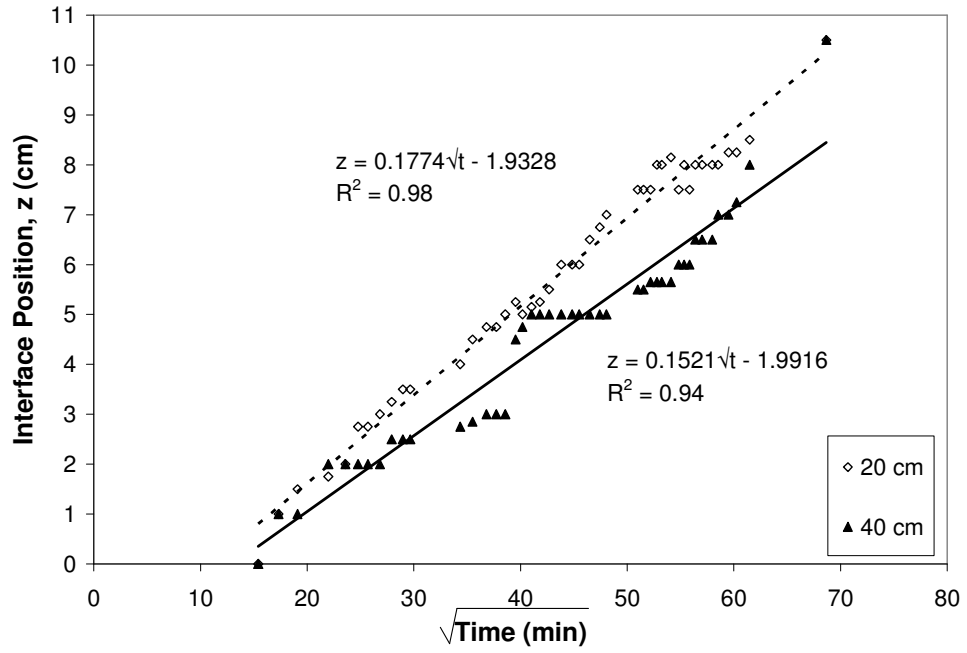


Figure C6 – Interface Advancement 20 and 40 cm from Model Top (Experiment #1)

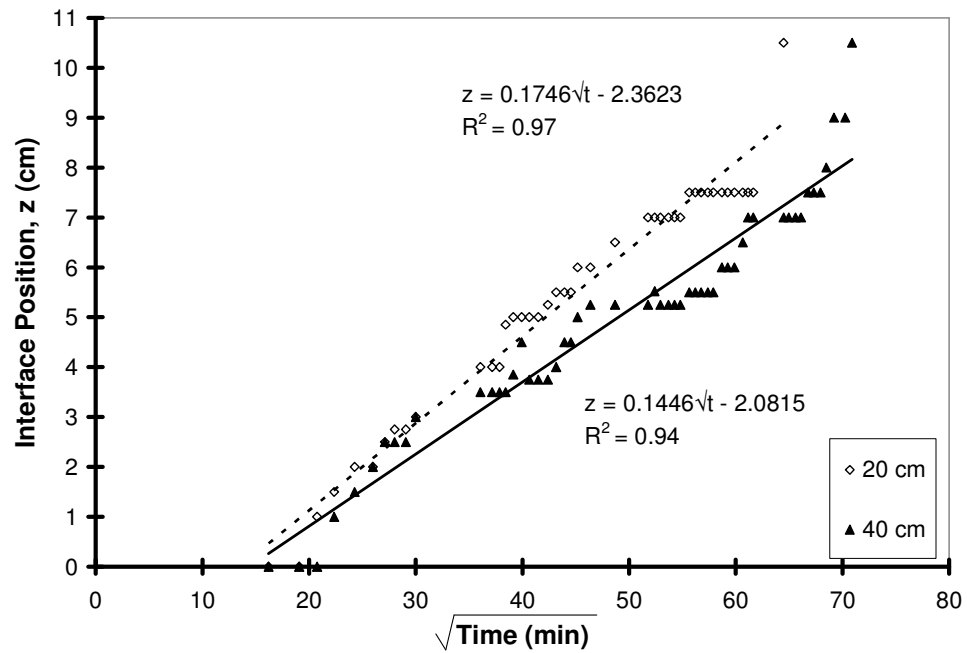


Figure C7 – Interface Advancement 20 and 40 cm from Model Top (Experiment #2)

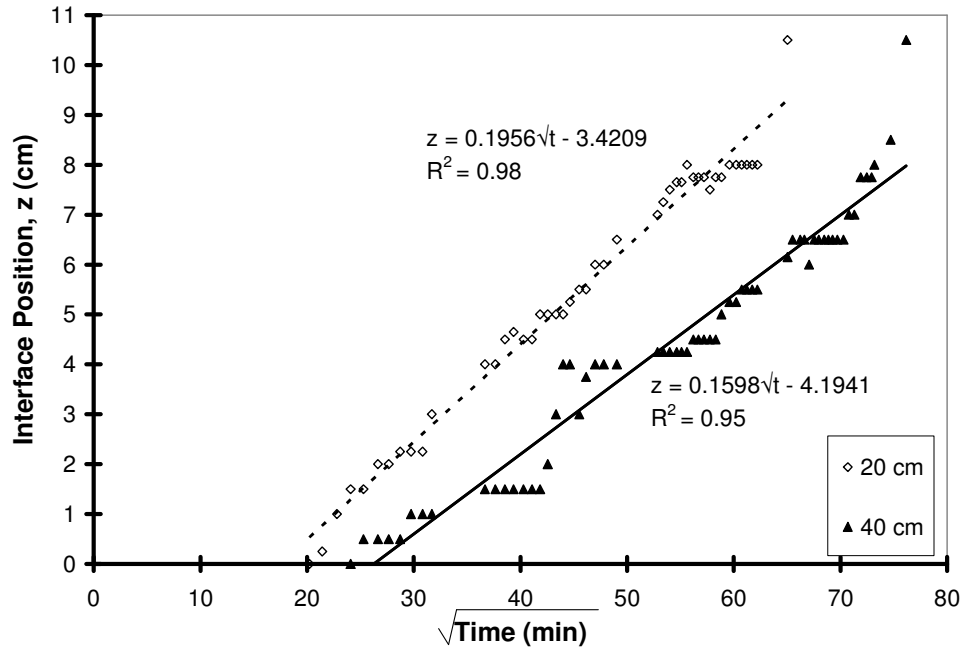


Figure C8 – Interface Advancement 20 and 40 cm from Model Top (Experiment #3)

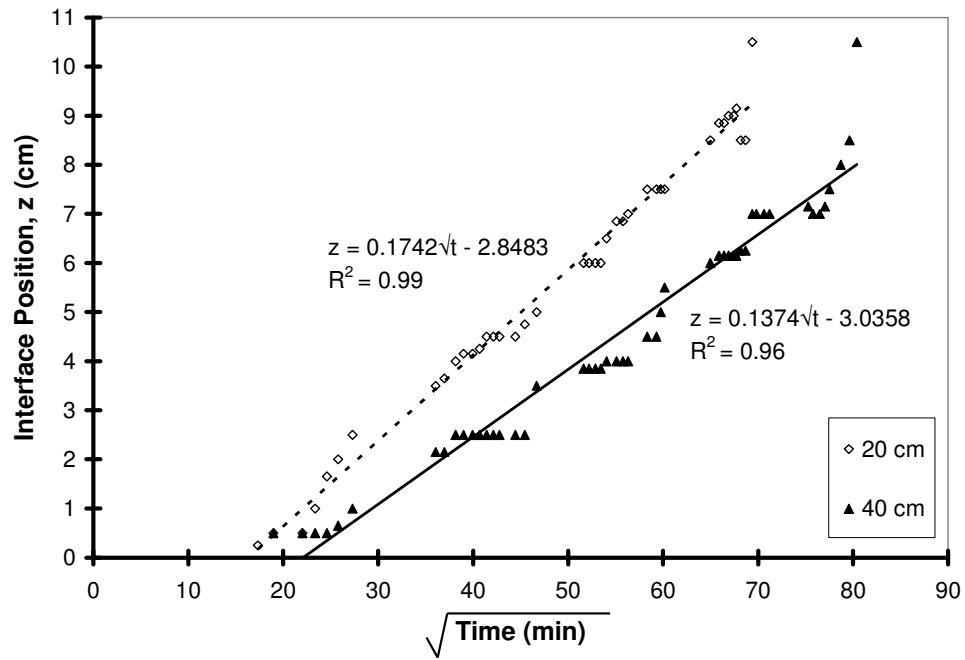


Figure C9 – Interface Advancement 20 and 40 cm from Model Top (Experiment #4)

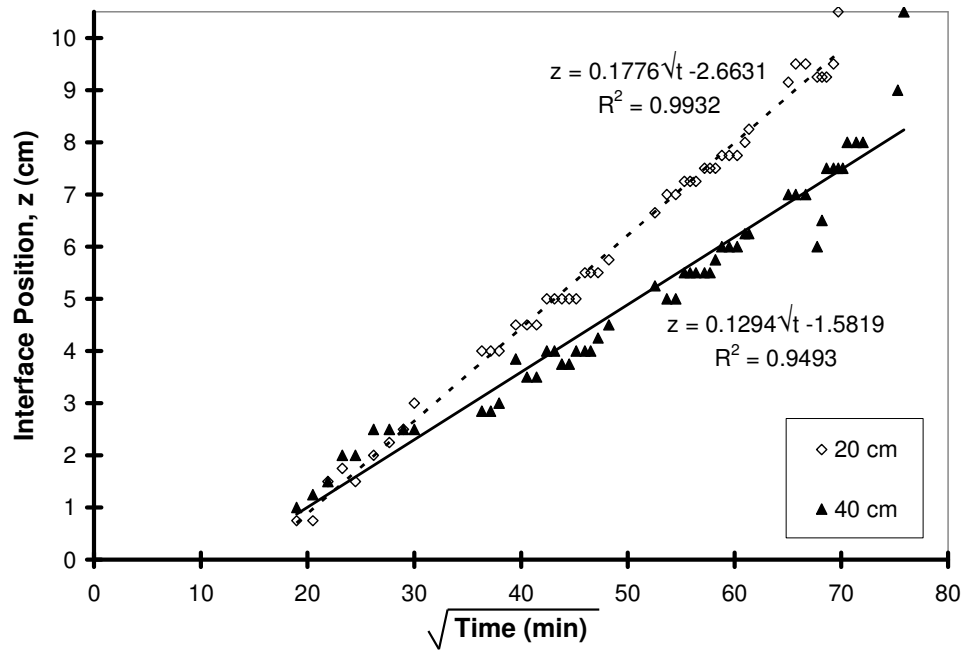


Figure C10 – Interface Advancement 20 and 40 cm from Model Top (Experiment #5)

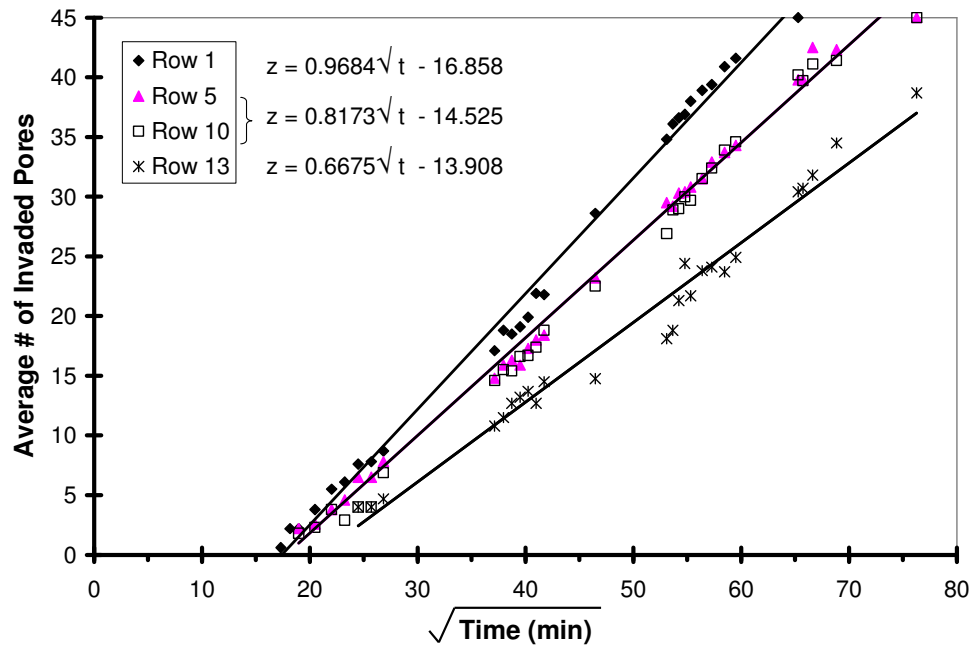


Figure C11 – Interface Advancement for Selected Rows (Experiment #7)

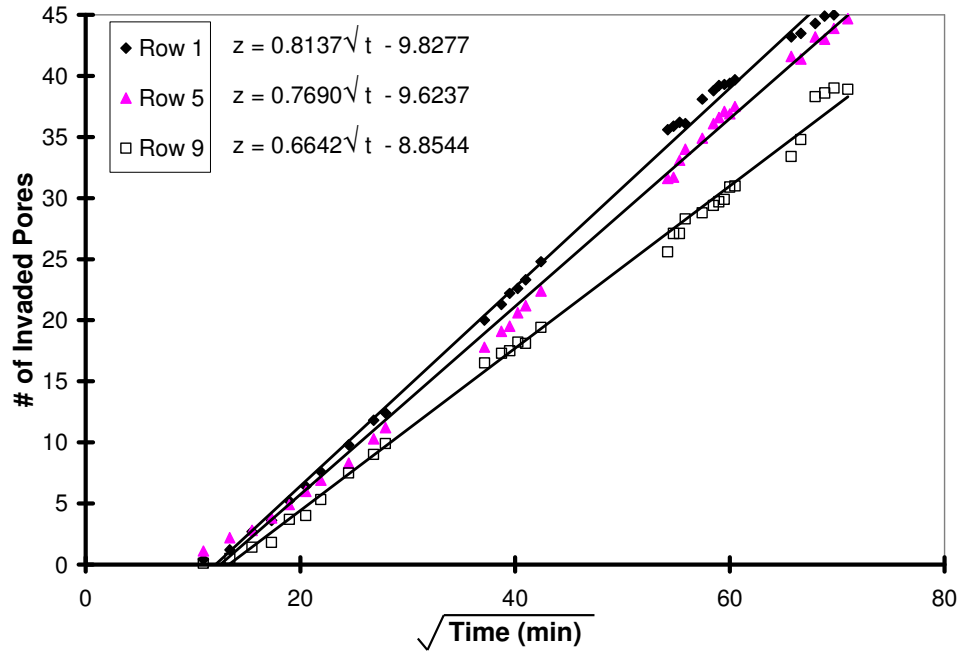


Figure C12 – Interface Advancement for Selected Rows (Experiment #8)

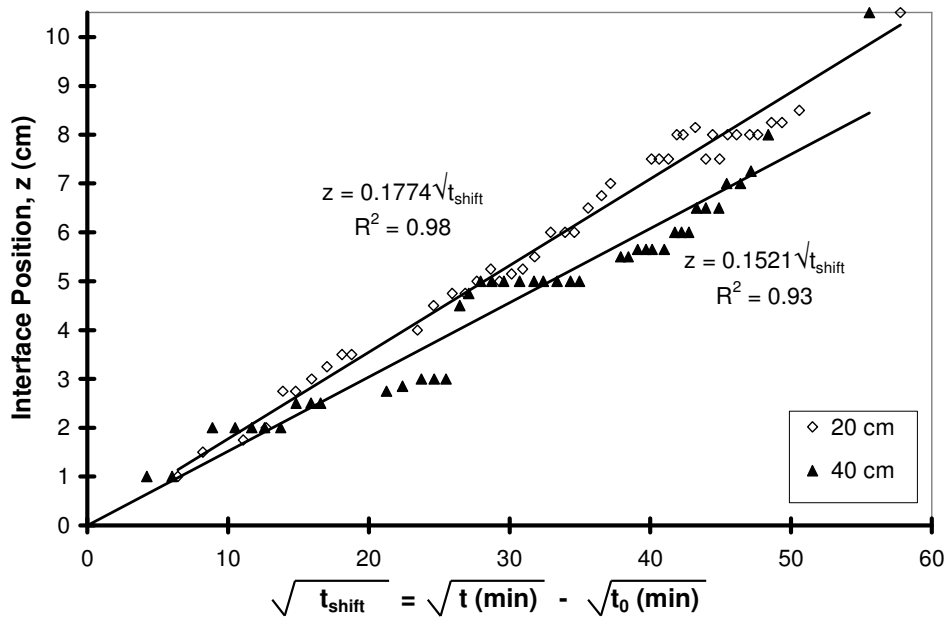


Figure C13 – Time Adjusted Interface Advancement 20 and 40 cm from Model Top (Experiment #1)

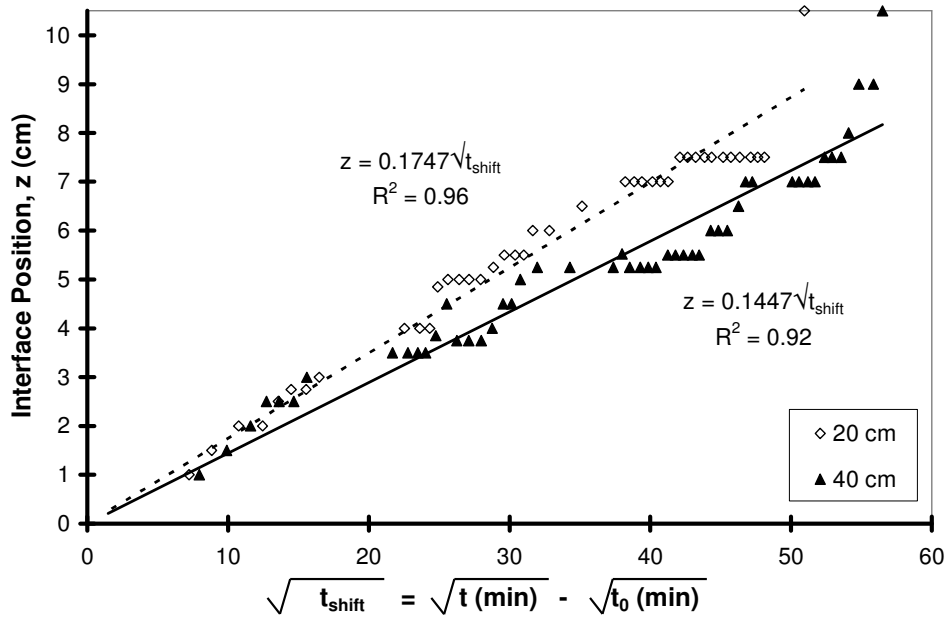


Figure C14 – Time Adjusted Interface Advancement 20 and 40 cm from Model Top
(Experiment #2)

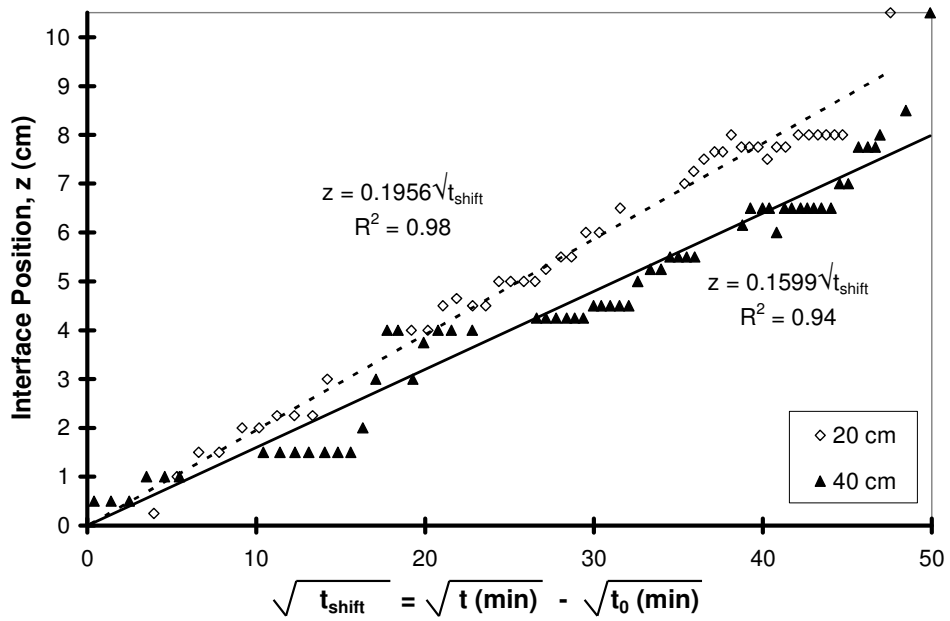


Figure C15 – Time Adjusted Interface Advancement 20 and 40 cm from Model Top
(Experiment #3)

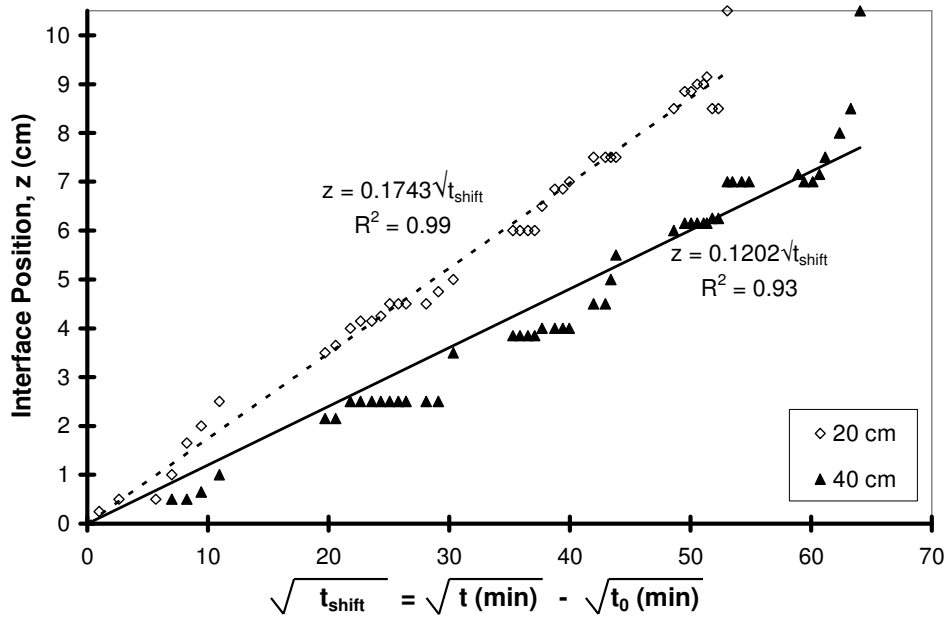


Figure C16 – Time Adjusted Interface Advancement 20 and 40 cm from Model Top
(Experiment #4)

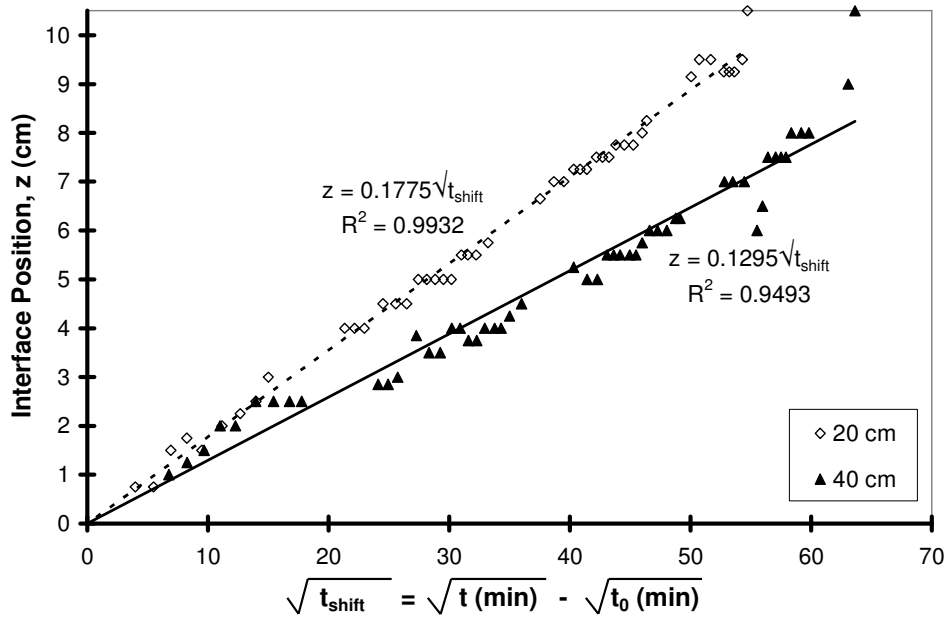


Figure C17 – Time Adjusted Interface Advancement 20 and 40 cm from Model Top
(Experiment #5)

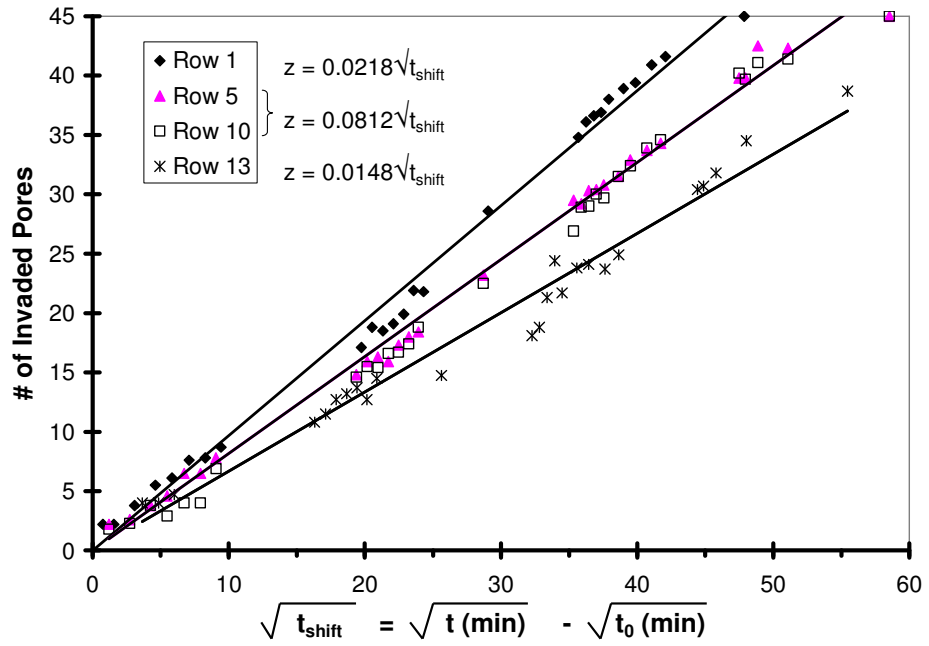


Figure C18 – Time Adjusted Interface Advancement for Selected Rows
(Experiment #7)

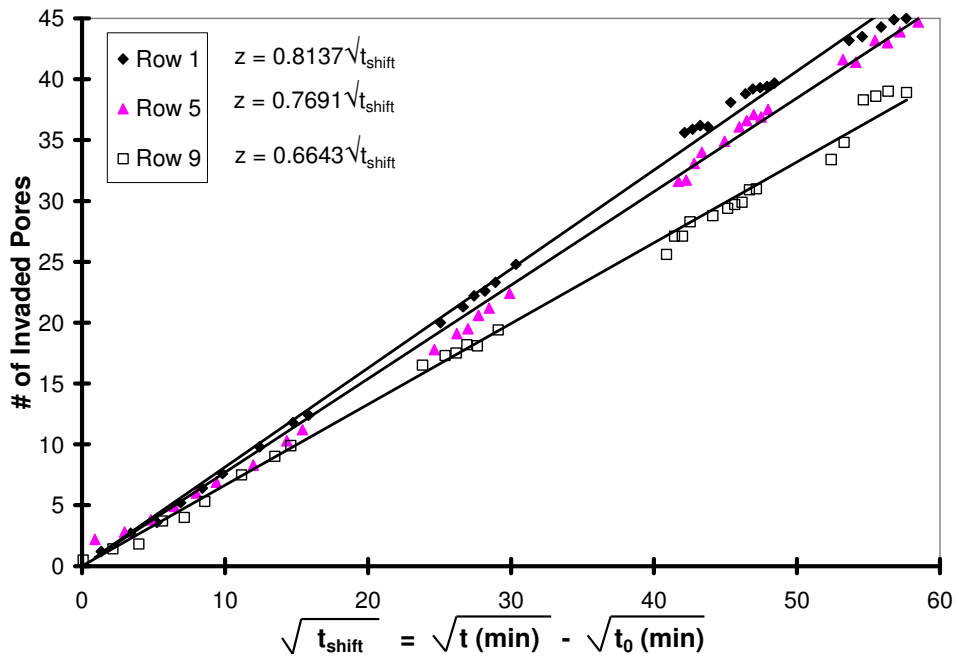


Figure C19 – Time Adjusted Interface Advancement for Selected Rows
(Experiment #8)

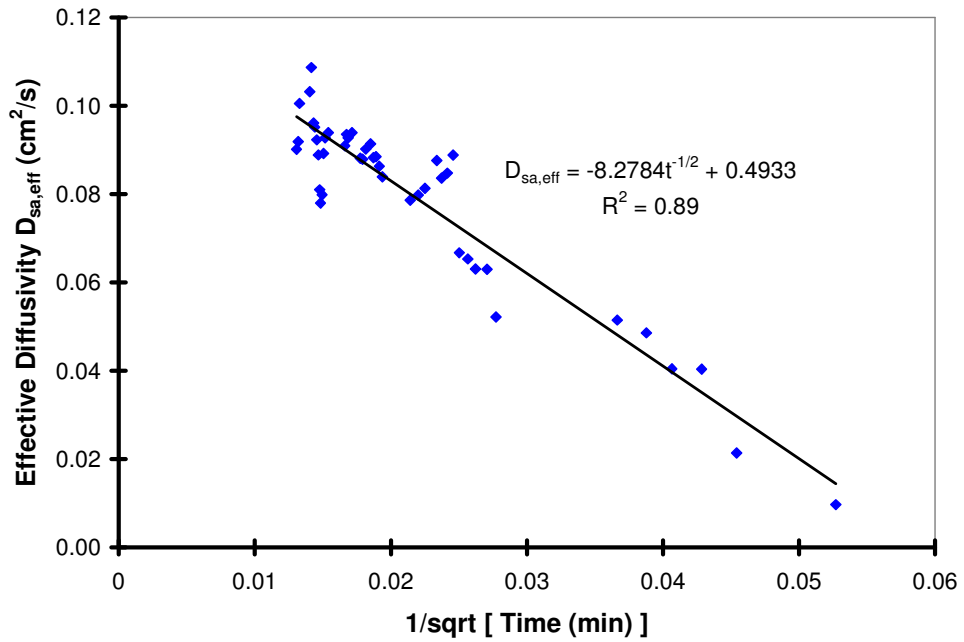


Figure C20 – Diffusivity-Time Relationship (Experiment #1)

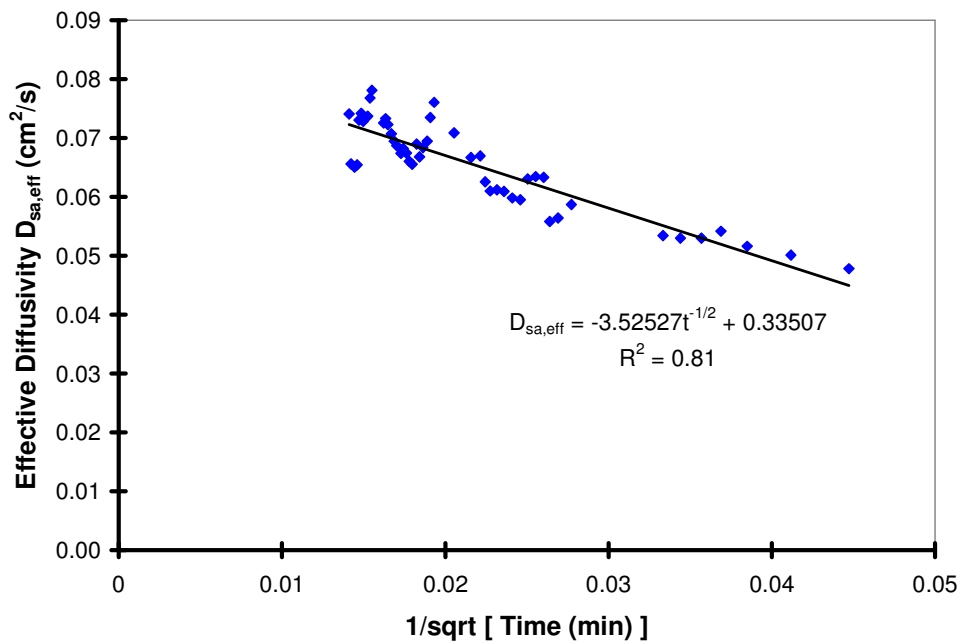


Figure C21 – Diffusivity-Time Relationship (Experiment #2)

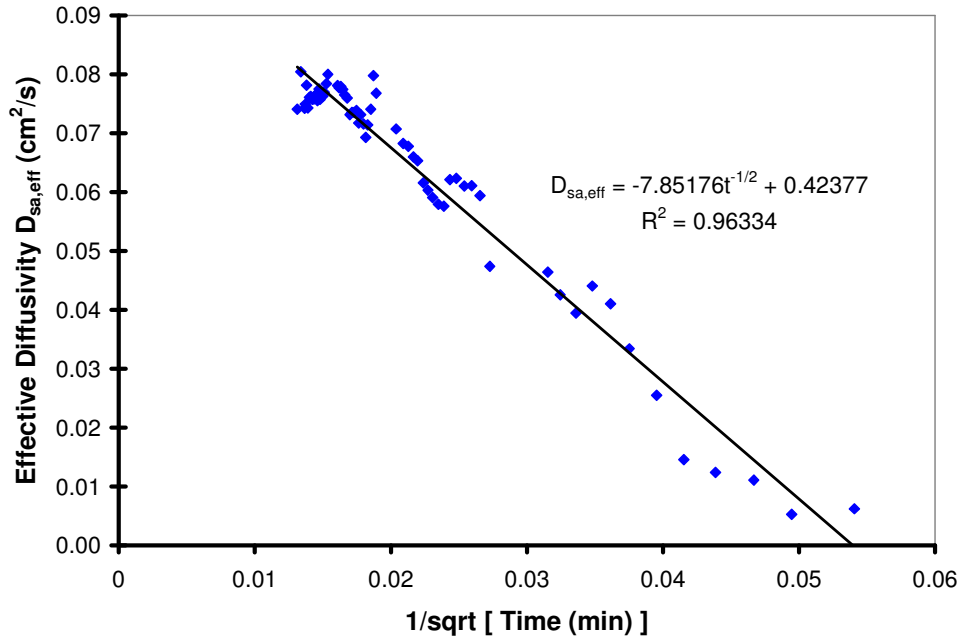


Figure C22 – Diffusivity-Time Relationship (Experiment #3)

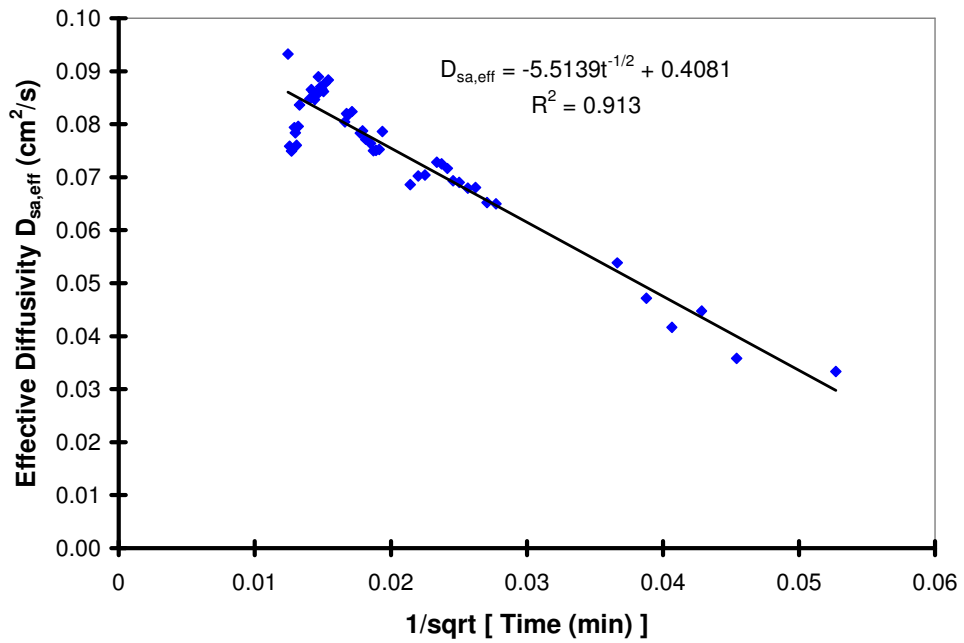


Figure C23 – Diffusivity-Time Relationship (Experiment #4)

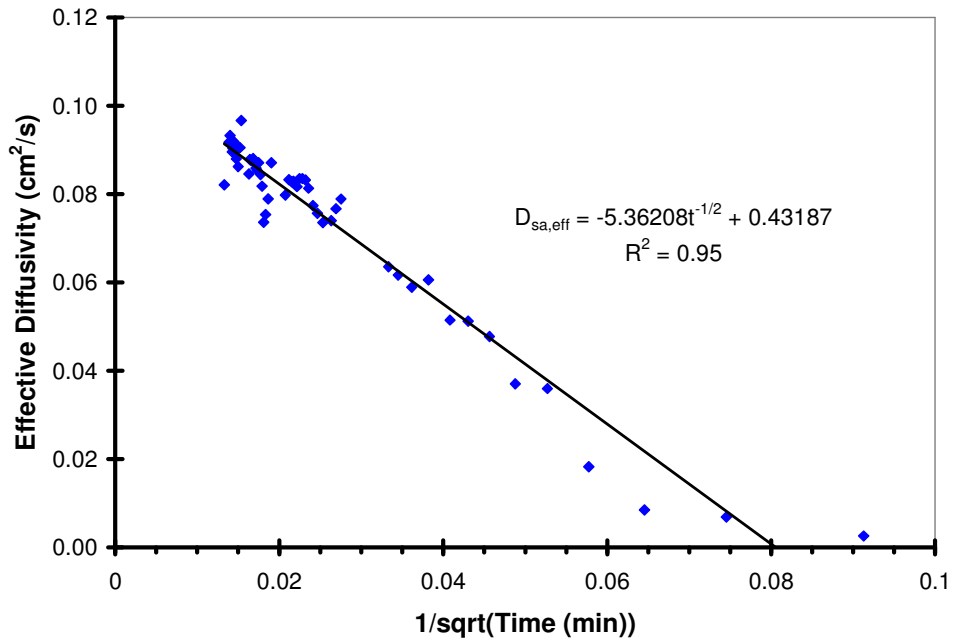


Figure C24 – Diffusivity-Time Relationship (Experiment #5)

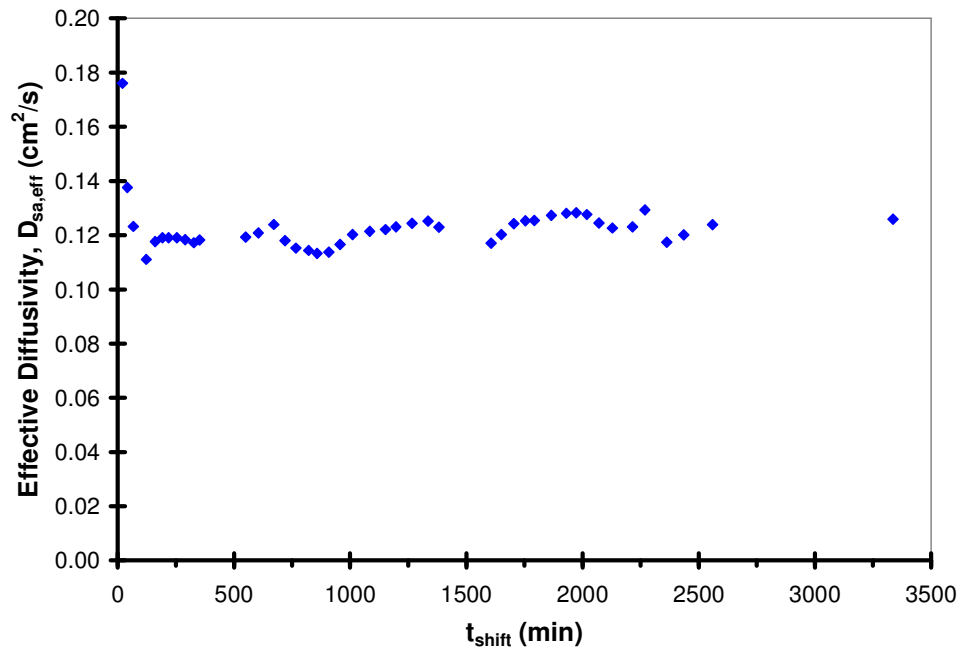


Figure C25 – Steady State Effect of Long Time Periods on Diffusivity Using Shifted Time (Experiment #1)

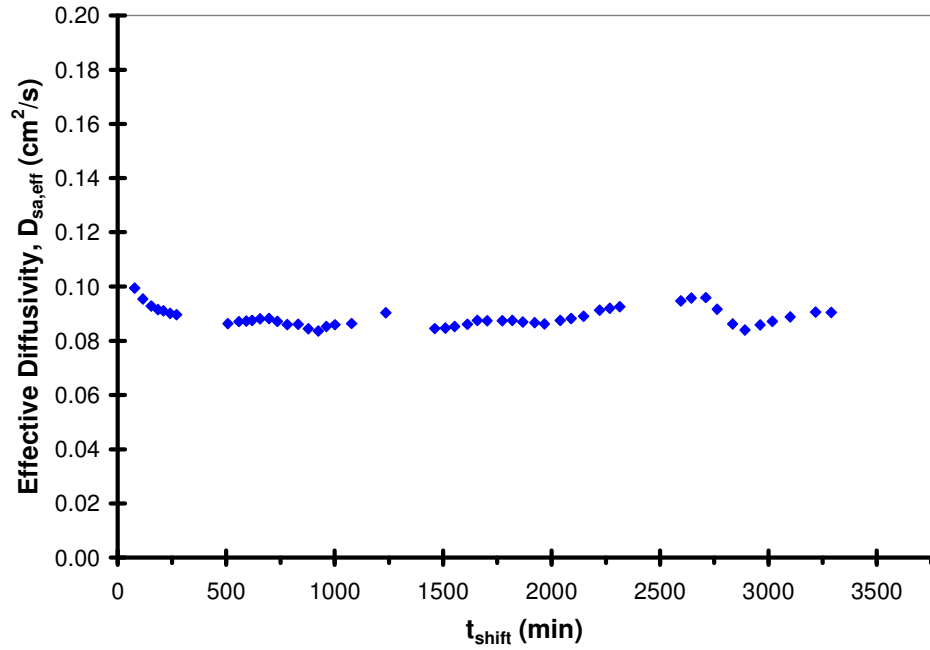


Figure C26 – Steady State Effect of Long Time Periods on Diffusivity Using Shifted Time (Experiment #2)

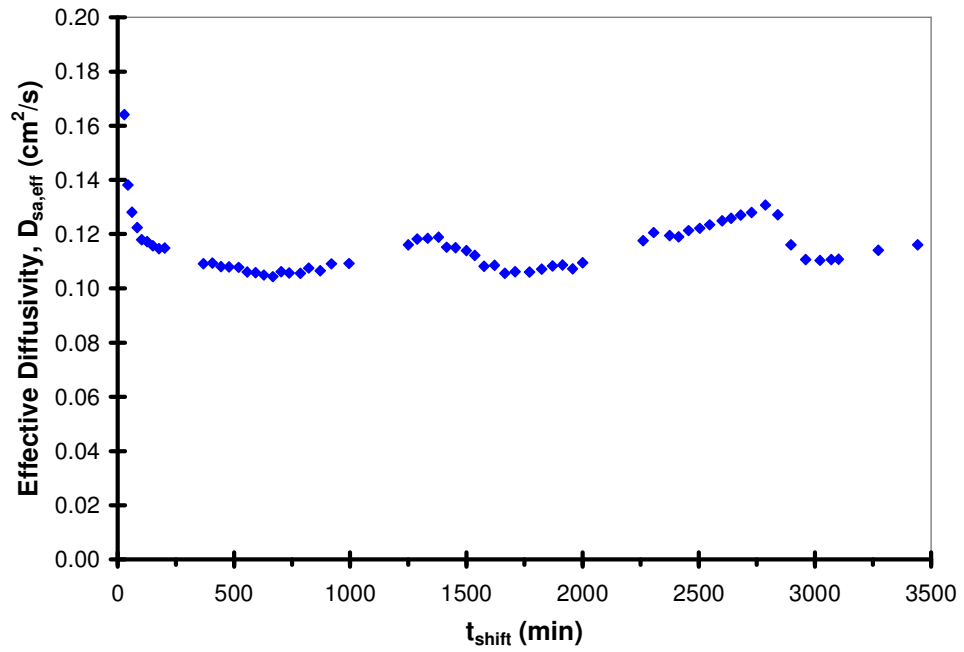


Figure C27 – Steady State Effect of Long Time Periods on Diffusivity Using Shifted Time (Experiment #3)

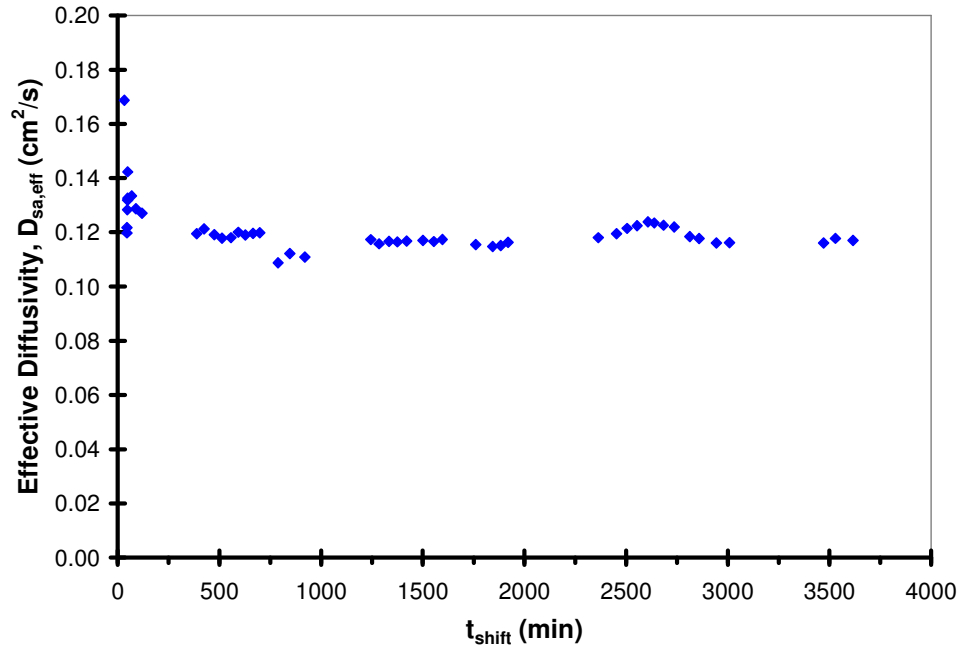


Figure C28 – Steady State Effect of Long Time Periods on Diffusivity Using Shifted Time (Experiment #4)

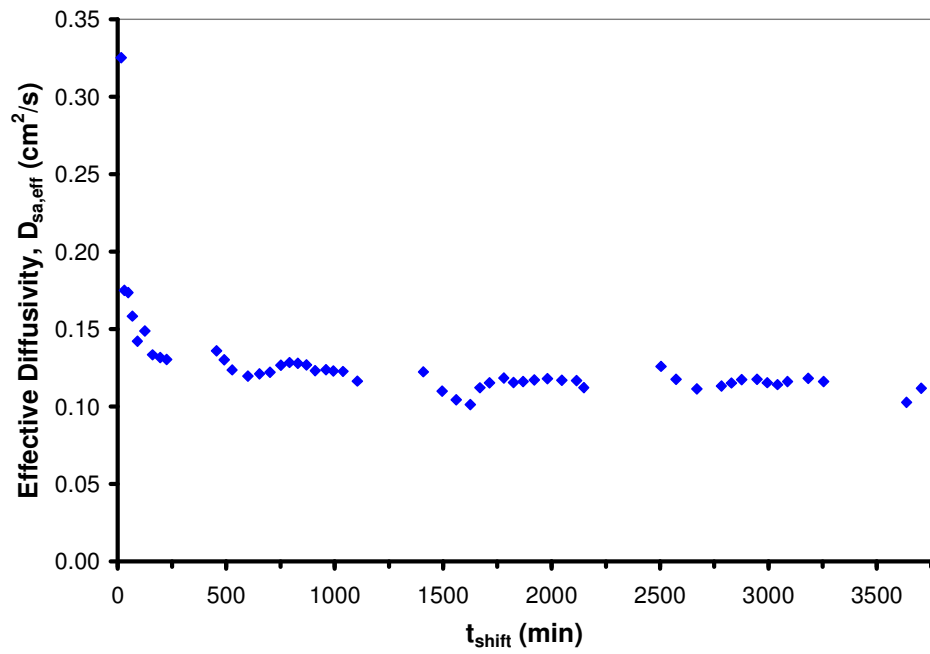


Figure C29 – Steady State Effect of Long Time Periods on Diffusivity Using Shifted Time (Experiment #5)

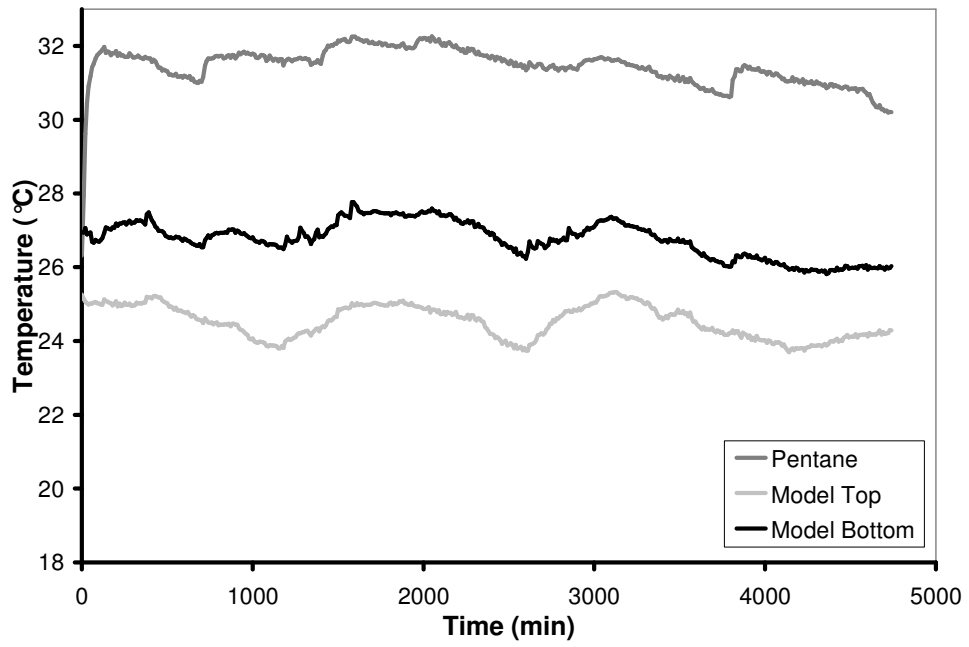


Figure C30 – Temperature History (Experiment #1)

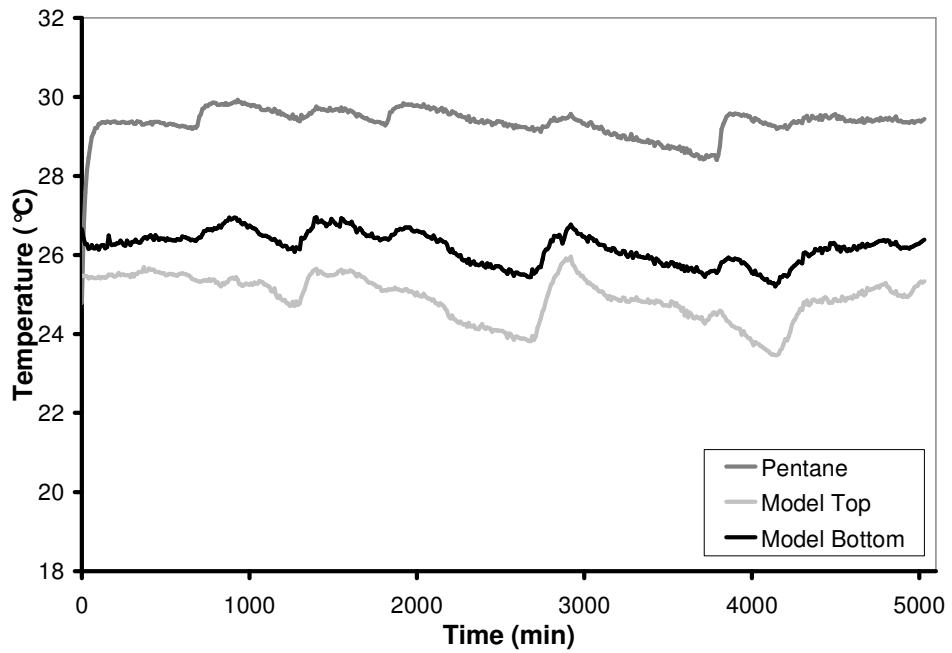


Figure C31 – Temperature History (Experiment #2)

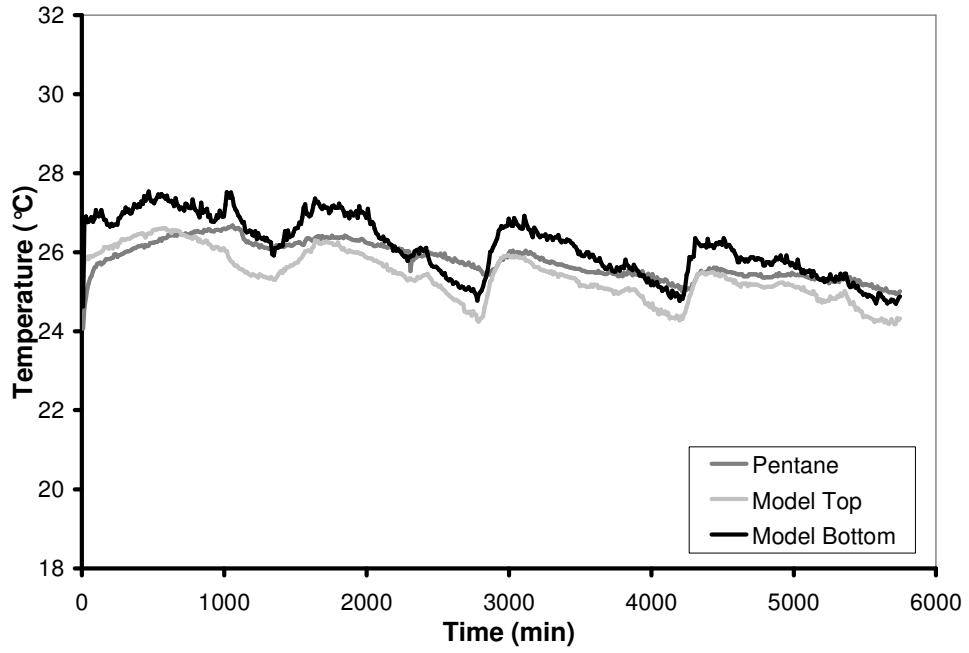


Figure C32 – Temperature History (Experiment #3)

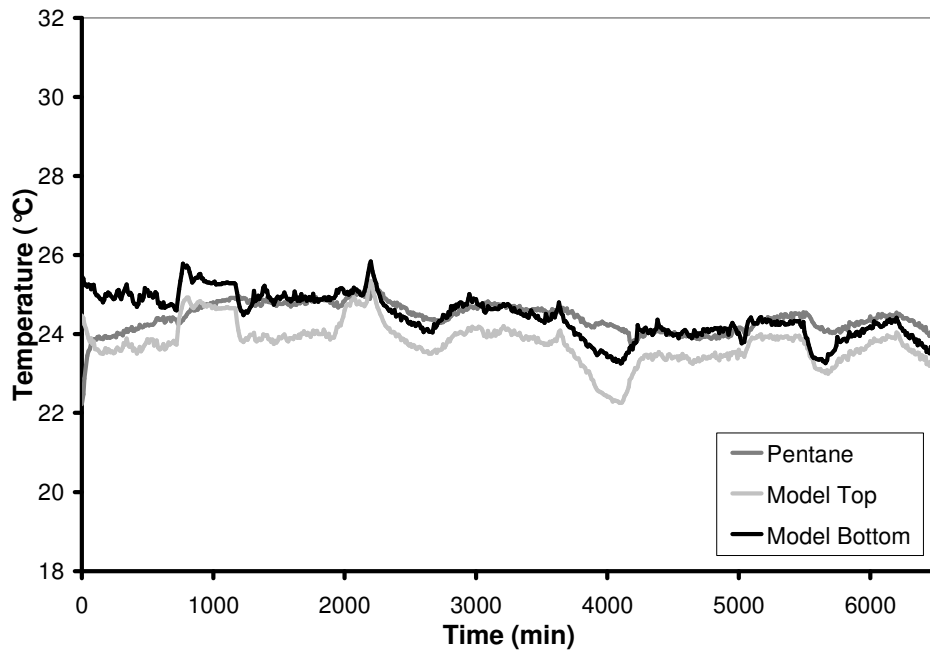


Figure C33 – Temperature History (Experiment #4)

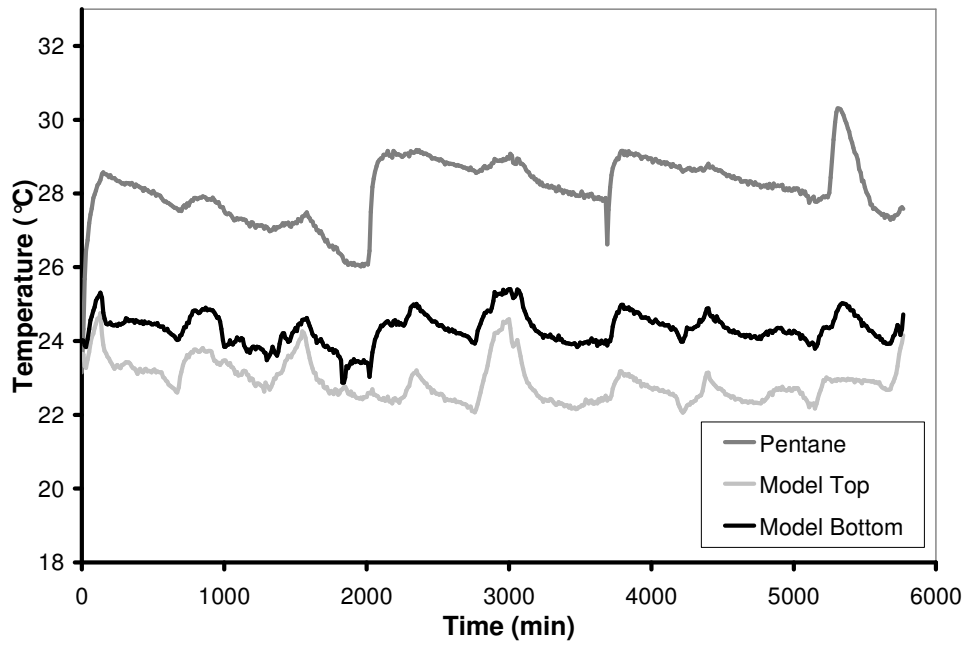


Figure C34 – Temperature History (Experiment #5)

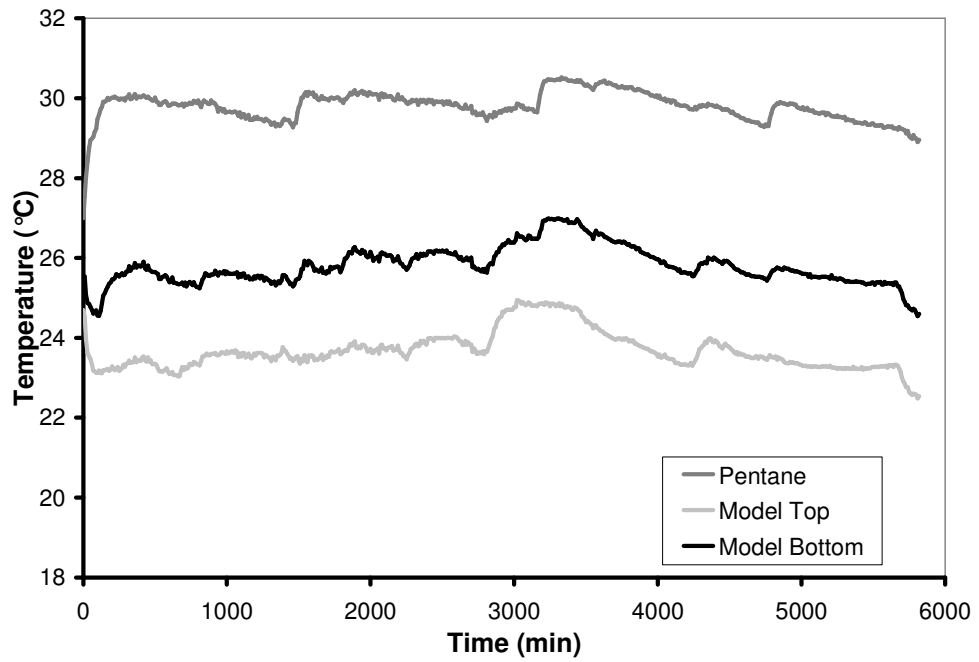


Figure C35 – Temperature History (Experiment #7)

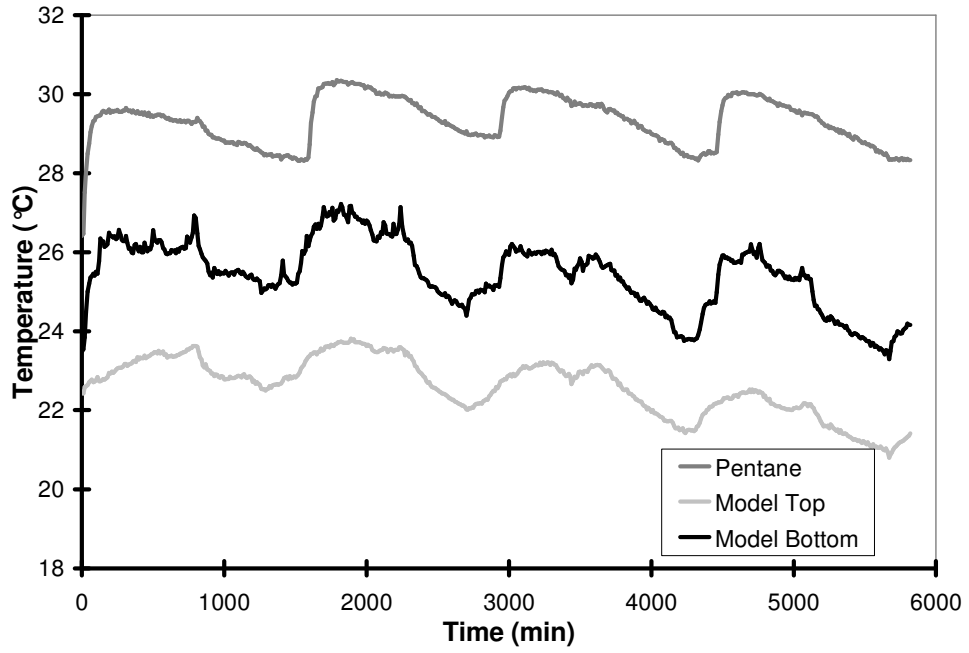


Figure C36 –Temperature History (Experiment #8)

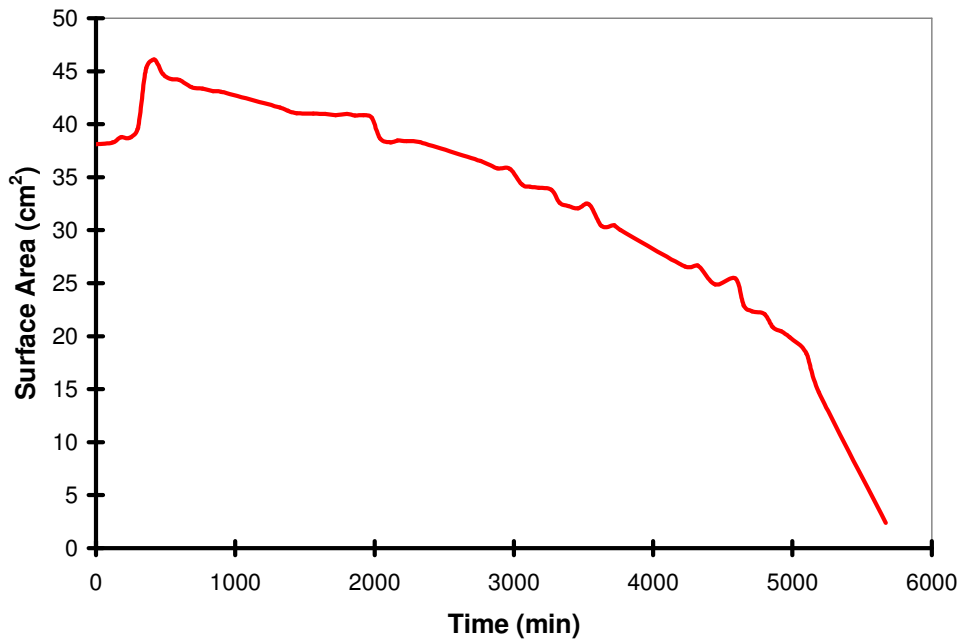


Figure C37 – Surface Area of Vapex Interface

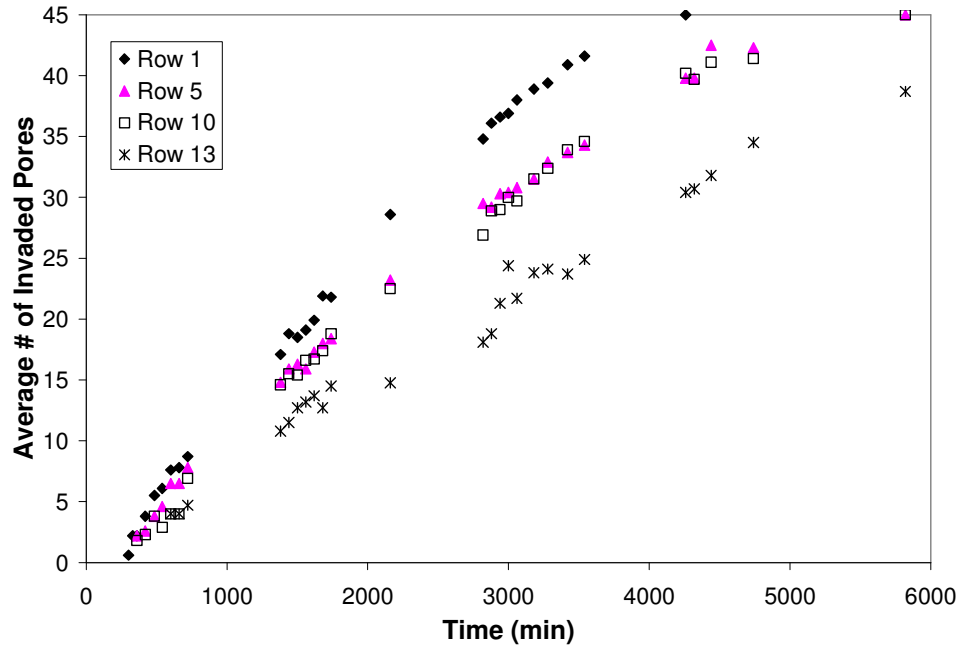


Figure C38 – Non-Linear Interface Advancement for Selected Rows (Experiment #7)

Table C.I – Residual Saturation by Sample Location

Exp't #	Sample Location						
	1	2	3	4	5	6	7
1	6.0	3.7	6.1	22.8	3.2	4.7	5.3
2	4.1	3.4	3.8	16.8	2.7	3.9	4.5
3	4.6	4.4	3.3	15.5	2.5	3.9	4.1
4	3.8	3.0	3.3	18.6	2.3	3.6	4.0
5	4.4	3.9	4.3	24.2	3.1	4.1	5.2